NOISY TRANSPORT IN REACTION-DIFFUSION SYSTEMS WITH QUENCHED DISORDER

BY

ANDREW ROYCE MISSEL

A.B., Cornell University, 2003
M.S., University of Illinois at Urbana-Champaign, 2005

DISSERTATION

Submitted in partial fulfillment of the requirements
for the degree of Doctor of Philosophy in Physics
in the Graduate College of the
University of Illinois at Urbana-Champaign, 2008

Urbana, Illinois

Doctoral Committee:

Professor Alfred Hübler, Chair
Associate Professor Karin A. Dahmen, Director of Research
Assistant Professor Smitha Vishveshwara
Professor Robert Clegg

Abstract

Reaction-diffusion (RD) models are useful tools for studying a wide variety of natural phenomena. The effects of quenched disorder in the reaction rates on RD models is not completely understood, especially in parameter regimes where internal noise or stochasticity is also important.

In the first part of this dissertation, I will examine an RD model in which both quenched disorder and stochasticity are important. The model consists of particles (labeled A) which diffuse around space and reproduce ($A \to 2A$), die ($A \to 0$), and compete with one another ($2A \to A$) with rates that depend on position. Specifically, birth is only allowed in localized patches called "oases," while death is allowed in the "desert" that comprises the rest of space. In the limit of low oasis density, transport through the system is achieved via rare "hopping" events when small concentrations of particles make it through the desert from one oasis to another. To correctly account for this hopping—and to accurately describe the nature of transport in the system—it is necessary to take stochasticity into account.

In order to determine the nature of transport in this system analytically, I will use a variety of tools drawn from disparate sources, including the theory of hopping conduction in doped semiconductors and first passage percolation. These tools will allow for predictions to be made for a number of important transport-related features: the infection time, or time needed for the population to traverse the system; the velocity of the front moving through the system; and the dynamic roughening of the front. I will also present the results of simulations of the system that largely confirm the analytical predictions. Finally, in the second part of the dissertation I will study a pair of closely related RD models, one of which exhibits an active to absorbing state phase transition.

To Jennine for agreeing to live so far from the ocean, to Dad for his ceaseless generosity, and to Mom for always making me do my homework, even when I really didn't want to.

Acknowledgments

Tony Leggett won a Nobel Prize less than three months after my arrival here—pure coincidence, I think—and the party that was held for him soon after the announcement was bursting with all of the good qualities of the UIUC Physics department: easy collegialism, a sense of fun, a lack of pretentiousness, and plentiful supplies of wine. It was, when I think about it now, perhaps a party better left for the *end* of one's tenure in Urbana; since that day, it has all been downhill.

In all seriousness, though, there are a number of people I would like to thank for making my experience here a largely positive one. First of all, there is my advisor, Karin Dahmen. Her enthusiasm, broad knowledge of the physics of disordered systems, and ability to ask probing questions greatly aided me in my quest to understand the various problems I attempted to solve. As one of her former students noted in the "Acknowledgments" section of his dissertation, her frequent "suggestions" to meet with visitors to the department quite often induced a lot of stress, but are now much appreciated; it is clear to me that I would not have learned as much—nor gained as much experience in the art of communicating months of research in five harrowing minutes at the blackboard—had I not had these meetings, and I certainly would not have volunteered to have these meetings without Karin's prodding.

I would also like to thank some of the fine teachers I have had here: Gordon Baym's utter disregard for factors of 2π, $\hbar$, and even $\imath$ was at first off-putting, but I eventually came to see it as a byproduct of his preternatural understanding of the essential elements of quantum mechanics, an understanding which he was often able to transfer to his students. Sometimes, in the pursuit of deeper truths, $2\pi\imath$ is simply not that important, and may even get in the way, but Baym never let it do so. Nigel Goldenfeld possesses a deep grasp of statistical mechanics (and better bookkeeping skills than Baym), and managed to convey most of the important truths of the subject in a way that made them seem obvious. Finally, Mike Stone's approach to his course on mathematical methods was pitch-perfect, and hearing him hold forth on the love lives, hobbies, and tragic ends of famous mathematicians was a welcome delight.

Ah, but what would graduate school be without friends to share the suffering? I do not have space to thank all of my fellow sufferers here, but there are a few people to whom I owe special thanks for helping me with

scientific matters: John Gergely, erstwhile drummer for the Born-Oppenheimer Breakdown/Starship and fellow Physical Revue organizer, helped me many times with programming matters; Bryan Clark also made many helpful suggestions concerning my simulations; and finally, Yang Liu and I had many illuminating discussions about both theoretical and numerical aspects of my work.

None of this would have been possible without the financial support of various government and university entities. The research contained herein was funded by NSF DMR grants 03-14279 and 03-25939 ITR (Materials Computation Center), by the UIUC Research Board (Account 08107RB), by a GAANN fellowship from the University of Illinois, and by the L.S. Edelheit Family Biological Physics Fellowship. The simulations I performed were run mostly on the Turing Cluster, a 1536-processor Apple G5 X-serve cluster maintained and operated by the Computational Science and Engineering Program at UIUC; I greatly appreciate the use of this fantastic computing resource.

Finally, I would like to thank my family. My parents have always provided support and encouragement in many different forms, and are a big reason why I have been able to complete this degree. My wife, Jennine Crucet, has always, always made me laugh, and continually reminds me why the world is beautiful enough to be worth studying in the first place.

Table of Contents

List of Tables

List of Figures

1 Introduction

Reaction-diffusion (RD) models are wonderful tools for exploring Nature: they are flexible enough that they can be applied to a wide variety of real-world systems; they are easy to simulate on a computer; and each one possesses a well-defined mean-field limit and unambiguous microscopic dynamics. Most of the well-studied RD models are homogeneous or translationally invariant in the sense that reactions are assumed to take place at the same rate everywhere in space. Models of this sort have proven to be very useful for studying many real-world systems, and have the advantage of being analytically tractable. One can employ a vast arsenal of tools—including a powerful set of field-theoretic methods—in order to determine the behavior of these models in various parameter regimes.

The trouble, of course, is that often Nature is dirty: reactions do not take place at the same rate everywhere, but instead have their rates set by environmental conditions. If those environmental conditions can be taken to be essentially constant over the time scale of interest, then the inhomogeneity can be modeled by quenched, or frozen in, disorder. Unfortunately, including quenched disorder in RD models makes them significantly harder to solve. In particular, the field-theoretic tools which have shone so much light on the nature of "clean" RD models are not all that useful when quenched disorder is introduced. If one is also interested in a parameter regime in which the internal noise or stochasticity in a given RD model is important, then the model becomes even more challenging to solve, as mean-field methods fail. With both mean-field theory and perturbative field-theoretic tools inapplicable—or at least exceedingly cumbersome to apply—one must dig deeper into the proverbial toolbox in these situations.

In this dissertation, I will consider a set of RD models in which quenched disorder and internal noise each plays a role. In order to tackle these models analytically, I will use tools drawn from a wide variety of sources as well as analogies to a number of other systems, including doped semiconductors in the hopping conduction regime, first passage percolation on a lattice, and the Eden model. In most cases, I will also present simulation results which by and large confirm the analytical predictions.

A brief outline of this dissertation: in Chapter 2, I will provide a brief introduction to reaction-diffusion models and the theory of stochastic systems. As this is a field that could not possibly be summarized in a single volume, let

alone a single chapter, the presentation will necessarily be idiosyncratic: I will focus on those topics which are essential for understanding the original research presented in later chapters. These topics include Markov processes and the master equation, mean-field theory, Langevin equations, the directed percolation (DP) class of active to absorbing state phase transitions in RD models, and fronts in RD models. Chapter 3 is also devoted to background material; specifically, I will discuss both lattice and off-lattice versions of first passage percolation and the Eden model.

Chapter 4 contains a number of analytical predictions about a particular RD model with quenched disorder in which internal noise must be taken into account. The model consists of particles which are allowed to diffuse around an inhomogeneous environment consisting of growth-promoting "oases" placed randomly in a deadly "desert." For the case of low oasis density (large average distance between oases), transport through the system is mediated by rare events in which a small number of particles manage to make it through the desert separating two oases. Because the number of particles involved in these events is low, mean-field theory is inadequate to the task of describing this type of transport; it is necessary to take into account discreteness effects. I will present a solvable model which takes into account such effects and correctly predicts the statistics of the transit time between two oases. I will then use this result, along with ideas from the theory of hopping conduction and first passage percolation, to make predictions for the time needed by a population to traverse a large system consisting of many oases and for the dynamic scaling of the coarse-grained front formed by occupied oases in such a system.

Chapter 5 is concerned with simulations. After a brief introduction to the kinetic Monte Carlo method, I will present the details and results of three sets of simulations designed to test the predictions made in Chapter 4. The first set tests the model used to predict the two-oasis transit time statistics. This is done by simulating the full RD model and comparing the generated transit time statistics to the analytical predictions. The second set of simulations tests the predictions for the infection time, or the time needed for a population to traverse a large system, and the third set tests the predictions for the dynamic scaling of the coarse-grained front that defines the border between occupied and unoccupied oases. For each set of simulations, I will first describe the algorithm used, the various approximations made, and the method of data analysis, and I will then present the results.

The second and third set of simulations presented in Chapter 5 are really simulations of a simplified model which has the same properties as the model of Chapter 4 in the limit of low oasis density and high oasis growth rate. This simplified model consists of points randomly placed in space with transit times between each pair of points picked from a distance-dependent probability distribution. In Chapter 6, I will explore the properties of this simplified model, which is a new kind of off-lattice first passage percolation model, using

both analytical tools and simulations. Specifically, I will look at what happens to the infection time as the oasis density and form of the transit time probability distribution are changed. I will then change the model by allowing the points to "die out" at some rate—thus turning the model into a kind of off-lattice contact process—and I will examine the nature of the phase transition that occurs as the death rate is raised.

2 Reaction-Diffusion Models

Reaction-diffusion (RD) models have proven to be very useful tools for the study of chemical [1], biological [2–7], and ecological [8, 9] systems. RD models typically consist of a set of particles which are allowed to diffuse and interact with one another and their environment in prescribed ways. By varying the types of allowed reactions, number of types of particles, and reaction rates, one can obtain a wide variety of behavior.

In this chapter, I will offer a brief introduction to those aspects of the theory of reaction-diffusion models relevant to the rest of this work. I will start by introducing the concept of a Markov process, then show how the master equation formalism can be derived from a few basic assumptions about stochastic processes together with the Markov property. I will then show, by example, how a collection of Poisson processes with given rates can be described by a master equation, and how a mean-field equation can be extracted from the master equation. The final two sections will be concerned with phase transitions and front propagation problems in reaction-diffusion systems.[1]

2.1 Preliminaries

2.1.1 Stochastic Processes and the Master Equation

Before delving into reaction-diffusion models, it is necessary to briefly review the theory of stochastic processes. The stochastic processes of most interest to physicists have largely been Markov processes—that is, processes which possess the property of being history-independent or memoryless [10]. This property can be defined explicitly, though it is first necessary to set up some preliminaries: consider a stochastic system defined by a state variable $N(t)$, where t represents time. This quantity N could be the number of particles in the system, or the position of a single particle, or some other quantity. The system is stochastic because its state at some future time t'—denoted by $N(t')$—is not a deterministic function of $N(t)$ and t, but rather a function of these quantities and some random variable which I will denote by X. $N(t)$ is

[1] Some of the material in this chapter has appeared before, in slightly altered form, in the following publications: A.R. Missel and K.A. Dahmen, Phys. Rev. Lett. **100**, 058301 (2008), Copyright 2008 by the American Physical Society; and A.R. Missel and K.A. Dahmen, submitted to Phys. Rev. E (2008), Copyright 2008 by the American Physical Society.

thus really $N_X(t)$.

In the spirit of Van Kampen [10], I will define the probability distributions that describe the system as follows: $P_k(n_k, t_k; \ldots; n_1, t_1)$ is the joint probability distribution for the variable N to take on the values $n_1, n_2, \ldots, n_k$ at times $t_1, t_2, \ldots, t_k$; and $P_{l|k}(n_{k+l}, t_{k+l}; \ldots; n_{k+1}, t_{k+1}|n_k, t_k; \ldots; n_1, t_1)$ is the conditional probability that N takes on the values $n_{k+1}, \ldots, n_{k+l}$ at the times $t_{k+1}, \ldots, t_{k+l}$, given that it took on the values $n_1, \ldots, n_k$ at the times $t_1, \ldots, t_k$. With these definitions in hand, it is now possible to define what is meant by a Markov process. A Markov process is a stochastic process for which [10]

$$P_{1|j-1}(n_j, t_j|n_{j-1}, t_{j-1}; \ldots; n_1, t_1) = P_{1|1}(n_j, t_j|n_{j-1}, t_{j-1}); \tag{2.1}$$

that is, if you know the state of the system at some time, it is not necessary to know anything about the history of the system to determine its future. This feature is known as memorylessness.

Why are systems that have the Markov property important? In large part it is because they are more easily dealt with than non-Markovian systems. For one thing, a Markov process can be completely described by two probability functions: $P_1(n_1, t_1)$ and $P_{1|1}(n_2, t_2|n_1, t_1)$ [10]. The second of these can be interpreted as a transition probability between the states n_2 and n_1. Consider the case where the transition probability depends only on the time difference $t_2 - t_1$; in this case, $P_{1|1}(n_2, t_2|n_1, t_1)$ is the probability that the system is in state n_2 a time $t_2 - t_1$ after definitely being found in state n_1 at time t_1. Now define $P(n_2|n_1, t)$ to be $P_{1|1}(n_2, t_1 + t|n_1, t_1)$, and assume that n can take one of an infinite number of discrete values ($n = 0, 1, 2, \ldots$). The Markov property makes it possible to write the following relation involving $P(n|0, t)$, known as the Chapman-Kolmogorov equation [10]:

$$P(n|0, t) = \sum_{n'} P(n|n', t - t')P(n'|0, t'). \tag{2.2}$$

This equation is valid for any value of t'.

Since the future evolution of the probability distribution functions of a Markov process depends only on its present state, one might hope to write down a differential equation for these functions. Indeed, it is possible to do so using (2.2) together with some facts about the nature of $P(n|0, t)$ for small times: as $t \to 0$, it is exceedingly unlikely that the system has time to jump from state $0 \to n' \to n$; it must go directly from $0 \to n$. This makes it possible to write

$$P(n|0, dt) \simeq W_{0,n}dt \tag{2.3}$$

for the case where $n \neq 0$, where $W_{0,n} \equiv \partial_t P(n|0, t)|_{t=0}$. If $n = 0$, then clearly $P(0|0, t)$ will decrease or remain the same for very small times since the

system only has time to leave the state 0:

$$P(0|0,dt) \simeq 1 - \left(\sum_{n' \neq 0} W_{0,n'} \right) dt. \tag{2.4}$$

Putting these results together, then, yields an expression for $P(n|0,dt)$ that is correct to first order in dt:

$$P(n|0,dt) \simeq \delta_{0,n} \left[1 - \left(\sum_{n'} W_{0,n'} \right) dt \right] + W_{0,n} dt. \tag{2.5}$$

Setting $t' = t - dt$ in (2.2) and using (2.5) leads to the following:

$$P(n|0,t) \simeq P(n|0,t-dt) + dt \left[\sum_{n'} W_{n',n} P(n'|0,t-dt) - W_{n,n'} P(n|0,t-dt) \right], \tag{2.6}$$

where the sum can be taken over all states. Letting $dt \to 0$ and rearranging leads to the celebrated master equation for $P(n|0,t)$:

$$\frac{\partial P(n|0,t)}{\partial t} = \sum_{n'} W_{n',n} P(n'|0,t) - W_{n,n'} P(n|0,t). \tag{2.7}$$

The master equation is thus a differential equation for the probability that a Markovian system is in the state n at time t, given that it was in the state 0 at time 0. The equation has a nice physical interpretation: the term $W_{n',n} P(n'|0,t)$ represents the rate of probability inflow into the state n from the state n', while $W_{n.n'} P(n|0,t)$ represents the rate of probability outflow from state n to state n' [10, 11]. By summing these rates over all states n', one gets the net rate of probability flow into the state n.

The master equation describes the evolution of a probability distribution that describes a stochastic process, but it still is not immediately clear what the microscopic description of the process should be. To see what kind of microscopic description is compatible with the Markov property and the master equation, consider the following simple system: particles (labeled A) are allowed to reproduce ($A \to 2A$) and die ($A \to 0$) with rates y and z. The system at any time time can be described by a single number n giving the number of particles present. I will use the following microscopic description of the process: at the birth of each particle, a time to that particle's death is picked from some distribution $p_d(\tau)$, and a time to that particle's splitting up (giving birth) is picked from some other distribution $p_b(\tau)$. In order for this microscopic description of events to be compatible with the Markov property, these distributions must be exponential distributions [10]. That is,

$$\begin{aligned} p_b(\tau) &= r_b e^{-r_b \tau} \\ p_d(\tau) &= r_d e^{-r_d \tau}, \end{aligned} \tag{2.8}$$

where r_b and r_d are called birth and death rates, respectively. I will not prove this assertion regarding the necessity of exponential distributions for describing stochastic events, but in the next chapter I will show explicitly how the exponential distribution is memoryless in the context of first passage percolation.

Events with such distributions to their time of occurrence are called Poisson processes [10]. Thus, a stochastic process can be described by a set of independent Poisson processes occurring in parallel. The master equation for the simple model described above is [10]

$$\frac{\partial P(n,t)}{\partial t} = r_b(n-1)P(n-1,t) + r_d(n+1)P(n+1,t) - (r_b + r_d)nP(n,t), \quad (2.9)$$

with the initial condition $P(n,0) = \delta_{n,n_0}$ (note that $P(n,t)$ is technically $P_{1|1}(n,t|n_0,0)$). Each particle contributes a birth rate of r_b and a death rate of r_d to the "total" birth and death rates, so that the rate for the system to go from a state with n particles to one with $n+1$ particles, for instance, is nr_b.

Processes with spatial dependence can also be handled by the master equation formalism. For example, the case of unbiased diffusion on a $d = 1$ lattice is described by the master equation

$$\frac{\partial P(\nu,t)}{\partial t} = \frac{w}{2}\left[P(\nu+1,t) + P(\nu-1,t) - 2P(\nu,t)\right], \quad (2.10)$$

where $P(\nu,t)$ is the probability for a particle to be at the lattice point ν at time t and w is the rate to hop away from the current site. By introducing a lattice spacing l_0 and allowing $l_0 \to 0$ while $w{l_0}^2 \to 2D$, it is possible to derive the continuum diffusion equation,

$$\frac{\partial P(x,t)}{\partial t} = D\frac{\partial^2 P(x,t)}{\partial x^2}, \quad (2.11)$$

where $x = \nu/l_0$ [10].

2.1.2 Mean-Field Theory and Beyond

As with most problems in statistical physics, the first approach to dealing with stochastic systems involves the neglect of fluctuations. For any master equation, it is possible to write down an associated "mean-field" equation for the average behavior of the system. There are formal ways of doing this—see Van Kampen [10] for a detailed discussion of some of these methods—but for my purposes it suffices to use the simplest approach possible. The easiest way to convey this approach is by example.

Take the master equation (2.9) for the simple birth-death system described in the last section, which is a differential equation for the probability of the system to be in a state with n particles at time t. By multiplying by n and summing over all values of n, one clearly arrives at an equation for the time

evolution of the *average* number of particles $\langle n(t)\rangle$:

$$\frac{\partial \sum_n nP(n,t)}{\partial t} = \frac{\partial \langle n(t)\rangle}{\partial t} = (r_b - r_d)\langle n(t)\rangle. \tag{2.12}$$

As one would expect, the average behavior of the system is described by a Malthusian equation, the solution of which is either exponential growth or exponential decay unless the birth and death rates exactly balance.

It is often easy to write down the proper mean-field equation simply by looking at the list of reactions and reaction rates of a given stochastic process. For instance, take the spatial birth-death process in $d = 1$, which consists of particles which are allowed to diffuse, die at some rate z, and reproduce at some rate y. It should be clear that the proper mean-field equation for the average density of particles $\langle n(x,t)\rangle$ is:

$$\frac{\partial \langle n(x,t)\rangle}{\partial t} = D\frac{\partial^2 \langle n(x,t)\rangle}{\partial x^2} + (y-z)\langle n(x,t)\rangle. \tag{2.13}$$

There are two major categories of advanced tools that can be used to extend the analysis of RD models beyond mean-field theory. The first class of tools comprises the use of stochastic differential equations to take into account the fluctuations present in a given RD model. The most popular method in this class is known as the Langevin approach, which consists of adding to the deterministic mean-field equation a stochastic term [10]. To see how this approach works, consider the spatial birth-death process just described: at a given time t, there should be fluctuations in the local density of particles $n(x,t)$ due to internal noise. Since the local density is really an average of particle occupation numbers over a large number of lattice sites, the size of these fluctuations should scale as $\sqrt{n(x,t)}$. Thus, the proper Langevin equation is [12]

$$\frac{\partial n(x,t)}{\partial t} = D\frac{\partial^2 n(x,t)}{\partial x^2} + (y-z)n(x,t) + \sqrt{n(x,t)}\,\xi(x,t), \tag{2.14}$$

where $\xi(x,t)$ is a random variable obeying the following relations:

$$\begin{aligned} \langle \xi(x,t)\rangle &= 0 \\ \langle \xi(x,t)\xi(x',t')\rangle &= \Gamma\delta(x-x')\delta(t-t'). \end{aligned} \tag{2.15}$$

The constant Γ must be determined by considering the steady-state fluctuations of $n(x,t)$ or by some other method.

While the Langevin approach is very popular, it is beset by some ambiguities and shortcomings. One alternative approach involves a systematic expansion of the master equation [10], but a far more popular set of methods comprises the second category of tools: field-theoretic methods. Doi was the first to use the creation and annihilation operator formalism (second

quantization) from quantum mechanics in the study of RD models, and this approach has grown in popularity ever since. Field-theoretic methods for RD models share many of the same advantages as their equilibrium cousins: in conjunction with ideas from the renormalization group, they allow for a clear grouping of models into universality classes; they make possible the quantitative calculation of critical exponents in an ϵ expansion about the upper critical dimension; and they make evident the appropriate mean-field equation for a given model.

2.2 Phase Transitions in Reaction-Diffusion Models

2.2.1 The Directed Percolation Universality Class

Although most of the original research presented in later chapters is concerned with the transport properties of RD systems, a portion is focused on the nature of a particular phase transition in an off-lattice RD model. For this reason, it is necessary to briefly review the vast literature on phase transitions in RD models. Much of the work in this field has been done on the phase transition between active (population survives as $t \to \infty$) and absorbing (population dies as $t \to \infty$) states [13–17], and it is this type of transition I am concerned with.

Consider a reaction-diffusion model comprised of particles (labeled, as usual, A) which are allowed to hop around a lattice in d dimensions, die with rate z, give birth with rate y, and compete with rate b. This last reaction is of the general form $kA \to lA$, where k and l are integers and $k > l$. In this work, I will only consider binary reactions ($k = 2$), although there are many interesting properties of reactions involving three or more particles [12, 17]. For the moment, I will take $l = 1$, so that the competition reaction is $2A \to A$. The state of the system at time t can be described by a set of occupation numbers $\{n\}$ giving the population at each lattice point. What is hopefully clear about this model is that it possesses only a single absorbing state; that is, there is only one state $\{n\}_{\text{abs}} = \{0, 0, \ldots\}$ (the state with no particles) from which escape is impossible. If the system reaches this state, it will stay there forever. But under what conditions will it reach this state?

The mean-field equation for the average particle concentration $\bar{n}(\boldsymbol{x}, t)$ in the continuum limit of this model can be written down fairly easily [17]:

$$\frac{\partial \bar{n}(\boldsymbol{x}, t)}{\partial t} = D\nabla^2 \bar{n}(\boldsymbol{x}, t) + (y - z)\bar{n}(\boldsymbol{x}, t) - b{\ell_0}^d \bar{n}(\boldsymbol{x}, t)^2, \tag{2.16}$$

where ℓ_0 is some microscopic length scale related to the distance within which particles are allowed to compete with one another. Consider what happens for $z > y$: mean-field theory predicts that the population should die out as $t \to \infty$; that is, it should reach the absorbing state. The total number of

particles $N(t) = \int d^d\boldsymbol{x}\, \bar{n}(\boldsymbol{x}, t)$ should decay like $N \sim e^{-(z-y)t}$ for small $N(t)$. But consider the case of $y = z$: for long times, the population should be sufficiently spread out so that the $\nabla^2\bar{n}(\boldsymbol{x}, t)$ term is negligible, leaving a simple equation for the mean concentration which is solved by $\bar{n}(\boldsymbol{x}, t) \sim 1/t$. Thus, the system still reaches the absorbing state, but the population decays according to a power law $\sim t^{-\alpha}$ with a critical exponent $\alpha = 1$. For $y > z$ the population survives as $t \to \infty$.

This type of phase transition is called an active to absorbing state transition. One would be correct in doubting the mean-field results just presented for the nature of the decay to the absorbing state; as mentioned in the previous section, this type of deterministic mean-field approximation should work very well only when the population is large, and this is certainly not the case in the vicinity of the transition at $y = z$. Because of the small particle concentrations involved in the decay, discreteness effects—fluctuations about mean-field theory—are important, and alter the critical behavior. Indeed, to get an accurate view of the nature of the transition, one needs to use one of the advanced methods discussed in Section 2.1.2. The use of such methods in the study of models like the one described above have led to the directed percolation (DP) hypothesis: for models with one type of particle, a single absorbing state, no disorder, and no special additional symmetries, the active to absorbing state transition should fall in the directed percolation universality class [12, 14, 17, 18].[2]

Various models in the DP universality class have been studied both analytically and through simulations; see Ref. [12] or Ref. [17] for an extensive review of these studies. A few features of the class are of particular interest: first, the upper critical dimension for the transition is $d_c = 4$; second, the effect of fluctuations is to shift the critical birth-minus-death rate $(y - z)_c$ to be > 0; finally, the critical exponents related to particle density decay, the spatial extent of the surviving population, and other quantities are of course different from their mean-field values for $d < d_c$.

2.2.2 The Effects of Quenched Disorder

Although RD models are supposed to be of wide applicability to real systems, there is scant experimental evidence for any active to absorbing state transitions in the DP class in nature [12, 17]. One possible reason for this is that real systems inevitably have disorder, and systems with disorder are not in the DP class. When speaking of disorder, it is important to distinguish

[2]The name "directed percolation" refers to the fact that the critical properties of such models in d dimensions are related to the critical properties of directed percolation in $d + 1$ dimensions. Directed percolation is a model in which bonds placed randomly between lattice sites can only be traversed in a preferred direction $\hat{x}_{d+1}$; if this direction is identified with time, then one can imagine each d-dimensional "layer" perpendicular to $\hat{x}_{d+1}$ corresponding to a configuration of the d-dimensional RD model at time t. The absorbing state is then identified with the DP regime in which there is no percolating cluster, while the active state corresponds to the DP regime in which there is a percolating cluster [16, 19].

between quenched and annealed disorder: quenched disorder is fixed in time or in space, while annealed disorder changes in time and space. In this work, I am concerned with quenched disorder in the reaction rates; that is, I am concerned with the case where some or all microscopic reaction rates are taken to be functions of position, but not of time.

The effects of quenched disorder in the reaction rates on the critical behavior of RD models—and of the DP transition in particular—have been difficult to determine. One simple way to check whether the presence of disorder will affect the critical properties of the DP transition is to use the Harris criterion [20, 21], which was first employed for this particular purpose by Kinzel [22] and Noest [23]: if $d\nu > 2$, where d is the spatial dimension and ν is a critical exponent related to the divergence of the characteristic length scale of fluctuation correlations at the critical point, then the disorder will *not* change the universality class of the transition. For the DP transition with $d < d_c = 4$, the Harris criterion is violated [12], and so quenched disorder, however weak, should change the nature of the DP active to absorbing state transition.

How does one deal with a system with quenched disorder? A straightforward renormalization group treatment using the field-theoretical approach described earlier leads to runaway flows [17, 24], but some progress has been made using other methods. Hooyberghs and coworkers [25, 26] have used real-space RG methods to study the transition, and have found that, for the case of large disorder, the critical behavior is governed by an infinite-disorder fixed point. Behavior of this type is characterized by logarithmically slow—rather than power-law—dynamics. For instance, for a lattice model with site occupation numbers s_i, one can define an average density $\langle \rho(t) \rangle$ by

$$\langle \rho(t) \rangle = \lim_{N_p \to \infty} \frac{1}{N_p} \sum_i \langle s_i(t) \rangle, \tag{2.17}$$

where N_p is the number of lattice points in the system and the averaging is over realizations of the process. At the critical point, this quantity is expected to decay as

$$\langle \rho(t) \rangle \sim \left[\log \left(t/t_0 \right) \right]^{-\bar{\delta}}, \tag{2.18}$$

where t_0 is some nonuniversal time scale and $\bar{\delta}$ is a critical exponent [27]. This is in contrast to a "clean" system, in which the density decays like $t^{-\alpha}$ at the critical point. For weak disorder, Hooyberghs *et. al* have obtained results that are somewhat ambiguous, but they have conjectured that there may be a line of fixed points corresponding to continuously varying critical exponents.

There have also been numerous simulations done to determine the nature of the disordered DP active to absorbing state transition. The contact process (CP) with disorder has been the most frequent subject of study, with the disorder taking a variety of forms. The contact process is a lattice model in

which each site i can either be infected ($s_i = 1$) or empty ($s_i = 0$). An empty site can be infected by an adjacent infected site with a rate $\lambda/2d$, where d is the dimensionality of the (square) lattice, and an infected site can become "healthy" with a rate μ. The ratio λ/μ can be tuned to control the behavior of the system: for large values of this parameter, the population survives, and for small values it dies out (reaches the absorbing state).

Disorder has been introduced into the contact process in a number of ways: Moreira and Dickman [28] and Vojta and coworkers [29, 30] have considered the diluted contact process, in which a fraction p of the lattice sites are randomly removed. So long as $p < p_c$, where p_c is the percolation threshold, there exists an infinite cluster of sites over which the population can travel, but for $p \geq p_c$, there is no active phase, and the population will eventually die. Vojta and Lee [29] have found that there are actually two phase transitions in this model: the first occurs for $p < p_c$ as the infection rate λ is lowered—this is the disordered DP phase transition from an active to an absorbing state, which has also been studied by Moreira and Dickman [28]. There is an additional transition from an active to an absorbing state as p is raised past p_c. The results obtained in these studies for the disordered DP transition can be summarized as follows: for $\lambda > \lambda_c(p)$, the system is in the active phase; for $\lambda < \lambda_c(0)$ (the critical point in the absence of disorder), the system decays to the absorbing state exponentially; and for $\lambda_c(0) < \lambda < \lambda_c(p)$, the system decays to the absorbing state very slowly (algebraically)—that is, this region is a Griffiths phase [31].[3] The slow relaxation to the absorbing state in the Griffiths phase can be attributed to the effects of rare regions without many sites removed. These regions are locally supercritical, but, since they are finite, they must eventually decay to the absorbing state, albeit only after a long time. In agreement with the theoretical work of Hooyberghs, these studies have found that the critical behavior of the transition at $\lambda_c(p)$ is not characterized by power laws, but is rather logarithmically slow for all values of p.

There have been a few other studies of disorder effects on the contact process and related models. Bramson and coworkers have studied a one-dimensional model in which each site is either "good"—has a low death rate—or "bad." They have found that there exists a third phase in this model, one in which the population survives but spreads sublinearly from a single "seed" site. Webman and coworkers [32] have found essentially the same thing in a similar one-dimensional model; however, as anticipated by Bramson *et. al*, this phase does not appear to exist for $d \geq 2$. Szabó and coworkers [33] have studied a $d = 2$ version of the contact process in which no sites are actually removed, but each site is randomly assigned one of two sets of birth and death rates. Their findings match those of Dickman and Vojta, although they have not looked at the portion of the absorbing phase in which the relaxation is

[3] At the clean critical point $\lambda_c(0)$, the decay appears to be of a stretched exponential character [30].

exponential (the portion corresponding to a high death rate). Vojta and Dickison [27] have considered a similar $d = 2$ model with "good" and "bad" sites, with similar results.

The general picture of the DP transition in the presence of disorder that is beginning to emerge is this: the transition is controlled by a strong disorder fixed point, and the dynamics are logarithmically slow [26, 30]; in the absorbing phase close to the transition, there is a Griffiths phase characterized by power-law decay towards the absorbing state; further away from the critical point, the relaxation to the absorbing state is exponential, as in the absorbing phase of the "clean" model. For $d = 1$, it appears that the active state is also broken up into two distinct regimes: close to the critical point, there exists a regime in which the population survives, but spreads sublinearly in time; further away from the critical point, the spreading is linear. This division of the active phase appears to not exist for $d \geq 2$.

2.3 Fronts and Transport in Reaction-Diffusion Models

2.3.1 Fisher Waves and Front Roughness

The subject of fronts in RD models has spawned a vast and diverse literature. In this section, I will attempt to summarize some of the features of fronts relevant to the results which will be presented in future chapters. Because I am mostly concerned with front roughening in this dissertation, I will not discuss problems related to depinning, nor will I discuss the very interesting subject of noise-induced fronts [34]. I will also not discuss the work that has been done on Fisher waves in random media [35–37], since these works have generally ignored discreteness effects. The focus will instead be on internal noise in Fisher waves and the features of fronts described by the KPZ equation.

Consider the RD model defined in the mean-field limit by (2.16). This equation is known as the Fisher/KPP equation, and it was first used to model the propagation of genes in a population [38]. For $y > z$, it admits a nontrivial $t \to \infty$ solution (at least in the mean-field limit): $\bar{n}(\boldsymbol{x}, t) = (y - z)/q$, where $q = b{\ell_0}^d$. If the initial condition is set so that one half of space—say, $x_d \leq 0$—is at the "carrying capacity" $(y - z)/q$ while the other half of space is empty, then clearly the time evolution of the system will consist of a front moving through space in the direction $\hat{x}_d$. In fact, the front will asymptotically reach a steady speed of $\sqrt{4D(y - z)}$ [39]—again, this is true for the mean-field limit. This front is known as a Fisher wave.

How does one include the effects of stochasticity in this equation? Rather than apply the field-theoretic machinery, it is simpler to just write down the

appropriate Langevin equation:

$$\frac{\partial \bar{n}(\boldsymbol{x},t)}{\partial t} = D\nabla^2 \bar{n}(\boldsymbol{x},t) + (y-z)\bar{n}(\boldsymbol{x},t) - q\bar{n}(\boldsymbol{x},t)^2 + \sqrt{\bar{n}(\boldsymbol{x},t)}\,\xi(\boldsymbol{x},t), \quad (2.19)$$

where the noise $\xi(\boldsymbol{x},t)$ is taken to be uncorrelated Gaussian noise. The source of this noise is essentially the discrete nature of the particles involved, and the fact that for a small number of particles the deviation from the mean behavior can be significant. This can also be modelled more directly by introducing a cutoff in the deterministic equation:

$$\frac{\partial \bar{n}(\boldsymbol{x},t)}{\partial t} = D\nabla^2 \bar{n}(\boldsymbol{x},t) + \left[(y-z)\bar{n}(\boldsymbol{x},t) - q\bar{n}(\boldsymbol{x},t)^2\right]\Theta(\bar{n}(\boldsymbol{x},t)-\epsilon), \quad (2.20)$$

where $\Theta(\cdot)$ is the Heaviside step function.

There are two features of the front that are of interest: the first is the front velocity, which is given in the mean-field limit by $\sqrt{4D(y-z)}$. How does this change when stochasticity is taken into account? By using a deterministic equation with a cutoff similar to (2.20), Brunet and Derrida [40] have been able to show that the front velocity converges to the mean-field limit from below like

$$v_f(\epsilon) \simeq v_f(0) - \frac{C}{\ln^2(\epsilon)}, \quad (2.21)$$

where C is some constant and $v_f(0)$ (in this case) is equal to $\sqrt{4D(y-z)}$.

The more interesting feature of the front is its roughness. In the mean-field limit, for any initial condition which depends only on x_d (the coordinate in the direction of front propagation), symmetry considerations require that the front be flat—that is, $\bar{n}(\boldsymbol{x},t)$ is just a function of x_d and t. However, the introduction of noise destroys that symmetry, and the front can roughen. The front can be defined by a height function $h(\boldsymbol{x}_\perp,t)$, where $\boldsymbol{x}_\perp$ is a position in the hyperplane perpendicular to $\hat{x}_d$ and $h(\boldsymbol{x}_\perp,t)$ is the largest value of x_d for which $\bar{n}(\boldsymbol{x},t)$ takes a given value for fixed $\boldsymbol{x}_\perp$. For the purposes of the following argument, assume that $h(\boldsymbol{x}_\perp,t)$ has had its average value subtracted: $h(\boldsymbol{x}_\perp,t) \to h(\boldsymbol{x}_\perp,t) - \left(\int d^{d-1}\boldsymbol{x}_\perp\, h(\boldsymbol{x}_\perp,t)\right)/L^{d-1}$, where L is the system size. In general, the roughness of the height function $h(\boldsymbol{x}_\perp,t)$ can be described using concepts of statistical self-similarity—that is, the front is self-affine. It is expected that, for some rescaling factor b, the statistics of the height function should be identical to those of some rescaled height function h' given by [41]

$$h'(\boldsymbol{x}_\perp,t) = b^{-\zeta} h(b\boldsymbol{x}_\perp, b^z t), \quad (2.22)$$

where ζ and z are two scaling exponents.

Consider the height difference correlation function $G(|\boldsymbol{x}_\perp - \boldsymbol{x}'_\perp|,t)$ $= \langle |h(\boldsymbol{x}_\perp,t) - h(\boldsymbol{x}'_\perp,t)| \rangle$. Using the scaling for for $h(\boldsymbol{x}_\perp,t)$ from above, one

arrives at the equation [41]

$$G(r,t) = b^{-\zeta} G(br, b^z t), \tag{2.23}$$

where $r = |\boldsymbol{x}_\perp - \boldsymbol{x}'_\perp|$. Without loss of generality, the scaling factor b can be set to $1/r$, leading to

$$G(r,t) = r^\zeta g\left(\frac{r}{t^{1/z}}\right), \tag{2.24}$$

where $g(\cdot)$ is some scaling function. Now clearly if the surface starts out flat, the height function at two distant points will not depend on r; thus, it is expected that, for large arguments, $g(x) \sim x^{-\zeta}$. On the other hand, for large times $G(r,t)$ should become time-independent, which implies that $g(x) \sim 1$ for small arguments. These considerations lead to an interpretation of the exponents z and ζ: since $G(r,t) \sim r^\zeta$ for large times, ζ describes the deviation of the front from flatness over a distance r, and is thus called the wandering exponent. To understand the significance of z, note that there is a characteristic time $t \sim r^z$ at which the function $g(x)$ begins to change from its small argument to its large argument form. This can be thought of as the time at which a point at r begins to "feel" the effects of some fluctuation that began at 0 at $t = 0$. Fluctuations therefore grow as $t^{1/z}$, and z is called the dynamic exponent [41]. It should be noted that these results are generally applicable to fluctuating fronts, not just to fronts in the Fisher/KPP equation.

Consider the case of a Fisher wave—or any other front exhibiting the self-similarity described above—propagating in a finite system of (perpendicular) size L. Clearly, the correlation function $G(r,t)$ will saturate after a time $t_{\text{sat}} \sim L^z$, and the front will not roughen any more. Family and Vicsek have used this observation to write down a scaling form for a surface roughness $w^2(L,t)$ [42]:

$$\sqrt{\langle w^2(L,t)\rangle} = \sqrt{\left\langle \frac{1}{L^{d-1}} \int d^{d-1}\boldsymbol{x}_\perp \left[h(\boldsymbol{x}_\perp, t) - \bar{h}(t)\right]^2 \right\rangle} = L^\zeta f\left(\frac{t}{L^z}\right), \tag{2.25}$$

where $\bar{h}(t)$ is given by $\bar{h}(t) = \left(\int d^{d-1}\boldsymbol{x}_\perp\, h(\boldsymbol{x}_\perp, t)\right)/L^{d-1}$ and the brackets denote averaging over realizations of the system (noise). The scaling function $f(\cdot)$ should be constant for large argument since the front roughness saturates; what about small arguments? For small t/L^z, the front does not "feel" the finite-size effects, and so the roughness should evolve independently of L. Thus, $f(x) \sim x^{\zeta/z}$ for small arguments [41]. For an infinite system, $\sqrt{\langle w^2(L,t)\rangle}$ will continue to grow like t^β ($\beta \equiv \zeta/z$) for all times.

2.3.2 The KPZ Equation

The stochastic Fisher/KPP equation belongs to the the KPZ universality class of front models [41, 43], and the height function is thus governed by the KPZ

equation [44]:

$$\frac{\partial h(\boldsymbol{x}_\perp, t)}{\partial t} = v + \sigma \nabla^2 h(\boldsymbol{x}_\perp, t) + \lambda \left[\nabla h(\boldsymbol{x}_\perp, t)\right]^2 + \zeta(\boldsymbol{x}_\perp, t), \tag{2.26}$$

where v is the mean front velocity (I have restored h to its original definition and added back the mean front position), σ is related to the surface tension, and $\zeta(\boldsymbol{x}_\perp, t)$ is a Gaussian noise term. The scaling exponents for the KPZ class are given in Table 2.1. The KPZ equation describes the roughness of a

Table 2.1: Table of KPZ exponents in $d = 2$ and $d = 3$, taken from Ref [12].

Exponent	$d = 2$	$d = 3$
$\beta \equiv \zeta/z$	1/3	.24
ζ	1/2	.38
z	3/2	1.58

front on mesoscopic length scales; that is, for a particular lattice model, it is sometimes necessary to average the height over many adjacent sites in order to recover KPZ-type scaling.

The roughness of the Fisher wavefront has not always been so well understood. Early simulations suggested that the exponents were not those of the KPZ class in d dimensions [45, 46], and Tripathy and coworkers conjectured that "pulled" fronts[4] like the one described by (2.19) cannot simply be described by writing down an effective interface theory like the KPZ equation. They in fact argued that taking into account the importance of the "empty" region ahead of the front—the region in which the field $\bar{n}(\boldsymbol{x}, t) \simeq 0$, in the present case—leads to the conclusion that the KPZ equation in $d + 1$ dimensions is appropriate for describing the dynamics of a d-dimensional front [47], and offered the closeness of the measured exponent values to those of the KPZ class in $d + 1$ dimensions as support for their argument. Blythe and Evans [48] and Moro [43], however, showed that by properly coarse-graining the front and taking into account the effects of the intrinsic width (see Section 3.1.3 for a discussion of the intrinsic width), one recovers the KPZ exponents in the expected number of dimensions.

2.4 Summary

In this chapter, I have endeavored to provide the information on reaction-diffusion models necessary to understand and place in context the main results of this dissertation. In Section 2.1, I offered an elementary introduction to the theory of stochastic processes, including a simple

[4] Pulled fronts are fronts in which the propagation speed matches the spreading speed of linear perturbations to the unstable phase. These fronts are thus "pulled along" by the growth in the unstable phase directly ahead of the front. For more, see Ref [39].

derivation of the all-important master equation. I then discussed the general approach to dealing with stochastic systems: figure out the mean-field limit, then either add noise or employ a field-theoretic method. In Section 2.2, I discussed the directed percolation (DP) active to absorbing state transition universality class, and the effects that quenched disorder has on this transition. Finally, in Section 2.3 I discussed Fisher waves, the scaling properties of fluctuating fronts, and the KPZ equation.

3 First Passage Percolation

First passage percolation (FPP) has been studied mostly in the mathematics community since being developed in the 1960s by Hammersley and Welsh [49], but its connections to the Eden model have earned it some attention from physicists [41]. I will be using many results from first passage percolation, and so it is necessary to provide some background on the origin of these results. In this chapter, I will provide this background. I will begin by introducing the classic FPP problem on a $d = 2$ lattice and will then present some of the well-known results for this problem. Next, I will discuss the connection between FPP and the Eden model for the case of exponentially distributed first passage times. Finally, I will discuss some off-lattice models of FPP and the Eden model that have been studied.

3.1 Lattice Models of First Passage Percolation

3.1.1 First Passage Percolation on a $d = 2$ Lattice

The canonical first passage percolation problem can be stated as follows: consider a 2D square lattice with links between each pair of adjacent sites. Unlike in regular percolation, all links are present in FPP. Now imagine that times are assigned to all the links, with each time picked from the same probability distribution function $f(t)$. This function is called the first passage time probability density function (FPT PDF), and will be referred to often in this chapter. Now for some pair of sites located at $\boldsymbol{a}$ and $\boldsymbol{b}$, there exists a path through the system which minimizes the passage time from $\boldsymbol{a} \to \boldsymbol{b}$ (or $\boldsymbol{b} \to \boldsymbol{a}$). I will denote this minimum passage time by $T(\boldsymbol{a}, \boldsymbol{b})$, in the spirit of Kesten [50], and I will call it the infection time.

There are a few important things to note before going any further. First, it should be obvious that the infection time will change from realization to realization as passage times between sites are re-picked. Second, the infection time will depend heavily on the FPT distribution $f(t)$. Finally, the mean first passage time $\langle T(\boldsymbol{a}, \boldsymbol{b})\rangle$ should depend only on $\boldsymbol{b} - \boldsymbol{a}$.

The first question I will address is the nature of the quantity $T(\boldsymbol{a}, \boldsymbol{b})/|\boldsymbol{b} - \boldsymbol{a}|$ as $|\boldsymbol{b} - \boldsymbol{a}| \to \infty$. For concreteness, I will take $\boldsymbol{a}$ to be the site at $(0, 0)$ (the origin) and $\boldsymbol{b}$ to be located at $(0, n)$—that is, $\boldsymbol{b}$ is on the y axis n sites away from the origin. I will call the infection time between these sites

$T(n)$; the quantity I am interested in is then $T(n)/n$. One of the most important results of first passage percolation theory is the following: as $n \to \infty$, $T(n)/n \to \mu$, where μ is called the *time constant* [50]. Note that μ as I have defined it is the time constant for two sites on the same axis—that is, two sites with the same x or y value. In general, the time constant depends on the direction $(\boldsymbol{b} - \boldsymbol{a})/|\boldsymbol{b} - \boldsymbol{a}|$ [51]. The value of μ obviously depends on the FPT PDF $f(t)$. For the case where $f(t)$ is an exponential distribution with mean T_1, for instance, simulations indicate that $\mu \simeq .4T_1$ [52]. Unfortunately, it is not clear how to predict the time constant theoretically for an arbitrary $f(t)$ [50]; nonetheless, there are some useful theorems about how the time constant depends on some general properties of $f(t)$, two of which I will quote here. The proofs for these theorems can be found in the cited references; I will not attempt to replicate them here since they are rather lengthy and not really needed for my purposes.

The first of these theorems provides a useful link between FPP and regular percolation:

$$\text{if } F(0) \equiv \lim_{\epsilon \to 0} \int_0^\epsilon dt\, f(t) \geq p_c, \text{ then } \mu = 0, \tag{3.1}$$

where $p_c = 1/2$ is the percolation threshold for $d = 2$ bond percolation on a square lattice [50]. In other words: if the probability of crossing a link with no time elapsing is great enough for there to be a system-spanning cluster of sites connected by such links, then any site can be reached from any other site in a time that scales sublinearly with n, and $T(n)/n \to 0$.

The second theorem concerns the bounds on μ [50]:

$$0 \leq \mu \leq T_1 = \int_0^\infty dt\, t f(t). \tag{3.2}$$

This upper limit is essentially the statement that the average value of the minimum of some set of paths is less than or equal to the minimum value of the set of average paths—that is, the paths resulting from replacing the time on each link by its average value T_1. It is important to note that, at least for the case of an exponential distribution, the time constant is not *that* much less than the upper limit: as mentioned before, μ is known to be $\simeq .4T_1$ when $f(t) = re^{-rt}$. This suggests that the "mean-field" view—replacing each link by its average value—is not too bad in this case, and only misses the time constant by a factor of $\simeq 2$. To put it another way: the infection time along the shortest path from $\boldsymbol{a}$ to $\boldsymbol{b}$ is, on average, not terribly different from the infection time along a straight line joining the two points for the case of an exponential FPT PDF.

In addition to the theorems about the time constant just discussed, there is one additional theorem and one conjecture which will be useful later on, and which I will thus introduce here. The theorem concerns the rate of

convergence of the mean infection time [53]:

$$0 \leq \langle T(n) \rangle - n\mu \leq \mathcal{O}(n^{1/2} \log(n)). \tag{3.3}$$

The mean infection time $\langle T(n) \rangle$ can thus be written as

$$\langle T(n) \rangle = n \left[\mu + \mathcal{O}\left(\log(n)/n^{1/2} \right) \right]. \tag{3.4}$$

The conjecture concerns the variance of the infection time, ${\sigma_T}^2(n)$, when $f(t)$ is the exponential distribution. As $n \to \infty$, it is believed that [54]

$${\sigma_T}^2(n) \equiv \langle T^2(n) \rangle - \langle T(n) \rangle^2 \propto n^{2/3}. \tag{3.5}$$

This is conjectured on the basis of first passage percolation's connection to the Eden model, which I will discuss in the next section.

3.1.2 First Passage Percolation and the Eden Model

First passage percolation can be regarded as an optimization problem: given a distribution from which times are picked, what is the shortest time path between two points? However, it is also possible to think of it as a dynamic process; in fact, FPP was originally formulated as a model for fluid flow in porous media [49]. Imagine that, at $t = 0$, all sites are colored red save the origin, which is blue. Now do the following: take the link from the origin with the smallest first passage time t_1^{min} and color the site that it connects to the origin blue. Repeat this process, at each step finding the site with the lowest infection time that has not yet been hit and coloring it blue. At a given time t, the set of blue sites is the set of sites with infection times lower than t. There are, in fact, numerous theorems having to do with the nature of this set [50], but I will not touch on any of these here.

It is natural to wonder whether anything can be said about the probability distribution of occupied (blue) sites—specifically, given that a set of sites is blue at time t, what is the probability that the next site to be occupied will be some site k, and what is the distribution of times to occupy the next site? The system can be described at time t by a set of occupation numbers $\{n\}$, with $n_i = 0$ if site i has not been hit yet and $n_i = 1$ if it has been hit. The time τ_{ne} to the next event (site infection) is given by:

$$\tau_{\text{ne}} = \min\{\tau_{ij} + t_i\} - t \tag{3.6}$$

where i runs over all occupied sites, t_i is the time at which the i-th site was infected, j runs over all unoccupied neighbors of i, and τ_{ij} is the FPT between sites i and j.

To answer the questions posed above, it is necessary to find the probability distribution function $p_{\text{ne}}(\tau_{\text{ne}})$ for the time τ_{ne} to the next event. To do this,

one starts by writing down the probability $\Theta(\tau_{\rm ne})$ that the next event has *not* occurred after a time $\tau_{\rm ne}$; this is simply the product of the probabilities that none of the possible link crossings $i \to j$ have occurred:

$$\Theta(\tau_{\rm ne}) = \prod_i \prod_{j \natural i} P_{\rm no}(t + \tau_{\rm ne} | !(t - t_i)). \tag{3.7}$$

The notation needs some explanation: $P_{\rm no}(t + \tau_{\rm ne}|!(t - t_i))$ is the probability that the link between i and one of its neighbors has not been crossed by time $t + \tau_{\rm ne}$ given that it had not been crossed by the time $t - t_i$ had passed after the site i was hit at time t_i; $j \natural i$ means "j is an unoccupied neighbor of i." Again, the product over i is only over occupied sites. Using Bayes' theorem, it is possible to write the function on the RHS of (3.7) in terms of marginal probabilities:

$$P_{\rm no}(t + \tau_{\rm ne}|!(t - t_i))\,[1 - F(t - t_i)] = P_{\rm no}(!(t - t_i)|t + \tau_{\rm ne})\,[1 - F(t + \tau_{\rm ne} - t_i)]\,, \tag{3.8}$$

where $F(t) \equiv \int_0^t dt'\, f(t')$ is the cumulative distribution function. The quantity $P_{\rm no}(!(t - t_i)|t + \tau_{\rm ne})$ is the probability that a link from i to a neighbor has not been crossed a time $t - t_i$ after site i was hit given that is has not been crossed at time $t + \tau_{\rm ne}$; this is clearly 1. Thus, the conditional probability $P_{\rm no}(t + \tau_{\rm ne}|!(t - t_i))$ can be written solely in terms of marginal probabilities:

$$P_{\rm no}(t + \tau_{\rm ne}|!(t - t_i)) = \frac{1 - F(t + \tau_{\rm ne} - t_i)}{1 - F(t - t_i)}. \tag{3.9}$$

Therefore,

$$\Theta(\tau_{\rm ne}) = \prod_i \prod_{j \natural i} \frac{1 - F(t + \tau_{\rm ne} - t_i)}{1 - F(t - t_i)}; \tag{3.10}$$

by definition, $p_{\rm ne}(\tau_{\rm ne}) = -\partial_{\tau_{\rm ne}} \Theta(\tau_{\rm ne})$.

It should be clear that, in general, (3.10) depends on the set of infection times t_i of the sites that are infected at time t. Thus, just knowing which sites are blue at time t is not sufficient to determine the future behavior of the system. But consider the case where $f(t) = re^{-rt}$—that is, the case of an exponential FPT PDF. The cumulative distribution function $F(t) = 1 - e^{-rt}$ for this case, and so

$$\Theta(\tau_{\rm ne}) = \prod_i \prod_{j \natural i} \frac{e^{-r(t + \tau_{\rm ne} - t_i)}}{e^{-r(t - t_i)}} = \prod_i \prod_{j \natural i} e^{-r\tau_{\rm ne}} = e^{-N_l r \tau_{\rm ne}}, \tag{3.11}$$

where N_l is the number of links connecting occupied to unoccupied sites at time t. Thus, for the case of an exponential FPT distribution, FPP is memoryless—all necessary information about the system is encoded in its current state. This should not be entirely surprising: in Chapter 2, I discussed briefly the theory of Markov processes and master equations, and touched on

the fact that the exponential distribution is the appropriate distribution for the microscopic description of Markov processes.

What about the probability $P_{\text{next}}(k)$ for a given uninfected site k to be the next site infected? Since each link is equally likely to be crossed according to (3.11), this is simply

$$P_{\text{next}}(k) = \frac{\sum_{i \in \text{n.n.}} n_i}{N_l}; \tag{3.12}$$

that is, $P_{\text{next}}(k)$ is simply the number of bonds connecting k to infected sites divided by N_l.

Together, these expressions for $p_{\text{ne}}(\tau_{\text{ne}})$ and $P_{\text{next}}(k)$ completely define the dynamics of FPP for the case where $f(t)$ is an exponential distribution. They also define the dynamics of one version of the Eden model, which was developed by Eden [55] as a model for biological morphogenesis. The version of the Eden model in question consists of a 2D lattice with sites connected by bonds; at each step of the process, a bond between an occupied and unoccupied site is chosen at random, the unoccupied site is infected, and time is advanced by a time chosen from $f(\tau) = N_l r e^{-N_l r \tau}$, where r is the rate for link crossing and N_l is the number of links connecting occupied to unoccupied sites. The reader should note that the Eden model is simply the contact process described in Chapter 2 with the death rate set to 0.

This version of the Eden model—the "type B" Eden model [41]—and the FPP problem are clearly thought of in different ways: for FPP, one usually imagines the times on the links being chosen to start things off, and the lattice then being infected as the time t passes the infection time of each lattice point; the Eden model, in contrast, is thought of as a stochastic process, with times picked for each link crossing each time a new site is hit. Whichever view one wishes to take, however, the two models are precisely the same for the case of an exponential FPT distribution. This is useful, as it is sometimes easier to picture the process as an optimization procedure and sometimes easier to picture it as a dynamic process. Perhaps more importantly, the correspondence immediately allows for some predictions to be made for FPP based on known features of the Eden model.

One such feature of particular interest is the nature of fronts in the model. Imagine that all lattice sites with $y \leq 0$ are initially infected—clearly, there will be a front that moves in the $+y$ direction with velocity $\sim 1/r$. As is usually the case with front problems, the first non-trivial question asked concerns the roughness of this front. For the $d = 2$ Eden model, the roughness of a front in a system infinite in the y-direction (direction of front travel) but finite in the x-direction is given by

$$w^2(\Lambda, t) = \frac{1}{\Lambda} \sum_{i=1}^{\Lambda} \left(h_i - \bar{h}\right)^2, \tag{3.13}$$

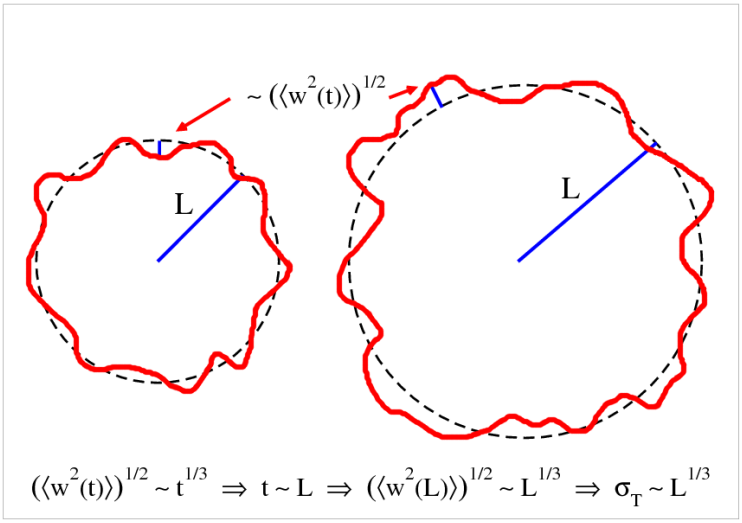

Figure 3.1: Plot showing a circular front in the Eden model at two different times. Since the typical width of the front goes as $t^{1/3}$ and the front travels at a constant average velocity, the width of a front passing through a circle of radius L goes as $L^{1/3}$; this should translate to a spread of infection times that also goes as $L^{1/3}$.

where Λ is the system size in the x-direction, h_i is the largest value of y for all infected sites with $x = i$, and $\bar{h} = \left(\sum_{i=1}^{\Lambda} h_i\right)/\Lambda$. Clearly the roughness $w^2(\Lambda, t)$ will be different for each realization of the system; the quantity of interest is therefore the roughness averaged over realizations, $\langle w^2(\Lambda, t)\rangle$.

The Eden model happens to be in the KPZ universality class [41, 44] discussed in Chapter 2, at least for $d = 2$ (there is some confusion about $d = 3$): the average roughness can be described by the scaling form

$$\sqrt{\langle w^2(\Lambda, t)\rangle} = \Lambda^{\zeta} f\left(t/\Lambda^{z}\right), \tag{3.14}$$

with $\zeta = 1/2$ and $z = 3/2$ in $d = 2$ and $f(\cdot)$ a scaling function. As discussed in Chapter 2, $f(x)$ has the small-argument behavior $f(x) \sim x^{\zeta/z}$, so that $\sqrt{\langle w^2(\Lambda, t)\rangle} \sim t^{\beta}$ ($\beta \equiv \zeta/z$) for small times. As $\Lambda \to \infty$, $\sqrt{\langle w^2(\Lambda, t)\rangle} \sim t^{\beta}$ for all times; the front roughness never saturates.

This result for the roughness can be used to make a prediction for the variance of the infection time ${\sigma_T}^2(L)$ in FPP, as can be seen from the following argument, adopted and slightly modified from one due to Krug and Spohn [41]. Consider a *circular* front moving through the system; this is the front that would result from a single site being infected at $t = 0$ rather than the entire half-space with $y \leq 0$. Now imagine a circular surface placed at a distance L from the origin (the underlying lattice structure is not really important to the argument, so the reader should not worry too much about the difficulties inherent in embedding a circle on a lattice). For large L, the set of infection times to the lattice points in the circle should be a good sample of

the infection time distribution, and so it should be possible to estimate ${\sigma_T}^2(L)$ by considering the spread of times at which the front crosses the circle. As Figure 3.1 should make clear, this is related to the the spatial spread of the front: as t increases, the width of the front increases as $t^{1/3}$; since the average time to reach the circle at L scales with L, the width of the front passing through the circle scales as $L^{1/3}$. Thus, the width of the distribution of infection times to points on the circle at L should scale like [41, 54]

$$\sigma_T(L) \sim L^{1/3}, \tag{3.15}$$

which is identical to the conjecture given in (3.5).[1]

3.1.3 Simulating the Eden Model

There are a number of subtle features of the Eden model that I have not mentioned, some of which have proved to be a hindrance to researchers attempting to simulate the model. Perhaps the most important of these features is the presence of an "intrinsic width" in the Eden model. The intrinsic width is a system-size-independent contribution to the width $\sqrt{\langle w^2(\Lambda,t)\rangle}$ coming from large steps (adjacent columns with very different heights), overhangs (columns with occupied sites higher than unoccupied sites), and holes (unoccupied sites surrounded by occupied sites)—that is, it is the contribution to the front width coming from "short-wavelength" fluctuations [56, 58]. For large system sizes, the intrinsic width is not very important, but it can wreak havoc on the analysis of simulation data from smaller system sizes.

It is possible to include the effects of the intrinsic width on the evolution of the front roughness by adding a term to (3.14) [58]:

$$\langle w^2(\Lambda,t)\rangle = \Lambda^{2\zeta}\left[f\left(t/L^z\right)\right]^2 + {w_i}^2(t), \tag{3.16}$$

where ${w_i}^2(t)$ is the intrinsic width. The intrinsic width saturates (reaches its $t \to \infty$ value) faster than the "long-wavelength"-related roughness, especially for larger system sizes. The new scaling equation (3.16) makes it easy to see what effect the intrinsic width has on the measured value of β: imagine doing a set of simulations and naïvely calculating $\beta \equiv \zeta/z$ from (3.14) via $\beta = d\log\sqrt{\langle w^2\rangle}/d\log t$. Assuming that the time is large enough for the very early ($\sqrt{\langle w^2\rangle} \sim t^{1/2}$) behavior to be done with and for the intrinsic width to have saturated, but still small enough that t/Λ^z is small and the first term in

[1] I have not told the whole story here: for the circular (or nearly circular) front resulting from growth from a single site on a 2D square lattice, the *very* long-time behavior of the roughness is actually proportional to L—$\sqrt{\langle w^2(t)\rangle} \sim L$—due to lattice anisotropy effects [56, 57]. However, since I will eventually apply the result for $\sigma_T(L)$ to an off-lattice system, I have ignored some of the subtleties associated with the underlying lattice structure. The argument given in Ref. [41] that relates the fluctuations in the front to $\sigma_T(L)$ on which I have based my argument is free of these lattice-related subtleties, but is not as transparent.

(3.16) is not too large compared to the second, the measured value of β will be approximately

$$\beta \simeq \frac{\zeta}{z} \frac{a^2 t^{2\zeta/z}}{a^2 t^{2\zeta/z} + {w_i}^2(\infty)}, \tag{3.17}$$

where a is a constant related to the saturated value of the width and ${w_i}^2(\infty)$ is the saturated value of the intrinsic width. Since the saturated value of the width—and thus the constant a—grows larger with increasing Λ, it should be clear that the measured value of β will be closer to the actual value ζ/z for larger system sizes.

In order to eliminate the effects of the intrinsic width, Kertész and Wolf developed the noise-reduction algorithm. The noise-reduction algorithm modifies the original Eden model in the following way: when a site is selected to be infected for the first time, this fact is recorded, but the site is not actually set to infected until m such events have occurred [58]. This makes it difficult for large fluctuations to occur on a small scale, but still allows for a long-wavelength roughness to develop. By using the noise-reduction algorithm, it was possible for researchers to minimize the effects of the intrinsic width without going to unreasonably large system sizes. This allowed for accurate measurements of the exponents ζ and z in $d = 2$ [59], measurements which confirmed that the Eden model is in the KPZ universality class in this dimension.

3.2 Off-Lattice Models of First Passage Percolation and the Eden Model

Off-lattice models of first passage percolation have not been nearly as well-studied as their lattice counterparts, despite the fact that they have some nice properties that lattice models typically lack. The most significant study of an off-lattice FPP model is due to Howard and Newman, who have considered a model called Euclidean FPP [51, 60, 61]. In Euclidean FPP, points are randomly placed with unit number density in a space of dimension d. Between each pair of points located at $\boldsymbol{r}_1$ and $\boldsymbol{r}_2$, a time τ is assigned according to

$$\tau(\boldsymbol{r}_1, \boldsymbol{r}_2) = |\boldsymbol{r}_1 - \boldsymbol{r}_2|^{\alpha}, \tag{3.18}$$

with α typically taken as being > 1. Between a given pair of points—one located at the origin, say, and the other at $\boldsymbol{L}$—there exists a path which minimizes the total time $T_\alpha(\boldsymbol{0}, \boldsymbol{L})$ (for $\alpha \leq 1$, this path is simply the single jump from the origin to $\boldsymbol{L}$).

The quantities of interest in Euclidean FPP are very similar to those in lattice FPP. One of the most important of these is the time constant μ,

defined as

$$\mu = \lim_{|\boldsymbol{L}|\to\infty} \frac{T_\alpha(\mathbf{0}, \boldsymbol{L})}{|\boldsymbol{L}|}. \tag{3.19}$$

Note that, unlike lattice FPP, the time constant in Euclidean FPP does not depend on direction; this is one of the aforementioned nice properties of Euclidean FPP that lattice FPP lacks. For $\alpha \leq 1$, $\mu = 0$ [60].

There have also been a few studies done of off-lattice Eden models. Wang and co-workers [62, 63] have devised an off-lattice Eden model in which balls of radius 1/2 randomly produce neighbors; when a ball has enough neighbors that another cannot possibly fit without overlapping, it is declared dead. At each time step, a "living" ball is selected at random to produce a neighbor. Somewhat unsurprisingly, the researchers recovered the KPZ exponents in $d = 2$; however, for $d = 3$ they found a different value of β for growth from a single ball (circular front) than they did for growth from a plane of balls (flat front) [63]. This further muddies the question of whether the Eden model in $d = 3$ is still in the KPZ universality class.

3.3 Summary

In this chapter, I have discussed a number of topics related to first passage percolation (FPP). I began in Section 3.1.1 by discussing the classic FPP problem on a lattice in $d = 2$, and quoted many of the most important theorems and conjectures, most of which will be used later on. In Section 3.1.2, I showed explicitly that FPP with an exponential distribution describes the same system as the type-B Eden model, and then described some of the known features of the Eden model. Section 3.1.3 was devoted to a discussion of one of the subtleties of the Eden model—the presence of an intrinsic width in the front—and how this has affected simulation results. Finally, Section 3.2 contained a discussion of the most prominent off-lattice FPP model, Euclidean FPP, and the most prominent off-lattice Eden model.

This chapter has by no means been an exhaustive review of first passage percolation problems; rather, the intent has been to introduce those concepts and results which will be needed later on, either as essential building blocks in the construction of analytic predictions or as useful guides in the interpretation of simulation results.

4 Transport in a Hostile Environment: Analytics

In this chapter, I will examine a particular reaction-diffusion model with inhomogeneity in the reaction rates. This model, which is an extension of a model previously studied by David Nelson and collaborators [4, 5], has some interesting properties which can be understood through an analogy with the theory of hopping conduction in doped semiconductors as developed by Ambegaokar and others in the 1970s [64, 65]. The theory of first passage percolation, which was introduced in Chapter 3, is also a useful tool for exploring this model, and allows for some predictions to made about the nature of fronts in the model.

As noted in Chapter 2, the issue of quenched disorder effects on absorbing state phase transitions in RD systems is a subtle one which is not as of yet completely understood. In this chapter, I will not examine the active to absorbing state phase transition, but rather the nature of transport under a particular set of assumptions about the relevant reaction rates and initial conditions in the model. In Chapter 6, I will relax some of the assumptions and explore the active to absorbing state phase transition in a related model.[1]

4.1 The Model: Oases and Deserts

Consider a reaction-diffusion model with a mean-field limit defined by the generalized Fisher/KPP equation

$$\frac{\partial \bar{c}(\boldsymbol{x},t)}{\partial t} = D\nabla^2 \bar{c}(\boldsymbol{x},t) - \boldsymbol{v}\cdot\nabla\bar{c}(\boldsymbol{x},t) + U(\boldsymbol{x})\bar{c}(\boldsymbol{x},t) - q\bar{c}(\boldsymbol{x},t)^2, \tag{4.1}$$

where $\bar{c}(\boldsymbol{x},t)$ represents the population density, D is the diffusion constant, $\boldsymbol{v}$ is a spatially uniform convection velocity (representing the flow of some liquid in which the particles exist), $U(\boldsymbol{x})$ is a spatially inhomogeneous growth term fixed in time, and $q = b{\ell_0}^d$ is a competition term (b is a competition rate and ℓ_0 is the microscopic length scale at which two particles will compete with one another). One of the simplest cases to consider is when $U(\boldsymbol{x}) = -z$ everywhere except a small patch near the origin, where $U(\boldsymbol{x}) = y$. The region of positive growth rate near the origin is called an "oasis," while the rest of space is

[1] Some of the material in this chapter has appeared before, in slightly altered form, in the following publications: A.R. Missel and K.A. Dahmen, Phys. Rev. Lett. **100**, 058301 (2008), Copyright 2008 by the American Physical Society; and A.R. Missel and K.A. Dahmen, submitted to Phys. Rev. E (2008), Copyright 2008 by the American Physical Society.

termed the "desert." This model was previously studied by Nelson and coworkers [4, 5], and a microscopic model (the contact process with disorder) with this mean-field limit was studied by Joo and Lebowitz [66]. Both sets of researchers found a transition in the $\langle U(\boldsymbol{x})\rangle$-$|\boldsymbol{v}|$ plane between extinct, localized, and delocalized phases in finite systems with periodic boundary conditions: for high average growth rate and high convection velocity, they observed a delocalized phase; for low average growth rate and high convection velocity they found that the population became extinct; and for low average growth rate and low convection velocity they found a localized phase. These predictions were tested in a laboratory setting using bacteria protected from harmful UV light (the "desert") by a mask (the "oasis"); the experiments largely confirmed the theoretical predictions summarized above [67].

In this chapter, I will study the nature of transport in a system consisting of many identical oases distributed randomly at low density in a desert. I will term this low oasis density regime "hostile"; the opposite case in which oases fill up most of space can be called "fertile." Because transport between oases in such a system involves the movement of a low population density, fluctuations about the mean-field theory (discreteness effects) will be important. I will thus be examining a particular stochastic process with a mean-field limit given by (4.1). This process is easiest to introduce on a $d = 1$ lattice; the generalization to higher dimensions is trivial. Identical particles (labeled A) occupy lattice sites without occupation number limits and are allowed to undergo the following processes: hopping to either side with rate $w/2$ (total hopping rate of w); death ($A \to 0$) with rate z if in the desert; reproduction ($A \to 2A$) with rate y if on an oasis; and competition/coagulation ($2A \to A$) with rate b everywhere. This process is governed by a master equation for the joint probability $P(\{c\}, t)$ to have occupation numbers $\{c\} \equiv \{\ldots, c_{\nu-1}, c_\nu, c_{\nu+1} \ldots\}$ on the lattice points ν at time t:

$$\begin{aligned}
\frac{\partial P(\{c\},t)}{\partial t} &= \frac{w}{2}\Big(\sum_\nu (c_{\nu-1}+1)P(\ldots, c_{\nu-1}+1, c_\nu - 1, \ldots, t) \\
&\qquad + (c_{\nu+1}+1)P(\ldots, c_\nu - 1, c_{\nu+1}+1, \ldots, t) - 2c_\nu P(\{c\},t)\Big) \\
&+ \sum_\nu z_\nu \left[(c_\nu+1)P(\ldots, c_\nu+1, \ldots, t) - c_\nu P(\{c\},t)\right] \\
&+ \sum_\nu y_\nu \left[(c_\nu-1)P(\ldots, c_\nu-1, \ldots, t) - c_\nu P(\{c\},t)\right] \\
&+ b\sum_\nu (c_\nu+1)c_\nu P(\ldots, c_\nu+1, \ldots, t) - c_\nu(c_\nu-1)P(\{c\},t).
\end{aligned} \tag{4.2}$$

Here $z_\nu = 0$ on the oases and z in the desert, and $y_\nu = 0$ in the desert and y on the oases.

This chapter is organized as follows: in Section 4.2, I will examine the nature of growth near a single oasis. Because the mean-field equation for the steady-state population density is exactly solvable in one dimension, one can

identify a length scale describing the distance away from the oasis at which fluctuations about the mean-field theory become important. I will also briefly discuss in this section the problem of extinction. In Section 4.3, I will look at transport between two oases. By using the fact that the $2A \to A$ competition process is unimportant far away from an oasis where the population is low, I will be able to devise a simpler model which captures the transport characteristics of the full model for large oasis separation. In Section 4.4, I will finally tackle the problem of transport in a system with many oases. By employing an analogy with the problem of hopping conduction in doped semiconductors, I will be able to estimate the time taken for a population to cross a large system. Using the theory of first passage percolation, I will analyze the nature of the coarse-grained front that moves through the system. Finally, I will offer a summary of results in Section 4.6.

4.2 Growth Near One Oasis

4.2.1 Mean-Field Description

I begin with a study of the nature of population growth near a single oasis in mean-field theory, starting with a 1D lattice with a single oasis of width $2a+1$ lattice points centered at the origin. The first step is to multiply $P(\{c\},t)$ by c_ν in Eq. (4.2) and sum over configurations to obtain an equation for the time evolution of the average particle concentration $\langle c_\nu \rangle(t)$:

$$\begin{aligned} \frac{\partial \langle c_\nu \rangle(t)}{\partial t} &= \frac{w}{2}\left[\langle c_{\nu+1}\rangle(t) + \langle c_{\nu-1}\rangle(t) - 2\langle c_\nu\rangle(t)\right] \\ &+ \left[y_\nu - z_\nu\right]\langle c_\nu\rangle(t) - b\langle c_\nu(c_\nu-1)\rangle(t). \end{aligned} \tag{4.3}$$

In order to obtain a "mean-field" description of the system, the term $\langle c_\nu(c_\nu-1)\rangle$ is replaced with $\langle c_\nu\rangle^2$. This replacement should work well when the population is large—i.e., near the oasis—since one would expect the relative fluctuations in particle number to be smaller in this case. (There are, of course, more formal ways of deriving the mean-field equation from the master equation. See, for instance, Ref. [10].) With this replacement, one can write a mean-field equation for $\bar{c}(\nu,t) \equiv \langle c_\nu\rangle(t)$:

$$\begin{aligned} \frac{\partial \bar{c}(\nu,t)}{\partial t} &= \frac{w}{2}\left[\bar{c}(\nu+1,t) + \bar{c}(\nu-1,t) - 2\bar{c}(\nu,t)\right] \\ &+ \left[y(\nu) - z(\nu)\right]\bar{c}(\nu,t) - b\bar{c}(\nu,t)^2. \end{aligned} \tag{4.4}$$

It is easier to consider the continuum version of this equation, which is obtained by introducing a lattice spacing ℓ_0 and redefining $\bar{c}(\nu,t) \to \bar{c}(\nu,t)\ell_0$, $b \to q/\ell_0$, and $\nu \to x/\ell_0$. The diffusion constant D is defined as $w{\ell_0}^2/2$. This leads to the $d=1$ version of (4.1), with $U(x) = (y+z)\Theta(a-|x|) - z$, where $\Theta(\cdot)$ is the Heaviside step function. The length scale ℓ_0 can be interpreted in

the continuum as the distance within which particles compete with one another.

There are two questions of particular interest: first, what does the mean-field concentration $\bar{c}(x,t)$ look like as $t \to \infty$? Second, what is the time scale on which a small population grows into a substantial population? Solving analytically for $\bar{c}(x,t)$ for all times is not feasible, but it is possible to solve for the steady-state $t \to \infty$ solution $\bar{c}(x, t=\infty) \equiv \bar{c}_{ss}(x)$ and thus answer the first question (see Appendix A for derivation). This function is given by

$$\bar{c}_{ss}(x) = \bar{c}_{ss}(0) - m_+ \,\mathrm{sn}^2\left(\sqrt{\frac{q|m_-|}{6D}}\,|x|,\, \imath\sqrt{\frac{m_+}{|m_-|}}\right) \quad |x| < a$$

$$\bar{c}_{ss}(x) = \frac{3z}{2q}\mathrm{csch}^2\left(\frac{\kappa}{2}(|x|-a) + C\right) \quad |x| > a, \tag{4.5}$$

where $\mathrm{sn}(u,k)$ is a Jacobi elliptic function, $\kappa \equiv \sqrt{z/D}$, $\bar{c}_{ss}(0)$ is the steady-state population at the origin, $C = \mathrm{csch}^{-1}(\sqrt{2q\bar{c}_{ss}(a)/3z})$ ($\bar{c}_{ss}(a)$ is the steady-state population at the edge of the oasis), and $m_{+,-}$ are defined as

$$m_{+,-} \equiv \frac{1}{2}\left[3\bar{c}_{ss}(0) - 3y/2q \pm \sqrt{(3y/2q - \bar{c}_{ss}(0))\,(3y/2q + 3\bar{c}_{ss}(0))}\right].$$

The constants $\bar{c}_{ss}(0)$ and $\bar{c}_{ss}(a)$ can be found by matching the solutions and their derivatives at $|x| = a$. This leads to a transcendental equation for $\bar{c}_{ss}(0)$:

$$\bar{c}_{ss}(0) = \frac{m_+ \,\mathrm{sn}^2\left(\sqrt{\frac{q|m_-|}{6D}}\,a,\, \imath\sqrt{\frac{m_+}{|m_-|}}\right)}{\left[1 - \sqrt{\frac{3y-2q\bar{c}_{ss}(0)}{3(y+z)}}\right]}. \tag{4.6}$$

Numerically, I have found that an excellent approximation to $\bar{c}_{ss}(0)$ is $\bar{c}_{ss}(0) \simeq (y - y_c)/q$, where y_c is the minimum growth rate at which the population does not die off as $t \to \infty$ when $q = 0$. This cutoff can be found by solving (4.1) with $q = 0$ (see Appendix A), which leads to the following transcendental equation for y_c:

$$y_c = z\cot^2\left(\sqrt{\frac{y_c}{D}}\,a\right). \tag{4.7}$$

At large distances from the oasis ($|x| \gg a$), $\bar{c}_{ss}(x) \simeq \bar{c}_\infty e^{-\kappa|x|}$, where $\bar{c}_\infty = 4\gamma^2\bar{c}_{ss}(a)e^{\kappa a}$ ($\gamma^{-1} = 1 + \mathrm{csch}(C)$). In the limit of high growth rate—$y \to \infty$ with all other rates fixed—$\bar{c}_{ss}(a) \to \infty$ and $\bar{c}_\infty \to 6ze^{\kappa a}/q$. For smaller values of y, $\bar{c}_{ss}(a)$—and thus $\bar{c}_\infty$—can be found by first solving for $\bar{c}_{ss}(0)$ using (4.6) and then using the relation (see Appendix A for derivation) $\bar{c}_{ss}(a) = \bar{c}_{ss}(0)\sqrt{\frac{3y-2q\bar{c}_{ss}(0)}{3(y+z)}}$.

In higher dimensions, one needs to consider a hyperspherical oasis of radius a. It is not possible to solve exactly the $t \to \infty$ nonlinear mean-field equation for $d > 1$, but it is easy to ascertain the asymptotic behavior of $\bar{c}_{ss}(\boldsymbol{x})$ far

away from the oasis. To do so, the nonlinear term is dropped from the mean-field equation (4.1) under the assumption that $\bar{c}_{ss}(\boldsymbol{x})$ is small far from the oasis. This leads to the linear equation

$$0 = D\nabla^2\bar{c}_{ss}(\boldsymbol{x}) - z\bar{c}_{ss}(\boldsymbol{x}), \tag{4.8}$$

which is valid far away from the oasis. In two dimensions, this is solved by $\bar{c}_{ss}(\boldsymbol{x}) \simeq \bar{c}_\infty K_0(\kappa r)$, where $r = |\boldsymbol{x}|$ and K_0 is a modified Bessel function of the first kind. In three dimensions, $\bar{c}_{ss}(\boldsymbol{x}) \simeq \bar{c}_\infty e^{-\kappa r}/\kappa r$. Because finding an exact solution for the entire space (including $r < a$) is no longer possible for $d = 2$ or 3, it is not possible to write down an analytic expression for the prefactors $\bar{c}_\infty$ in front of these asymptotic functional forms.

The question of the time scale on which a small population grows into a substantial population has been addressed by Nelson and coworkers [4, 5]. They analyzed the eigenvalue spectrum of the linearized ($q = 0$) version of (4.1) and found that the largest eigenvalue Γ_0 is given by [5]

$$\Gamma_0 = (y+z)f\left(\sqrt{D/a^2(y+z)}\right) - z, \tag{4.9}$$

where $f(x)$ is a monotonically decreasing function of x which goes as $1 - \pi^2x^2/4$ for $x \ll 1$ and $1/x^2$ for $x \gg 1$ In the limit of large y, then, $\Gamma_0 \simeq y$, and the time scale on which a small population grows up is $\sim 1/y$. Thus, for large y the population reaches a sizable level rather quickly.

4.2.2 Fluctuations and Extinction

It has been known for some time that fluctuations can drive a system to extinction even when mean-field theory predicts a stable active state. In fact, this phenomenon was discussed in Chapter 2 for RD systems with homogeneous reaction rates: in the case of a continuous homogeneous system with the same reactions as the system being studied—$A \to 2A$ with rate y, $A \to 0$ with rate z, and $2A \to A$ with rate b—there is an active phase only when $z - y < r_c$, where r_c depends on dimension but is less than zero for $d = 1, 2, 3$ [17]. Mean-field theory, on the other hand, predicts an active phase for $y > z$; fluctuations drive the critical growth rate up. The disparity between mean-field and stochastic behavior is even greater in the case of a $d = 0$ system: mean-field theory predicts a $t \to \infty$ steady state which is reached for any nonzero initial condition, but solving the master equation leads to the conclusion that, for any $z > 0$, the population will eventually become extinct [10]. The mean extinction time in this case can be calculated exactly as a function of y, z, b, and the starting population n_0, although the resulting expression is cumbersome to work with [10].

For the case of a single oasis in an infinite desert, it seems clear that the population will become extinct as $t \to \infty$ for $d = 1, 2, 3$: the finite oasis cannot

compete with the infinite desert, regardless of how high the growth rate y is. For the problem I will be considering, it is important that the oases not die out too early, and thus it is necessary to know the dependence of the mean extinction time on the various parameters of the problem. The field-theoretic tools used to analyze systems with translational invariance are hard to apply to this case, as are the various methods (see Ref. [68] for one such method) used to analyze $d = 0$ systems. Nonetheless, one can try to place a lower limit on the extinction time. To do so, I will return to the lattice case in one dimension; the results will be applicable to the continuum case and to other dimensions.

Consider the case of a perfectly deadly desert, $z \to \infty$. This effectively turns the system into a finite system with $2a + 1$ lattice points and absorbing boundaries. The "effective" death rate is of the order of w, the hopping rate. Now consider a $d = 0$ system with the same birth and competition rates which has a death rate of w, the hopping rate in the original system. The $d = 1$ system will certainly live longer than this system, on average: the number of events needed to extinguish the population completely is much larger. As mentioned above, the mean extinction time for this $d = 0$ system can be calculated explicitly, with the result that $T_{\text{extinct}} \sim e^{cy}$, where c is a constant, for large y [10]. This suggests that the mean extinction time should rise at least exponentially with y in the one oasis problem when y is large. By choosing a large y, then, it is possible to ensure that extinction will in all likelihood not invalidate any results obtained by assuming no extinction. From here on, I will assume that the growth rate on the oases is large enough that extinction is unlikely on the transport time scales in question.

4.3 Transport Between Two Oases

4.3.1 Transport as a First Passage Process

The eventual goal of this chapter is to understand the transport of a population across a system filled with oases at low density. The first step towards such an understanding is to determine the nature of transport between two oases. Consider two oases of radius a in d dimensions. The center of one oasis is located at the origin, and the center of the other oasis is located at position $\boldsymbol{R}$. At $t = 0$, the first oasis is populated and the second oasis is empty. I wish to find the infection time—that is, the time it takes for a population to take hold and reach a significant level on the second oasis. This time can be roughly broken into two parts: T_{transit}, the time it takes particles from the first oasis to reach the second oasis; and T_{growth}, the time it takes the population to rise to a significant level once the second oasis has been reached. I will assume that the first particle to reach the second oasis will reproduce and that its offspring will not die out; in other words, I will take T_{transit} to be the first passage time (FPT) of the process. This assumption can be satisfied

in two ways: the first way is simply to make the growth rate y of the oases very high. In this case, it is possible to estimate how the survival probability—the probability that a particle reaching the second oasis reproduces and starts a new population—increases as y increases. Consider again the case of a very deadly desert: if the particle diffuses off the oasis, it is certainly dead; thus, there is an effective death rate of order $D/{\ell_0}^2$. For the case of a very small oasis, then, a toy model of the oasis is a $d = 0$ system with death rate of $D/{\ell_0}^2$. For this case, it is known that the survival probability goes like $1 - D/y{\ell_0}^2$ [10], and thus making y very high assures that the population will take hold and survive. A second way of satisfying the first passage assumption is to seed the oases with a second species of particles, B, which interact with the A particles via the reaction $A + B \to 2A$ at a very high rate.

The time T_{growth} that it takes the initially small population on the second oasis to grow to a macroscopic size should go roughly like $1/y$ for large y, and so choosing a large y should also serve to make $T_{\text{growth}} \ll T_{\text{transit}}$. For the remainder of the chapter, I will assume that y is large enough so that this is the case. Note that taking y to be very high accomplishes three things: first, it ensures that a small population which reaches a new oasis grows into a sizable population and does not die out, which allows for the identification of the first passage time with the transit time; second, it makes the time for this growth small compared to the transit time; and finally, as mentioned in the previous section, it ensures that extinction will only occur on a time scale much larger than the one associated with transit. In Chapter 6, I will study a related model in which the equivalent of the oases are allowed to die out.

Consider the case where the two oases are close together: particles from the first oasis diffuse out in a front, its amplitude decaying due to the death term in the desert and competition effects. However, so long as the second oasis is close enough that the edge of the front is almost certain to possess many particles (the number will vary from realization to realization of the stochastic process), the transit time should simply go as R, the oasis separation. However, once R is well above some length scale I will call R_{lin}, this is no longer true: the front simply does not exist in most realizations of the system, as the number of particles present at this distance from the first oasis is quite small for all times. In this regime, the second oasis is reached not by a front but by a stray particle (or some stray particles) that manages to make it through the desert; it is essentially a noise-induced growth process. R_{lin} can thus be roughly defined as the distance from the oasis at which the large-time average concentration falls to $1/{\ell_0}^d$. I have already analyzed the mean-field equations for the average concentration as $t \to \infty$, and found that, except in $d = 1$, there are no closed-form solutions. In one dimension, setting the mean-field $t \to \infty$ average concentration (4.5) for large y equal to $1/\ell_0$ and

solving for R_{lin} leads to

$$R_{\text{lin}} = a + \sqrt{\frac{4D}{z}}\,\text{csch}^{-1}\left(\sqrt{\frac{2b}{3z}}\right), \tag{4.10}$$

where a is the radius of the oases. In the limit of large z/b, this simplifies to $R_{\text{lin}} \simeq a + \sqrt{D/z}\ln(6z/b)$, where b is q/ℓ_0. This expression is valid as $y \to \infty$; if y is smaller, the relevant length scale will also be smaller. It seems reasonable that this length scale should be of the same order of magnitude in higher dimensions, and so (4.10) should also provide a rough estimate of R_{lin} for $d = 2$ and $d = 3$.

4.3.2 A Simpler Linear Model With a Source

As particles move further from the first oasis, the competition process $2A \to A$ becomes less and less important, especially if b is small compared to the other rates in the problem. Due to this fact, it is natural to wonder if ignoring these interactions altogether might be the first step in the creation of a tractable model with the same large distance first passage properties as the full model with competition. I will now propose such a model: consider replacing the first oasis with desert, and then placing a point source in the middle that produces non-interacting particles at some average rate g. The master equation for this process on a lattice in $d = 1$ can be written as

$$\begin{aligned}
\frac{\partial P(\{n\},t)}{\partial t} &= \frac{w}{2}\Big(\sum_{\nu}(n_{\nu-1}+1)P(\ldots,n_{\nu-1}+1,n_\nu-1,\ldots,t) \\
&\qquad + (n_{\nu+1}+1)P(\ldots,n_\nu-1,n_{\nu+1}+1,\ldots,t) - 2n_\nu P(\{n\},t)\Big) \\
&+ z\sum_{\nu}\left[(n_\nu+1)P(\ldots,n_\nu+1,\ldots,t) - n_\nu P(\{n\},t)\right] \\
&+ g\left[P(\ldots,n_0-1,\ldots,t) - P(\{n\},t)\right],
\end{aligned} \tag{4.11}$$

where $P(\{n\},t)$ is the joint probability to have occupation numbers $\{n\} \equiv \{\ldots,n_{\nu-1},n_\nu,n_{\nu+1}\ldots\}$ on the lattice points ν at time t. For an appropriately chosen g, the mean flux of particles past the surface at R_{lin} should match that of the model with competition; beyond that point, the model with a source differs from the model with competition only in that it ignores the rare annihilation interactions between particles.

While it certainly seems likely—or at least plausible—that the linear model with a source just introduced will have the same large oasis separation first passage properties as the full model with competition, it cannot be proven without the help of simulations. For the remainder of this chapter, I will simply focus on the properties of the linear model with a source, using it to make predictions about the behavior of the model with competition. In Chapter 5, I will show simulation results that indicate that the linear model

with a source *does* capture the large oasis separation behavior of the full model with competition.

As with the full nonlinear model with competition (hereafter referred to as the nonlinear model), it is useful to analyze the mean-field behavior of the linear model with a source. The master equation (4.11) can be multiplied by n_ν and summed over configurations to obtain an equation for the time evolution of the average number of particles $\bar{n}(\nu,t)$:

$$\begin{aligned}\frac{\partial \bar{n}(\nu,t)}{\partial t} &= \frac{w}{2}\left[\bar{n}(\nu+1,t)+\bar{n}(\nu-1,t)-2\bar{n}(\nu,t)\right] \\ &\quad -z\bar{n}(\nu,t)+g\delta_{\nu,0}. \end{aligned} \tag{4.12}$$

I will study the continuum version of this equation in detail in one, two, and three dimensions. Taking the continuum limit of (4.12) (and changing $\partial_x^2 \to \nabla^2$ for $d>1$) results in:

$$\frac{\partial \bar{n}(\boldsymbol{x},t)}{\partial t} = D\nabla^2\bar{n}(\boldsymbol{x},t)-z\bar{n}(\boldsymbol{x},t)+g\delta^d(\boldsymbol{x}). \tag{4.13}$$

Unlike the mean-field equation for the model with competition, this equation can be solved exactly in all dimensions. Assuming an initial condition with no particles present, a Laplace transform in time and Fourier transform in space leads to:

$$\widetilde{\bar{n}}(\boldsymbol{k},s) = \frac{g}{s(s+D\boldsymbol{k}^2+z)}. \tag{4.14}$$

Transforming back into the time domain gives:

$$\widetilde{\bar{n}}(\boldsymbol{k},t) = \frac{g\left[1-e^{-(z+D\boldsymbol{k}^2)t}\right]}{D\boldsymbol{k}^2+z}. \tag{4.15}$$

I am interested in the long-time, steady-state behavior in all dimensions. Letting $t\to\infty$ and transforming in space gives the following solutions for $\bar{n}_{ss}(\boldsymbol{x}) \equiv \bar{n}(\boldsymbol{x},t=\infty)$:

$$\begin{aligned}\bar{n}_{ss}(x) &= \frac{ge^{-\kappa|x|}}{\sqrt{4Dz}} \qquad \text{1D} \\ \bar{n}_{ss}(r) &= \frac{gK_0(\kappa r)}{4\pi D} \qquad \text{2D} \\ \bar{n}_{ss}(r) &= \frac{ge^{-\kappa r}}{4\pi D r} \qquad \text{3D}\end{aligned} \tag{4.16}$$

There is one additional case of interest: the $d=1$ lattice case. The relevant mean-field equation in this case is simply (4.12). After a Laplace transform, one is left with a difference equation which can be solved with the ansatz $\widetilde{\bar{n}}(\nu+1,s) = e^{-f(s)}\widetilde{\bar{n}}(\nu,s)$ for $\nu>0$. The solution is

$$\widetilde{\bar{n}}(\nu,s) = \frac{ge^{-f(s)|\nu|}}{sw\sinh(f(s))}, \tag{4.17}$$

where $f(s) = \cosh^{-1}(1 + (s+z)/w)$. One can immediately get the $t \to \infty$ behavior of $\bar{n}(\nu, t)$ from this expression by multiplying by s and letting $s \to 0$, resulting in

$$\bar{n}_{ss}(\nu) \equiv \bar{n}(\nu, t \to \infty) = \frac{g e^{-f|\nu|}}{w \sinh(f)}, \tag{4.18}$$

where $f \equiv f(0)$.

The functional forms of the continuum solutions in (4.16) are the same as those of the solutions for the asymptotic ($r \gg a$) steady-state nonlinear ($b \neq 0$) equations discussed in Section 4.2.1. For a properly chosen creation rate g, the mean-field solutions of the two models should match at long distances. In Chapter 5, I will use this method of matching mean-field solutions to determine g for the purposes of making numerical predictions of first passage properties in the nonlinear model.

In practice, one can solve the nonlinear steady-state mean-field equations numerically, and then find g by matching the long-distance behavior to the appropriate solution from (4.16). It is possible, however, to match the $d = 1$ solutions analytically: using the results of Section 4.2.1 together with (4.16) results in

$$g = 8\sqrt{Dz}\,\gamma^2 \bar{c}_{ss}(a) e^{\kappa a}, \tag{4.19}$$

where $\gamma^{-1} = 1 + \sqrt{2q\bar{c}_{ss}(a)/3z}$, as before. The constant $\bar{c}_{ss}(a)$ can be found as described in Section 4.2.1. As $y \to \infty$, $g \to 12\sqrt{Dz^3}\, e^{\kappa a}/q$. For higher dimensions, it is necessary to numerically solve the mean-field equations for the nonlinear model to accurately calculate g.

4.3.3 Analytic Predictions from the Linear Model with a Source

With a method in place for determining g from the parameters of the nonlinear model, it is now possible to use the linear model with a source to make predictions about first passage properties of the two oasis system. To do this, begin by noting that, since the particles in the linear model with a source are non-interacting, the full multi-particle FPT PDF $f_N(\boldsymbol{x}, t)$—that is, the probability per unit time that the first particle from the first oasis reaches the second oasis between t and $t + dt$—can be written in terms of the one-particle FPT PDF $f_1(\boldsymbol{x}, t)$. (Note that the vector $\boldsymbol{x}$ is a stand-in for all the geometric particulars of the system. For instance, for a spherical or circular oasis, $f_N(\boldsymbol{x}, t)$ depends on the distance of the center of the oasis from the origin R and the radius a of the oasis. These geometrical particulars are not important for the present discussion, and so f_N is expressed as a function of the generic vector $\boldsymbol{x}$.) This is accomplished as follows: assume the source is at the origin, and that it releases N particles per unit time Δt.[2] Define

[2]There is a subtle but ultimately unimportant inconsistency here: in writing the master equation for the linear model with a source, I implicitly assumed that the creation process at

$S(\boldsymbol{x},t) = 1 - \int_0^t dt'\, f_1(\boldsymbol{x},t') = 1 - P_{\rm hit}(\boldsymbol{x},t)$ to be the probability that a particular particle released from the origin at $t = 0$ has *not* reached the target oasis by time t. If one defines $P_{\rm none}(\boldsymbol{x},t)$ to be the probability that *no* particles from the source have hit the target oasis by time t, then

$$P_{\rm none}(\boldsymbol{x},t) \;=\; \prod_{\tau=0,\Delta t,\ldots}^{t} [S(\boldsymbol{x},\tau)]^N. \tag{4.20}$$

Taking the logarithm of this expression gives

$$\ln\left[P_{\rm none}(\boldsymbol{x},t)\right] = \sum_{\tau=0,\Delta t,\ldots}^{t} g\Delta t\, \ln\left[S(\boldsymbol{x},\tau)\right], \tag{4.21}$$

where $g \equiv N/\Delta t$ is the creation rate. Taking the limit $\Delta t \to 0$ with g fixed and exponentiating both sides leads to a closed equation for $P_{\rm none}(\boldsymbol{x},t)$ in terms of $S(\boldsymbol{x},t)$:

$$P_{\rm none}(\boldsymbol{x},t) = \exp\left(g\int_0^t dt'\, \ln S(\boldsymbol{x},t')\right). \tag{4.22}$$

Since I am interested in oasis separations large enough that a given single particle has a low probability of ever reaching the second oasis, $S(\boldsymbol{x},t)$ is close to 1 even as $t \to \infty$. This allows for the quantity $\ln S(\boldsymbol{x},t) = \ln(1 - P_{\rm hit}(\boldsymbol{x},t))$ to be approximated by $-P_{\rm hit}(\boldsymbol{x},t)$, leading to a simpler expression for $P_{\rm none}(\boldsymbol{x},t)$:

$$P_{\rm none}(\boldsymbol{x},t) \simeq \exp\Big[-g\int_0^t dt'\,(t-t')f_1(\boldsymbol{x},t')\Big]. \tag{4.23}$$

The full FPT PDF $f_N(\boldsymbol{x},t)$ is simply $-\partial_t P_{\rm none}(\boldsymbol{x},t)$.

There is one more useful way to write $P_{\rm none}$: since the integral appearing in the exponent in (4.23) is a convolution of t and $f_1(\boldsymbol{x},t)$, its Laplace transform is simply a product of the two functions' individual Laplace transforms. Explicitly:

$$P_{\rm none}(\boldsymbol{x},t) \simeq \exp\left(-g\mathcal{L}^{-1}\left[\widetilde{f}_1(\boldsymbol{x},s)/s^2\right]\right), \tag{4.24}$$

where $\mathcal{L}^{-1}[u(s)]$ is the inverse Laplace transform of $u(s)$ and $\widetilde{f}_1(\boldsymbol{x},s)$ is the Laplace transform in time of $f_1(\boldsymbol{x},t)$. Often it is easier to compute $\widetilde{f}_1(\boldsymbol{x},s)$ than $f_1(\boldsymbol{x},t)$, and in these cases (4.24) can be very useful.

In order to make predictions using (4.23) or (4.24), it is necessary to compute the one-particle FPT PDF $f_1(\boldsymbol{x},t)$. I will do this now for the continuum case in all relevant dimensions and the lattice case in $d = 1$, starting with the continuum case. The diffusion equation governing the

the source was a Poisson process. However, I am now treating it as a deterministic process in which particles are released at regular intervals. The mean-field equation for the linear model with a source is the same in either case, and so there is no ambiguity in fixing g.

probability distribution $p_1(\boldsymbol{x}, t)$ of a particle released into the desert from the origin at $t = 0$ is

$$\frac{\partial p_1(\boldsymbol{x}, t)}{\partial t} = D\nabla^2 p_1(\boldsymbol{x}, t) - z p_1(\boldsymbol{x}, t), \tag{4.25}$$

with boundary condition $p_1(\text{oasis surface}, t) = 0$. This boundary condition is of course not true in the model—particles arriving at the oasis will not immediately die—but it is used as a device to extract first passage properties (see Ref. [69]). By writing $p_1(\boldsymbol{x}, t) = \phi_1(\boldsymbol{x}, t)e^{-zt}$, it is possible to eliminate the death term in (4.25) and arrive at a simple diffusion equation for $\phi_1(\boldsymbol{x}, t)$. The FPT PDF $f_1(\boldsymbol{x}, t)$ can be obtained by considering the flux of probability into the oasis [69]:

$$f_1(\boldsymbol{x}, t) = D \int_{\substack{\text{oasis} \\ \text{surface}}} dA\ \hat{n} \cdot \nabla\phi_1(\boldsymbol{x}, t)e^{-zt}, \tag{4.26}$$

where dA is an element of the oasis surface and $\hat{n}$ is a unit vector pointing out from the oasis. Since $\phi_1(\boldsymbol{x}, t)$ is the solution to a simple diffusion equation, $D \int dA\, \hat{n} \cdot \nabla\phi_1(\boldsymbol{x}, t) = f_1^{z=0}(\boldsymbol{x}, t)$, where $f_1^{z=0}(\boldsymbol{x}, t)$ is the FPT PDF in the case where there is no desert. This fact can be combined with (4.26) to arrive at the conclusion

$$f_1(\boldsymbol{x}, t) = f_1^{z=0}(\boldsymbol{x}, t)e^{-zt}. \tag{4.27}$$

The Laplace-transformed FPT PDF $\widetilde{f}_1(\boldsymbol{x}, s)$ is thus related to the $z = 0$ function by

$$\widetilde{f}_1(\boldsymbol{x}, s) = \widetilde{f}_1^{z=0}(\boldsymbol{x}, s + z). \tag{4.28}$$

These results are convenient due to the fact that, for circular or spherical oases, exact solutions exist for $f_1^{z=0}(\boldsymbol{x}, t)$.

In one dimension, $f_1^{z=0}(x, t) = |x|e^{-x^2/4Dt}/\sqrt{4\pi D t^3}$ [69]. This means that

$$f_1(x, t) = \frac{|x|e^{-x^2/4Dt}e^{-zt}}{\sqrt{4\pi D}\, t^{3/2}} \tag{4.29}$$

when there is a desert present. Plugging this into (4.23) and doing the integration [70] gives

$$\begin{aligned} P_{\text{none}}(x, t) \quad \simeq \quad & \exp\left[-\frac{g}{4z}\left(e^{\kappa|x|}\,\zeta^+ \operatorname{erfc}(\zeta^+/\sqrt{4zt}\,)\right.\right. \\ & \left.\left. -e^{-\kappa|x|}\,\zeta^- \operatorname{erfc}(\zeta^-/\sqrt{4zt}\,)\right)\right], \end{aligned} \tag{4.30}$$

where $\zeta^\pm = \zeta^\pm(x, t) = \kappa|x| \pm 2zt$. This function is shown in Figure 4.1. For large times, $P_{\text{none}}(x, t) \sim \exp\left(-ge^{-\kappa|x|}t\right)$. The j-th moment of $f_N(x, t)$ is given by $\langle T^j(x)\rangle = j \int_0^\infty dt\, P_{\text{none}}(x, t)t^{j-1}$; although it is not possible to perform this integral analytically, one can extract its $|x| \to \infty$ (large oasis

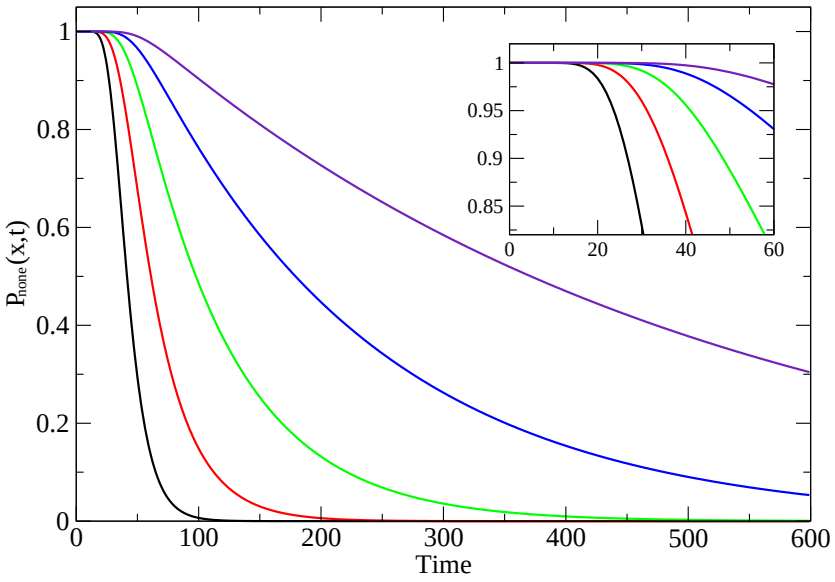

Figure 4.1: Main window: plot showing $P_{\rm none}(x,t)$ in $d=1$. The lines represent, from left to right, the function for $x = 16, 18, 20, 22$, and 24. Inset: a blowup showing the early-time behavior of $P_{\rm none}$.

separation) behavior (see Appendix B):

$$\langle T^j(x)\rangle = j!\,\frac{e^{\kappa|x|j}}{g^j}. \quad \text{(1D continuum)} \tag{4.31}$$

In two and three dimensions, it becomes more convenient to solve for $\widetilde{f}_1(\boldsymbol{x},s)$ and then use (4.24) to obtain $P_{\rm none}$. The single-particle FPT PDF is a function of the separation of the center of the target oasis from the origin ($\boldsymbol{R}$) and the radius of the oasis (a), so I will from now on write it as $f_1(R,a,t)$, where $R = |\boldsymbol{R}|$. The FPT PDF in frequency space in the absence of a desert ($z=0$) is known for these cases [69]; using (4.28) gives

$$\widetilde{f}_1(R,a,s) = \left(\frac{a}{R}\right)^{d/2-1} \frac{K_{d/2-1}\left(\sqrt{\frac{s+z}{D}}\,R\right)}{K_{d/2-1}\left(\sqrt{\frac{s+z}{D}}\,a\right)}, \tag{4.32}$$

where K_n is the n-th order modified Bessel function of the first kind. This equation also holds in $d=1$; redefining $x = R-a$ and using the definition of $K_{1/2}$ leads to the Laplace transform of (4.29).

In $d=2$, using (4.24) and (4.32) gives

$$P_{\rm none}(R,a,t) \simeq \exp\left[-\frac{g}{2\pi\imath}\int_{\mathcal{L}} ds\,\frac{e^{st}K_0\left(\sqrt{\frac{s+z}{D}}\,R\right)}{s^2 K_0\left(\sqrt{\frac{s+z}{D}}\,a\right)}\right]. \tag{4.33}$$

The exponent can be reduced to an analytic function plus a real integral (see

Appendix B)

$$\begin{aligned} P_{\rm none}(R,a,t) &= e^{-gY(R,a,t)} \\ Y(R,a,t) &= \frac{t\,K_0\left(\kappa R\right)}{K_0\left(\kappa a\right)} \\ &- \frac{RK_0\left(\kappa a\right)K_1\left(\kappa R\right) - aK_0\left(\kappa R\right)K_1\left(\kappa a\right)}{\sqrt{4Dz}\left[K_0\left(\kappa a\right)\right]^2} \\ &+ \frac{2R^2e^{-zt}}{\pi D}\int_0^\infty du\,\frac{u\,e^{-Dtu^2/R^2}\,Z_0(u,\frac{a}{R})}{\left[u^2+\kappa^2R^2\right]^2}, \end{aligned} \tag{4.34}$$

where

$$Z_0\left(u,\frac{a}{R}\right) = \frac{J_0(\frac{a}{R}u)Y_0(u) - J_0(u)Y_0(\frac{a}{R}u)}{J_0(\frac{a}{R}u)^2 + Y_0(\frac{a}{R}u)^2}. \tag{4.35}$$

The large t behavior of $P_{\rm none}$ is given by $P_{\rm none}(R,a,t)$ $\sim \exp\left(-g\left[K_0(\kappa R)/K_0(\kappa a)\right]t\right)$. The moments asymptotically approach

$$\langle T^j(R,a)\rangle = j!\left(\frac{K_0(\kappa a)}{gK_0(\kappa R)}\right)^j \quad \text{(2D contin.)} \tag{4.36}$$

as $R\to\infty$.

The three dimensional case is easy to treat. Since $K_{-n}(z) = K_n(z)$, looking at (4.32) immediately shows that $\widetilde{f}_1(R,a,s)$ for $d=3$ is identical to the $d=1$ case save for a factor of a/R. Making the replacements $|x|\to R-a$ and $g\to ga/R$ in (4.30) gives $P_{\rm none}(R,a,t)$; making the same replacements gives the $t\to\infty$ decay $P_{\rm none}(R,a,t)\sim\exp\left(-g(a/R)e^{-\kappa(R-a)}t\right)$. The moments approach

$$\langle T^j(R,a)\rangle = j!\left(\frac{R}{a}\right)^j\frac{e^{\kappa(R-a)j}}{g^j} \quad \text{(3D contin.)} \tag{4.37}$$

as $R\to\infty$.

The final case I will consider is the $d=1$ lattice case. Recall that for this case, w is the total hopping rate and the integer ν denotes the lattice point. The single-particle FPT PDF $f_1(\nu,t)$ is [69]

$$f_1(\nu,t) = \frac{|\nu|e^{-(w+z)t}I_\nu(wt)}{t}, \tag{4.38}$$

where I_ν is the ν-th order modified Bessel function of the first kind. It is more convenient to use the frequency space function:

$$\widetilde{f}_1(\nu,s) = \frac{w^{|\nu|}}{\left[s+w+z+\sqrt{(s+z)(s+z+2w)}\right]^{|\nu|}}. \tag{4.39}$$

Using this together with (4.24) gives an expression for $P_{\text{none}}(\nu, t)$:

$$\begin{aligned} P_{\text{none}}(\nu,t) &\simeq e^{-gY(\nu,t)} \\ Y(\nu,t) &= e^{-f|\nu|}\left(t - \frac{|\nu|}{w\sinh(f)}\right) \\ &+ \frac{e^{-(w+z)t}}{\pi w}\int_0^\pi d\theta\, \frac{\sin(\theta)\sin(|\nu|\theta)e^{wt\cos(\theta)}}{\left[1+\frac{z}{w}-\cos(\theta)\right]^2}. \end{aligned} \tag{4.40}$$

This function decays as $P_{\text{none}}(\nu,t) \simeq \exp\left(-ge^{-f|\nu|}t\right)$ as $t \to \infty$. As in the continuum case, P_{none} cannot be integrated analytically, but an asymptotic analysis (similar to the one for the continuum case described in Appendix B) shows that, as $|\nu| \to \infty$,

$$\langle T^j(\nu)\rangle = j!\,\frac{e^{f|\nu|j}}{g^j}. \quad \text{(1D lattice)} \tag{4.41}$$

4.3.4 Convection Effects on First Passage Properties

In this section, I will determine the effects of a small, uniform convection velocity $\boldsymbol{v}$ on the first passage properties of a two oasis system. Physically, such a convection velocity might represent the effects of a moving liquid medium in which the particles exist. By "small," I mean that the velocity does not push the population off the oasis very much. To quantify this, consider the effects of a convection velocity on the mean-field steady state of a population near an oasis in $d = 1$. The equation governing this system is given by (4.1) with the left side equal to 0. If one goes far enough away from the oasis, the nonlinear term can be neglected, leading to

$$0 = D\frac{\partial^2 \bar{c}_{ss}(x)}{\partial x^2} - v\frac{\partial \bar{c}_{ss}(x)}{\partial x} - z\bar{c}_{ss}(x). \tag{4.42}$$

Defining $\xi_{ss}(x) = \bar{c}_{ss}(x)e^{-vx/2D}$ leads to a simple, solvable equation for $\xi_{ss}(x)$ and the result that

$$\bar{c}_{ss}(x) \sim e^{vx/2D}e^{-\kappa_v x}, \tag{4.43}$$

where $\kappa_v = \sqrt{z/D + v^2/4D^2}$. I am interested in convection velocities small enough that the $vx/2D$ term is much larger than the shift in κ due to v; that is, where $v \ll \sqrt{4Dz}$. From here on, I will assume that v fulfills this condition.

Consider a two oasis system in $d = 2$ or $d = 3$. To determine the effects of a convection velocity, I will first need to find $f_1(R, a, t)$. For a small, uniform convection velocity, the diffusion equation governing $p_1(\boldsymbol{x}, t)$ is

$$\frac{\partial p_1(\boldsymbol{x},t)}{\partial t} = D\nabla^2 p_1(\boldsymbol{x},t) - zp_1(\boldsymbol{x},t) - \boldsymbol{v}\cdot\nabla p_1(\boldsymbol{x},t). \tag{4.44}$$

It is essential to simplify this equation before proceeding with a Laplace transform. As with (4.25), one can define a new function $\phi_1(\boldsymbol{x}, t) = p_1(\boldsymbol{x}, t)e^{zt}$

and eliminate the $-zp_1(\boldsymbol{x},t)$ term from the equation. Next, the function $\chi_1(\boldsymbol{x},t)$ can be defined as $\phi_1(\boldsymbol{x},t) = e^{\boldsymbol{v}\cdot\boldsymbol{x}/2D}\chi_1(\boldsymbol{x},t)$, leading to

$$\frac{\partial\chi_1(\boldsymbol{x},t)}{\partial t} = D\nabla^2\chi_1(\boldsymbol{x},t) - \frac{v^2}{4D}\,\chi_1(\boldsymbol{x},t). \tag{4.45}$$

The last term on the right can be handled by defining $\chi_1(\boldsymbol{x},t) = \psi_1(\boldsymbol{x},t)e^{-v^2\,t/4D}$, leading to a simple diffusion equation for ψ_1.

The flux into the oasis can be used, as before, to find $f_1(R,a,t)$:

$$\begin{aligned} f_1(R,a,t) &= Da^{d-1}\int d\Omega\ \partial_r p_1(\boldsymbol{x},t) \\ &= Da^{d-1}e^{-(z+v^2/4D)t}\int d\Omega\ e^{\boldsymbol{v}\cdot\boldsymbol{x}/2D}\partial_r\psi_1(\boldsymbol{x},t), \end{aligned} \tag{4.46}$$

where $d\Omega$ is a differential element of angle in 2D, and of solid angle in 3D. All that must be done is to find $\psi_1(\boldsymbol{x},t)$. This function is the solution to a simple diffusion equation with initial condition $\psi_1(\boldsymbol{x},0) = e^{-\boldsymbol{v}\cdot\boldsymbol{R}/2D}\delta^d(\boldsymbol{x}-\boldsymbol{R})$. Thus,

$$f_1(R,a,t) = Da^{d-1}e^{-(z+v^2/4D)t}e^{-\boldsymbol{v}\cdot\boldsymbol{R}/2D}\int d\Omega\ e^{\boldsymbol{v}\cdot\boldsymbol{x}/2D}\partial_r\Omega_1(\boldsymbol{x},t), \tag{4.47}$$

where $\Omega_1(\boldsymbol{x},t)$ is the solution to the simple diffusion equation without convection. I am interested in the case where $R \gg a$, and so a decent approximation of $f_1(R,a,t)$ is given by

$$f_1(R,a,t) \simeq e^{-v^2t/4D}e^{\boldsymbol{v}\cdot\boldsymbol{R}/2D}f_1^{\boldsymbol{v}=0}(R,a,t). \tag{4.48}$$

Note that in the above equation, I have reversed the sign of $\boldsymbol{R}$ since it is more natural to take the source as the origin rather than the center of the target oasis. This result can be used to determine the moments of $f_N(R,a,t)$. By making the replacements $z \to z + v^2/4D$ and $g \to ge^{\boldsymbol{v}\cdot\boldsymbol{R}/2D}$ in the expressions for the moments of $f_N(R,a,t)$, one arrives at the following expression, valid in any dimension:

$$\langle T^j(R,a)\rangle_{\boldsymbol{v}} = j!\left(\frac{R}{a}\right)^{(d-1)j/2}\frac{e^{-j\boldsymbol{v}\cdot\boldsymbol{R}/2D}e^{\kappa_{\boldsymbol{v}}(R-a)j}}{g(\boldsymbol{v})^j}, \tag{4.49}$$

where $\kappa_{\boldsymbol{v}} = \sqrt{z/D + v^2/4D^2}$. Note that g may depend on $\boldsymbol{v}$; that is, if a given g correctly captures the first passage properties of a given nonlinear system with no convection, then some new $g(\boldsymbol{v})$ will capture the first passage properties of the nonlinear system with a convection velocity $\boldsymbol{v}$.

It is important to note that the dominant contribution to the change in the FPT comes from the term $e^{-\boldsymbol{v}\cdot\boldsymbol{R}/2D}$. The reason for this is that, although $v \equiv |\boldsymbol{v}| \ll \sqrt{4Dz}$, it is *not* necessarily much smaller than D/R, where R is the oasis separation. Expanding out $\kappa_{\boldsymbol{v}}$ and taking $g(\boldsymbol{v}) \simeq g(0)$ (remembering $\boldsymbol{v}$ is

small) leads to

$$\langle T^j(R,a)\rangle_{\boldsymbol{v}} \simeq e^{-j\boldsymbol{v}\cdot\boldsymbol{R}/2D}\, e^{j\kappa_0 v^2(R-a)/4Dz}\langle T^j(R,a)\rangle_{\mathbf{0}}, \tag{4.50}$$

where $\langle T^j(R,a)\rangle_{\mathbf{0}}$ is the j-th moment of the FPT PDF with $\boldsymbol{v}=0$. Unless the angle θ between $\boldsymbol{v}$ and $\boldsymbol{R}$ is near $\pm\pi/2$, the first exponential will be far bigger than the second, and

$$\langle T^j(R,a)\rangle_{\boldsymbol{v}} \simeq e^{-j\boldsymbol{v}\cdot\boldsymbol{R}/2D}\langle T^j(R,a)\rangle_{\mathbf{0}}. \tag{4.51}$$

4.4 From Two Oases to Many

4.4.1 The Connection with Hopping Conduction

With results for the two oasis system in hand, I will now turn my attention to a system with many oases at low density. For concreteness, consider a continuum system in d dimensions ($d>1$) comprised of identical oases of radius a and growth rate y placed around randomly distributed points with number density n in a desert of death rate z. I am interested in the low density regime; that is, the regime in which the average distance between oases $R_{\text{avg}} \propto n^{-1/d}$ is larger than the length scale R_{lin} identified in (4.10). The oases are allowed to overlap, although this shouldn't happen too often at the low oasis densities being considered. Imagine starting with one or more oases populated at $t=0$ and waiting for a particular oasis or one of a number of oases situated far away to become populated. I will call the total time for this to take place $T_{\text{infection}}$, the infection time. Because of the exponential dependence of the mean FPT on oasis separation for large oasis separations (see (4.31), (4.36), and (4.37)), the time taken to cross the largest oasis separations (or links) on the path should, on average, be *much* greater than the time taken to cross the shorter links. The situation is somewhat analogous to that of hopping conduction in doped semiconductors [71]: the oases in this system play the role of the impurity sites in the semiconductor, and the mean transit time between oases is akin to the resistance between impurity sites. In doped semiconductors, the resistance between impurity sites depends exponentially on their separation like $e^{\alpha R}$, where R is the impurity separation and $\alpha \equiv 2/a$, where a is an effective Bohr radius describing the width of the impurity wavefunctions [71]. This is similar to the way the mean transit time (and, indeed, all other moments of the distribution for large separation) depends exponentially on oasis separation in the oasis system. There are a couple of significant differences between the two systems: first, there is no equivalent in the semiconductor problem of the growth time, the time needed for the population on a newly inhabited oasis to rise to a significant level; second, the resistances between impurity sites are not the averages of stochastic variables like the mean transit times, but rather definite quantities.

The first of these differences is insignificant since it has already been assumed that T_{growth} is much smaller than a typical value of T_{transit} for oases separated by a large distance. The second difference is more important, and some of its implications will be discussed in detail later in this chapter.

The problem of determining the resistivity (or conductivity) of a doped semiconductor in the hopping regime was first tackled satisfactorily using ideas from percolation theory by Ambegaokar and coworkers [64, 65]. They found that the resistivity is dominated by the largest links in the network of impurity sites spanning the system. Any links with much larger resistances are effectively shunted by the smaller resistances, and are not important in determining the macroscopic resistivity. The size of the largest link R_{max} in the spanning cluster can be determined using continuum percolation theory, which works in roughly the following way: a circle (or sphere) is drawn around each impurity site, and the radius of each circle is increased. When an impurity site center comes within the circle centered around another impurity site, the two are said to be linked. When the radii of the circles are increased to the point where a cluster of linked sites connects one side of the system to another, the percolation threshold has been reached. The last link to form as the radii of the circles are increased is clearly the longest link, and its length is R_{max}. This length varies from sample to sample, but has a well-defined limit as the system size goes to infinity [71]:

$$R_{\text{max}} = \left[\frac{B_c(d)}{n\, V_d} \right]^{1/d}, \tag{4.52}$$

where $B_c(d)$ is the dimensionally-dependent *bonding criterion*, V_d is the volume of a d-dimensional unit hypersphere, and n is the number density of impurity sites. The quantity $B_c(d)$ has an interpretation as the mean number of connected neighbors for members of the percolation cluster [71].

It is natural to suppose that, in the semiconductor problem, the resistivity of a sample might be minimized by including some resistances larger than R_{max}. To see this, imagine starting with the critical percolation cluster—the spanning cluster formed when the circles around each site are expanded to R_{max}—and allowing the circles to expand further out. More resistances will now be included in the cluster, and, though these resistances are higher than R_{max}, they also serve to provide new parallel pathways for current to go through [71]. As the radii of the circles surrounding the impurity sites are increased to $R > R_{\text{max}}$—and thus more large resistances are included in the cluster—the correlation length L_0 of the spanning cluster decreases. It is expected that, just as in lattice percolation, L_0 should decrease according to a power law, with the mean number of bonds per site $B = n\pi R^2$ taking the place of the percolation probability p [72]:

$$L_0 \sim (B - B_c(d))^{-\nu}, \tag{4.53}$$

where $\nu = 4/3$ in $d = 2$ and $\simeq .9$ in $d = 3$. These are the same power laws governing the divergence of the correlation length as $p \to p_c$ in lattice percolation [73].

To determine the resistivity of the system at some value of R, it is necessary to know something about the structure of the cluster—namely, it is necessary to know what the typical separation of large links is. One model of the cluster structure is the links-nodes-blobs picture [71, 73], which suggests that the cluster can be thought of as a network of nodes separated by a distance on the order of L_0 connected by one-dimensional links and clusters (or blobs) of links. Since the resistance of a link depends exponentially on its length, the largest one-dimensional links of approximate size R largely determine the resistance between nodes. If a large chunk of material of linear size $L \gg L_0$ has its resistance Ω measured, Ω should be $\sim (L/L_0)^{2-d} e^{\alpha R}$, since there are $\sim (L/L_0)^{d-1}$ chains of resistors connecting the edges of the system, each with resistance $\sim (L/L_0) e^{\alpha R}$. The resistivity ρ is then given by [73]

$$\rho = L^{d-2}\Omega = e^{\alpha R} {L_0}^{d-2}. \tag{4.54}$$

It is possible to minimize this resistivity with respect to R. First, L_0 must be written as a function of R [72]:

$$L_0 \sim (B - B_c(d))^{-\nu} \sim [n(R - R_{\max})(R + R_{\max})]^{-\nu} \quad \text{(d=2)} \tag{4.55}$$

$$\sim \left[n(R - R_{\max})(R^2 + {R_{\max}}^2)\right]^{-\nu} \quad \text{(d=3)}, \tag{4.56}$$

where I have assumed in the $d = 3$ equation that R is not too different from $R_{\max}$. The values of ν and the oasis density n in the two equations above are, of course, different from one another. For $d = 3$, minimizing (4.54) with respect to R gives $\alpha R_{\rm opt} = \alpha R_{\max} + \nu$. To obtain a numerical value for L_0, it is necessary to multiply (4.53) by some typical length scale—say $n^{-1/3}$—giving

$$L_0 \simeq \frac{(\alpha R_{\max})^\nu}{n^{1/3}}. \tag{4.57}$$

Note that various numerical prefactors have been left out of this expression; what is important is the scaling of L_0 with ν and the dependence on $\alpha R_{\max}$.[3]

For $d = 2$, minimizing (4.54) leads to $R_{\rm opt} = R_{\max}$ and $L_0 = \infty$. Simulations actually indicate that $R_{\rm opt}$ is very close to $R_{\max}$ in $d = 2$ [72], but clearly the expression for L_0 is unacceptable. How to remedy this? A heuristic argument due to Shklovskii allows for an estimate of L_0 [71]: links with resistances much more than $e^{\alpha R_{\max}+1}$ should be shunted by the rest of the cluster, and so the correlation length should be roughly equal to that of the

[3] According to Hunt and others [72], there exists another length scale l which, together with L_0, characterizes the structure of the cluster in $d = 3$. This length scale is associated with the distance between large links along the direction of current motion. Using this picture of the cluster, Hunt has obtained $\alpha R_{\rm opt} = \alpha R_{\max} + 2\nu$.

spanning cluster which includes such links as its largest members. Plugging $\alpha R = \alpha R_{\max} + 1$ into (4.55) gives an estimate for L_0:

$$L_0 \simeq \frac{(\kappa R_{\max})^{\nu}}{n^{1/2}}, \tag{4.58}$$

where I have again multiplied by a length scale to obtain a value of L_0 with the correct units.

In addition to being the correlation length of the spanning cluster, L_0 is also the length scale at which sample-to-sample variations in $\alpha R_{\max}$ become relatively small, of order 1 [71]. That is, if $R_{\max}(L)$ is defined as the largest link in the cluster that spans a *finite* system of size L, then the width of the probability distribution for $R_{\max}(L)$ becomes small around $L = L_0$. Above the length scale L_0, the system can be regarded as homogeneous, and so the resistivity of a large system of size $L \gg L_0$ is roughly equal to the resistivity of a system of size L_0; this fact is captured in (4.54).

4.4.2 Dynamics of Transport in a Macroscopic System: Infection Time

Now I return to the problem of oases in a desert. Recall that the dominant contribution to the transit time in any dimension comes from the exponential $e^{\kappa R}$ with $\kappa \equiv \sqrt{z/D}$; thus, substituting κ for α in (4.57) or (4.58) gives a length scale which can be identified with the typical separation between large oasis separations:

$$L_0 \simeq \frac{(\kappa R_{\max})^{\nu}}{n^{1/d}}, \tag{4.59}$$

where n is now the number density of oases. Consider a system of size L_0 with one oasis initially infected at one edge of the system. In the hopping conduction problem, the goal is to find the resistance between the edges of the system; in the oasis problem, it is to find the first passage time between the starting oasis and either a specific oasis on the opposite edge or any oasis in a thin layer close to the opposite edge. Unlike the hopping conduction problem, the oasis problem is dynamic in nature; an additional difference is that, as mentioned previously, the first passage times are random variables with a distribution whose mean increases exponentially with oasis separation rather than fixed resistances with an exponential dependence on link size. The mean FPT across the system is thus an average of a minimum: for a fixed set of oases, each realization of the dynamic process yields a path with minimal first passage time which may differ from the paths from other realizations. However, there is at least one large link of size $\simeq R_{\text{opt}}$ which must be crossed in order for the population to reach the opposite edge of the system, and the time to cross this link sets the time scale to cross the system in the same way the that the resistance of the largest link sets the scale of the resistance in the

hopping conduction problem. Thus,

$$\langle \text{time to cross system of size } L_0 \rangle \simeq \langle T(R_{\text{opt}}, a) \rangle, \tag{4.60}$$

where $T(R_{\text{opt}}, a)$ is given by (4.36) or (4.37) depending on the dimensionality of the system. This approximation should work better as $\kappa R_{\max}$ increases, just as the estimate for the resistivity in (4.54) should work better as $\alpha R_{\max}$ increases [65, 74].

Now consider a very large system. The desired quantity is the mean infection time $\langle T_{\text{infection}}(L) \rangle$—that is, the mean time for the population to travel between oases separated by some large distance $L \gg L_0$. This time is roughly equal to the mean FPT in the current parameter regime (that is, the limit of high growth rate on the oases). Because this time depends on the distance L—it is an extensive quantity—it is *not* analogous to the resistivity in the semiconductor problem, which is an intensive quantity. It seems reasonable that, for large L, $\langle T_{\text{infection}}(L) \rangle \propto L$, but this should not be taken for granted. In order to show that this is the case and to arrive at an expression for $\langle T_{\text{infection}}(L) \rangle$, I will now employ some ideas from the theory of first passage percolation first introduced in Chapter 3.

Consider the oasis system as consisting of nodes placed on a square ($d = 2$) or cubic ($d = 3$) lattice with lattice spacing L_0 with one large link of size R_{opt} in between each node; this is essentially the links-nodes-blobs picture of the system. For the time being, I will ignore the time to cross the shorter links and the variations in the oasis configurations from one correlation-length-sized chunk to another. The population starts at one node, and the desired quantity is the first passage time to some distant node located a distance L away along a lattice basis vector (or, equivalently, $n = L/L_0$ lattice points away). If the reader has read Chapter 3, she may recognize this as the basic problem of *first passage percolation*. As discussed in that chapter, one of the main results of FPP is that, as the separation between nodes $n \to \infty$, the FPT $\langle T(n) \rangle$ divided by n goes to a constant μ, conventionally called the time constant. Thus, the mean FPT rises linearly with distance between sites (with sublinear corrections of order $n^{1/2} \log(n)$, as discussed in Chapter 3), indicating that the proper intensive quantity for the problem is the mean FPT divided by oasis separation. This is reassuring, as it reinforces the common-sense notion that $\langle T_{\text{infection}}(L) \rangle \propto L$ for large L. The value of μ depends on the underlying FPT probability distribution, but a general result is that $\mu \leq T_1$, where T_1 is the average time to cross one link [50]. For the case where the times are chosen from an exponential distribution, $\mu \simeq .4T_1$ in two dimensions [52].

One consequence of the intensive quantity being $\langle T_{\text{infection}}(L) \rangle / L$ is that the optimal oasis separation R_{opt} is now $R_{\max}$ in both $d = 2$ and $d = 3$. This is due the fact that the advantage gained in raising R_{opt} from $R_{\max}$ to some higher value in the hopping conduction problem—more parallel paths added to

lower the resistance—is completely absent here. Explicitly, trying to minimize

$$\langle T_{\text{infection}}(L)\rangle \sim \frac{L}{L_0}\langle T(R_{\text{opt}}, a)\rangle \tag{4.61}$$

with respect to R_{opt} leads to $R_{\text{opt}} = R_{\max}$. For the remainder of this chapter and the next two, then, I will cease using R_{opt} and use only $R_{\max}$. The correlation length L_0 will still be given by (4.59), however, as the Shklovskii method can be used to obtain this value.

Since there is approximately one large link of size $R_{\max}$ in between each node, the time T_1 is given approximately by $\langle T(R_{\max}, a)\rangle$. Furthermore, the distribution of times to cross the largest link is nearly exponential for large $R_{\max}$ (see (4.36) or (4.37)); this suggests that the time constant for the oasis problem in $d = 2$ should be of the order $.4T_1$. The exact value is unimportant; the important fact is that the time constant is not too different from T_1. Thus, to obtain a rough estimate of the infection time, one can simply use T_1 (the mean time to cross one link) as an estimate for $\langle T_{\text{infection}}\rangle/n$. This gives the following:

$$\langle T_{\text{infection}}(L)\rangle \simeq \frac{L}{L_0}\langle T(R_{\max}, a)\rangle, \tag{4.62}$$

where $\langle T(R_{\max}, a)\rangle$ is again given by (4.36) in $d = 2$ and (4.37) in $d = 3$, and L_0 is given by (4.53). This result is important, and deserves to be written out for $d = 2$ and $d = 3$ with all factors explicitly stated:

$$\langle T_{\text{infection}}(L)\rangle \simeq \sqrt{\frac{B_c(2)}{\pi}}\,\frac{L}{(\kappa R_{\max})^{4/3}R_{\max}}\,\frac{K_0(\kappa R_{\max})}{gK_0(\kappa a)} \qquad \text{(2D)}; \tag{4.63}$$

$$\langle T_{\text{infection}}(L)\rangle \simeq \left(\frac{3B_c(3)}{4\pi}\right)^{\frac{1}{3}}\,\frac{L}{(\kappa R_{\max})^{.88}}\,\frac{e^{\kappa(R_{\max}-a)}}{ga} \qquad \text{(3D)}. \tag{4.64}$$

In the above equations, $B_c(d)$ is, as before, the bonding criterion, equal to $\simeq 4.5$ in $d = 2$ and $\simeq 2.7$ in $d = 3$ [71].

Since (4.63) and (4.64) are of great importance to the rest of this chapter and the next, it is worth remarking on them. First, note that the numerical prefactors involving $B_c(d)$ (the bonding criterion) in both equations—prefactors that come from expanding the functional form for L_0 given in (4.59)—should not be taken too seriously. These prefactors are of order 1, so ignoring them is not difficult. Note also that g is a function of the birth rate y, the oasis size a, the competition rate b, the death rate z, and the diffusion constant D, but *not* the oasis number density n; thus, as n is varied to change $R_{\max}$, g should remain constant. As mentioned in Section 4.3.2, g must be determined numerically by matching the long-distance steady-state solutions of the mean-field equations for both the model with competition and the linear model with a source.

Before continuing, it is probably good to stop at this point and briefly recall the approximations made to obtain the results quoted in (4.63) and

(4.64): first, I have ignored the growth time on the grounds that it is small compared to the transit time between oases; second, I have simplified the picture of transport on the scale of L_0, replacing the mess of oases with a single link of size $R_{\max}$; and third, I have used an upper limit on the time constant rather than the time constant itself. It should be noted that the first and second approximations tend to lead to underestimating $\langle T_{\text{infection}} \rangle$, while the third tends to lead to overestimating it.

In addition to the mean infection time, it is possible to estimate the variance of the infection time in $d = 2$ using the analogy to first passage percolation. Recall from Chapter 3 that in $d = 2$ the standard deviation of the FPT to lattice point $(0, n)$, $\sigma_T(n)$, goes as $\sim n^{1/3}$ for large n [41, 54]. This suggests that fluctuations in the infection time $T_{\text{infection}}$ might also grow as $L^{1/3}$; that is:

$$\sigma_T(L) \equiv \sqrt{\langle T_{\text{infection}}(L)^2 \rangle - \langle T_{\text{infection}}(L) \rangle^2} \propto L^{1/3} \tag{4.65}$$

as $L \to \infty$. Some care must be taken in evaluating this claim; in Chapter 5, I will discuss this problem further.

The results of this section can be summarized as follows: for a large system consisting of many oases at low density, the time $\langle T_{\text{infection}}(L) \rangle$ taken for a population to traverse a distance L should be dominated by the time to cross the largest links which must be crossed, which are of size $R_{\max}$. These links are separated by a distance $\sim L_0$, so that $\langle T_{\text{infection}}(L) \rangle \simeq L \langle T(R_{\max} \rangle / L_0$.

4.5 Front Properties

In the preceding sections, I used an analogy with the theory of hopping conduction to argue that the largest oasis separations that a population must cross largely determine the transit time across a large system filled with oases at low density. In this section, I will investigate the nature of the front that moves through such a system. Imagine again a system comprised of a desert with death rate z into which identical circular ($d = 2$) or spherical ($d = 3$) oases of growth rate y and radius a are placed at density n. As before, y is high enough that the growth time on the oases is negligible and the threat of extinction is virtually nonexistent. At $t = 0$, all oases with centers with $x_d \leq 0$ are infected, where x_d is a Euclidean spatial coordinate. It should be clear that, as time goes on, a front will move through the system in the direction of $\hat{x}_d$. There are two interesting questions that can be asked: what is the front velocity v and how rough is the front?

4.5.1 Front Velocity

The first of these questions is easy to answer, as long as an order-of-magnitude estimate is all that is required. Recall that the population takes a time the order of $\langle T(R_{\max}, a)\rangle$ to cross a distance of order L_0; this suggests that the front velocity v should be approximately given by

$$v \simeq \frac{L_0}{\langle T(R_{\max}, a)\rangle}. \tag{4.66}$$

To see the dependence of the front velocity on the various model parameters, one need only divide (4.63) (in $d = 2$) or (4.64) (in $d = 3$) by L and invert the resultant expression. Again, the key feature to note is the exponential dependence on $\kappa R_{\max}$.

4.5.2 Front Roughness

The question of the front's roughness is significantly more subtle, if for no other reason than the fact that even *defining* what is meant by "roughness" is not entirely clear. Recall from Chapter 2 the discussion of the roughness of Fisher waves in homogeneous media (spatially uniform growth rate y). As mentioned in that discussion, there was, for a short period of time, some debate as to the correct roughness exponents for a Fisher wave in d dimensions, but Moro [43] showed that the KPZ roughness exponents for d dimensions are correct. The key to resolving this ambiguity was to define the interface properly; once that was accomplished, the KPZ exponents in d dimensions were recovered unambiguously.

A similar difficulty regarding how to define the front exists in the present problem. There are three important length scales present: ℓ_0, a microscopic length scale; R_{avg}, the average distance between oases; and L_0, the correlation length of the particle-carrying network. Imagine trying to construct a front by looking at the scale ℓ_0 or R_{avg}: essentially, there are only particles present on and immediately surrounding the oases at these scales. For this reason, the roughness is entirely determined at these scales by the random placement of the oases, and thus the front is very rough and craggy; this is not really too interesting.

Now consider the length scale L_0. According to the simplified picture of the particle current-carrying cluster presented in Section 4.4.1, one can picture the system as roughly consisting of large oasis separations $R_{\max}$ which must be crossed separated by a distance on the order of L_0. The connection between this picture and lattice FPP was exploited to justify the scaling of $\langle T_{\text{infection}}(L)\rangle$ with L , but it can be exploited further. Recall from Chapter 3 the connection between FPP with exponentially distributed first passage times on the links and the Eden model: they are the same model, with the same statistical properties. Now clearly the passage time across some swath of

material of size $\simeq L_0$ is not an exponentially distributed quantity, but, as I mentioned in Section 4.4.1, it *is* a quantity whose moments are dominated by the moments to cross the largest link of size $R_{\max}$, and those moments are close to those of an exponential distribution for large $R_{\max}$. It seems plausible, then, that a coarse-graining on the scale of L_0 might produce a front with the same roughness as the Eden model. As discussed in Chapter 3, the Eden model in $d = 2$ is described by the KPZ equation, and its roughness is thus given by the KPZ exponents.

How to accomplish this coarse-graining? There are numerous valid ways to define such a transformation; I will describe the simplest. Consider breaking the system up into boxes of edge length ξ, where ξ is of the same order as L_0. When the oasis number density is n, such a box should have, on average, $N_{\text{avg}} \equiv n\xi^2$ oases. An individual oasis can be called "infected" when its population reaches a sizable level; the exact definition is unimportant. At some time t, all the infected oases in a given box are counted; if the number of infected oases $N_{\text{inf}} \geq \lambda N_{\text{avg}}$, where λ is some some arbitrary number close to $1/2$, then the box is said to be occupied. At $t = 0$, then, the system consists of a set of boxes below the plane $x_2 = 0$ which are occupied and a set of boxes above $x_2 = 0$ which are unoccupied.

With a coarse-graining procedure in place, one can define the front roughness in the usual way. Consider a system of size $\Lambda\xi$ in the direction perpendicular to the front (that is, a system with Λ boxes in each "layer") and infinite in the direction of the front. Each box in such a system can be labeled by its location $r_\perp$ in the plane perpendicular to $\hat{x}_2$ and its position $r_\parallel$ above that plane (measured in the number of boxes, of course). The roughness $w(\Lambda, t)$ is then given by

$$w^2(\Lambda, t) = \frac{1}{\Lambda} \sum_{r_\perp} \left(h(r_\perp) - \bar{h} \right)^2 , \tag{4.67}$$

where the height $h(r_\perp)$ is the value of $r_\parallel$ of the occupied box with the largest $r_\parallel$ value of all boxes in the same "column" at $r_\perp$ and $\bar{h}$ is the average over $r_\perp$ of $h(r_\perp)$. If the (coarse-grained) front is well-described by the Eden model, then the average of $w^2(\Lambda, t)$ over many realizations should be given by (see Chapter 3 for a further discussion)

$$\sqrt{\langle w^2(\Lambda, t) \rangle} = \Lambda^\zeta f\left(\frac{t}{\Lambda^z} \right) , \tag{4.68}$$

where ζ and z are the KPZ exponents and $f(x)$ is some function. For a finite system size, the width saturates after a long time, and so $\sqrt{\langle w^2 \rangle} \sim \Lambda^\zeta$. As the system size grows to infinity, the width must lose its dependence on system size, and thus $f(x) \sim x^{\zeta/z}$ for small values of x. The KPZ values of the exponents in $d = 2$ are $\zeta = 1/2$ and $z = 3/2$.

4.6 Summary

In this chapter, I examined transport in a particular reaction-diffusion model with disorder in the reaction rates. In Section 4.1, I introduced the model and explicitly gave the master equation for the $d = 1$ lattice version. In Section 4.2, I examined the mean-field equation for the model near one oasis and discussed the problem of extinction. I then introduced a simplified model in Section 4.3 to study the nature of transport between two oases; this model allowed me to make predictions for the first passage properties between two oases.

In Section 4.4, I used the predictions from the simplified model together with some ideas from the theory of hopping conduction in doped semiconductors and the theory of first passage percolation to estimate the average time needed for a population to traverse a large system consisting of many oases. I also made a prediction for the variance of this time. Finally, in Section 4.5 I examined the nature of the coarse-grained front in the multi-oasis system and predicted that it should be in the KPZ universality class of front propagation models.

5 Transport in a Hostile Environment: Numerics

In order to test the predictions made in the previous chapter, I wrote two simulations: a kinetic Monte Carlo (KMC) simulation of the full model with competition for the case of two oases in $d = 1$, which was used to test the validity of the linear model with a source; and a simulation of a large system with many oases in $d = 2$, which was used to test the predictions for the infection time and front roughness. In this chapter, I will discuss the algorithms used in these simulations and present the results I obtained.[1]

5.1 Introduction to Stochastic Simulations

For a system described by a master equation, the individual events can be taken to be Poisson processes [10]. As discussed in Chapter 2, this means that the probability distribution $p(t)$ for the time to a particular event j is governed by an exponential distribution:

$$p_j(t) = r_j e^{-r_j t}, \tag{5.1}$$

where r_j is the rate associated with the event. The reader will recall from the discussion of lattice FPP in Chapter 3 the following two important properties of a system whose events are governed by exponential distributions: first, the probability distribution $P(t)$ for the time to the next event is given by

$$P(t) = r_{\text{tot}} e^{-r_{\text{tot}} t}, \tag{5.2}$$

where $r_{\text{tot}} \equiv \sum_j r_j$ is the *total rate*; second, the probability of the next event being some event k is simply r_k / r_{tot}.

These two facts are all that are needed to formulate an exact algorithm for simulating a stochastic system described by a master equation. The algorithm goes under many names—kinetic Monte Carlo (KMC), dynamic Monte Carlo, the stochastic simulation algorithm (SSA)—but whatever it is called, it works as follows [11, 75]:

1. Choose an event. To do this, first choose a random number u_1,

[1] Some of the material in this chapter has appeared before, in slightly altered form, in the following publications: A.R. Missel and K.A. Dahmen, Phys. Rev. Lett. **100**, 058301 (2008), Copyright 2008 by the American Physical Society; and A.R. Missel and K.A. Dahmen, submitted to Phys. Rev. E (2008), Copyright 2008 by the American Physical Society.

$0 \leq u_1 < 1$, and pick the first event k for which $\sum_{i=1}^{k} r_i/r_{\text{tot}} > u_1$.

2. Sample the PDF for the time t to the next event; that is, choose another random number u_2, $0 < u_2 \leq 1$ and take $t = -\log(u_2)/r_{\text{tot}}$.

3. Execute the event and update the list of possible events and the total rate.

The obvious bottleneck in terms of efficiency lies in the first step. Luckily, there is a more efficient way to choose the correct event than searching through each possible event: the so-called "n-fold way." This method involves dividing the possible events in the system into n classes and then choosing first a class, and then an event from that class [11, 76]. For example, if there are two types of events—say birth and death—then the probability of a death event being the next event to occur is simply $N_{\text{death}} r_{\text{death}}/r_{\text{tot}}$, where r_{death} is simply the death rate (the rate at which individuals die) and N_{death} is the number of possible death events in the system. One can simply generate a random number and quickly decide whether the next event should be a birth or death event, and then search through just the events of the given type. All events of the same type have the same rate, and so each has an equal probability of being the next event. There are numerous clever ways of grouping events together to minimize the search time—see Ref. [11] for a summary—but perhaps the simplest method is just to put all events of the same type together, just as in the example given above.

5.2 Simulations of a Two Oasis System in $d = 1$

5.2.1 Testing the Linear Model With a Source

The introduction of the linear model with a source in Section 4.3.2 was an essential step in the process of making analytic predictions about the dynamics of transport in a large system of oases at low density. Recall the justification for introducing this simplified model: far away from an oasis—where the average population density is low—interactions between particles are a relatively unimportant source of particle destruction compared to the death process $A \to 0$. It thus might be permissible to ignore interactions between particles in such areas, especially if the interaction rate b is low. If the oasis is replaced by desert and a source which spits out particles $(0 \to A)$ into the desert at some rate g, then, for an appropriately chosen g, the mean concentration of particles at large distances from the oasis should be the same as for the full model with competition, and it seems likely that the first passage properties between two oases might also be the same, in the limit of large oasis separation.

This certainly seems plausible, but it needs numerical verification, seeing as how the subsequent arguments presented in Chapter 4 rest on the features of

the FPT PDF for two oases predicted using this simplified model. In order to do the testing, I wrote a kinetic Monte Carlo simulation of the full nonlinear model on a $d = 1$ lattice. By doing enough runs, I was able to get accurate values for the low moments of the FPT PDF as well as an idea of its general shape. I was then able to compare these with the analytic predictions from the linear model with a source to assess the validity of that model.

It should be noted that the decision to perform the two oasis simulation in $d = 1$ was made due to several factors. First of all, the assumptions behind the linear model with a source—namely, that the $2A \to A$ process can be ignored when trying to determine the FPT properties for oases separated by a large distance ($> R_{\text{lin}}$) and that the proper source strength g can be found by matching mean-field solutions—are the same in all dimensions, and so if the linear model works well in $d = 1$, it should work well in higher dimensions, as well. Since the computational time rises with the number of dimensions in the simulation, it would be inefficient to simulate a higher dimensional system for the purposes of confirming the applicability of the linear model with a source. A second reason for performing a $d = 1$ simulation is that, given the difficulties in simulating a continuum system on a lattice, it would be simpler to compare lattice simulation results with *lattice* analytical results; however, these are only available for $d = 1$ (see the end of Section 4.3.3).

The procedure for verifying the linear model with a source is as follows:

1. Pick a set of parameters (birth rate, death rate, etc.). The parameters should be such that the population on the starting oasis will not die out too quickly, but, because the simulation employs the KMC method (every event simulated), the birth rate cannot be too high, either.

2. Solve the mean-field equation for the full model with competition (4.4) numerically for this set of parameters. By matching the large time, long-distance values of the particle concentration to the analytic form from the linear model with a source (4.12), determine the correct value of the source strength g.

3. Run the full model with competition many times using the KMC simulation to determine the moments of the FPT PDF $f_N(R, t)$ for large values of R. Compare these with the values obtained from the linear model with a source with the value of g determined above.

The mean-field equation for the full model with competition on a $d = 1$ lattice is easily solved numerically, since it is already in the form of a difference equation in space. Thus, the main difficulty in this procedure comes from the third step—that is, running the KMC simulation of the full nonlinear model. In the next section, I will describe the way this simulation works.

5.2.2 Details of the Two Oasis Simulation

The two oasis simulation proceeds as follows: a lattice is set up in $d = 1$ of M points, with M an odd integer. At the center of the system, an oasis of $2a + 1$ lattice points is placed with growth rate y; every other lattice point is assigned a death rate z. The central lattice point of the oasis at $\nu = 0$ is initialized with $c_0(0)$ particles—that is, an array of length M holding the number of particles at each lattice point c_ν is initialized with zeroes everywhere except at index $(M-1)/2$, where it is set to $c_0(0)$.

Throughout the simulation, the n-fold way algorithm described in Section 5.1 is employed: the event type is first selected with the correct probability, and then an event of that type is chosen at random. It is thus necessary to know, at all steps, the number of possible events of each type. These are given by:

$$\begin{aligned} N_{\text{compete}} &= \sum_{\nu} c_\nu \left(c_\nu - 1\right), \\ N_{\text{birth}} &= \sum_{\text{oasis}} c_\nu, \\ N_{\text{death}} &= \sum_{\text{desert}} c_\nu, \\ N_{\text{move left}} &= \sum_{\nu} c_\nu \equiv N_{\text{tot}}, \\ N_{\text{move right}} &= N_{\text{tot}}. \end{aligned} \tag{5.3}$$

The initial values of the event numbers are $N_{\text{birth}} = N_{\text{tot}} = c_0(0)$, $N_{\text{death}} = 0$, $N_{\text{compete}} = c_0(0)[c_0(0) - 1]$. Denoting the competition rate by b and the total hopping rate by w, the total rate for each type of event is thus given by:

$$\begin{aligned} r_{\text{compete}} &= bN_{\text{compete}}, \\ r_{\text{birth}} &= yN_{\text{birth}}, \\ r_{\text{death}} &= zN_{\text{death}}, \\ r_{\text{move left}} &= \frac{w}{2}N_{\text{tot}}, \\ r_{\text{move right}} &= \frac{w}{2}N_{\text{tot}}. \end{aligned} \tag{5.4}$$

Once the population array and event numbers are initialized, the simulation proceeds one event at a time. The algorithm for the simulation is as follows:

1. Choose an event type i with probability $p_i = r_i/r_{\text{tot}}$, where $r_{\text{tot}} = \sum_i r_i$.
   (a) If the event is a birth event, choose a random number $u, 1 \le u \le N_{\text{birth}}$ and begin searching at the left end of the oasis at $\nu = -a$ for the u-th particle. The smallest value of μ for which $\sum_\nu^\mu c_\nu \ge u$ is the lattice point at which a particle will give birth.
   (b) If the event is a death event, choose a random number

$u, 1 \leq u \leq N_{\text{death}}$ and begin searching at the desert just to the right of the oasis for the u-th particle. The search proceeds by jumping back and forth from the right to the left of the desert; that is, from $\nu = a+1 \to -a-1 \to a+2 \to -a-2 \to \ldots$. Since most particles are located near the oasis, this search method is fairly efficient, and is very easy to implement.

(c) If the event is a move to the left or to the right, choose a particle in a manner similar to that described above, beginning at the center of the system and moving out, alternating between the left and right sides of the oasis. Use periodic boundary conditions, so that a particle at the left edge of the system which hops to the left ends up at the right edge of the system.

(d) If the event is a competition event, choose an event in a similar manner, remembering that the number of competition events per lattice point is $c_\nu(c_\nu - 1)$.

2. With the lattice point μ of the event participant(s) in hand, update the number of possible events of each type.

(a) If the event is a death event, $N_{\text{compete}} \to N_{\text{compete}} - 2(n_\mu - 1)$, $N_{\text{death}} \to N_{\text{death}} - 1$, and $N_{\text{tot}} \to N_{\text{tot}} - 1$.

(b) If the event is a birth event, $N_{\text{compete}} \to N_{\text{compete}} + 2n_\mu$, $N_{\text{birth}} \to N_{\text{birth}} + 1$, and $N_{\text{tot}} \to N_{\text{tot}} + 1$.

(c) If the event is a competition event, $N_{\text{compete}} \to N_{\text{compete}} - 2(n_\mu - 1)$ and $N_{\text{tot}} \to N_{\text{tot}} - 1$. If the event is occurring on the oasis, $N_{\text{birth}} \to N_{\text{birth}} - 1$; otherwise $N_{\text{death}} \to N_{\text{death}} - 1$.

(d) If the event is a move left (move right) event, then $N_{\text{compete}} \to N_{\text{compete}} + 2[n_{\mu-1} - (n_\mu - 1)]$ ($N_{\text{compete}} \to N_{\text{compete}} + 2[n_{\mu+1} - (n_\mu - 1)]$). If $\mu = -a$ ($\mu = +a$), then $N_{\text{birth}} \to N_{\text{birth}} - 1$ and $N_{\text{death}} \to N_{\text{death}} + 1$; if $\mu = a + 1$ ($\mu = -a - 1$), then $N_{\text{death}} \to N_{\text{death}} - 1$ and $N_{\text{birth}} \to N_{\text{birth}} + 1$.

3. Update the population array ($n_\mu \to n_\mu + 1$ for a birth event, etc.).

4. Choose a time Δt for the event from an exponential distribution with parameter r_{tot}; that is, $\Delta t = -\ln(U)/r_{\text{tot}}$, where $0 < U \leq 1$ is a uniformly distributed random number.

5. Update the rates for each event type and then r_{tot} using the newly updated number of possible events of each type and the relations given in (5.4).

This algorithm is repeated until a target lattice point $R_<$ is reached for the first time. When this happens, the time is recorded and the target is moved one lattice point further away and the simulation continues. When the target

Table 5.1: Parameters used in the first of three sets of simulations of a two oasis system in $d = 1$.

Parameter	Description	Value
a	oasis radius	2
$R_<$	min. dist. measured	10
$R_>$	max. dist. measured	30
w	hopping rate	1.0
y	birth rate	.25
z	death rate	0.1
b	compet. rate	.001
$c_0(0)$	starting pop.	125
N_{sims}	number of runs	5000

reaches some set maximum value $R_>$ and is hit for the first time, the population, event numbers, and event rates are reset, and the simulation restarts. This is repeated a total of N_{sims} times. In practice, it is necessary to make the system size M a few times larger than the maximum target distance so that the periodic boundary conditions do not affect the results.

The astute reader will note that this algorithm is not fully optimized.[2] For instance, the search for the lattice point of the u-th event of whatever type is chosen could be done better by keeping track of the *cumulative* number of events of each type at each lattice point and then performing a binary search. This would help in particular when searching for movement events. However, given the small system sizes being simulated, the speed difference between the algorithm employed and a fully optimized algorithm is really not great, and the algorithm as described has the advantage of being very easy to implement.

5.2.3 Two Oasis Simulation Results

I will now present results from the KMC simulations and compare them with the predictions from the linear model with a source. There are three parameter sets for which I ran simulations; for each of these parameter sets, I will list the parameters, compare some of the low moments of the measured FPT PDF $f_N(R, t)$ to the predicted values, and compare the extrapolated form of $f_N(R, t)$ with the analytic prediction.

The first set of simulations was performed with the parameters listed in Table 5.1. Solving the mean-field equation (4.4) with these parameters and matching with the analytic solution of the mean-field equation of the linear model with a source leads to a value of 116.845 for the parameter g. Using this

[2] Actually, the algorithm used to generate some of the data presented in the next section was even less optimized: searching for movement and competition events began from the edge of the system, where the population was low; also, the system size was larger than the maximum distance to which first passage times were measured. The first of these sub-optimal features was present simply because it was very easy to implement, and the second was present to allow the system to continue to evolve for large times for the purpose of making a movie.

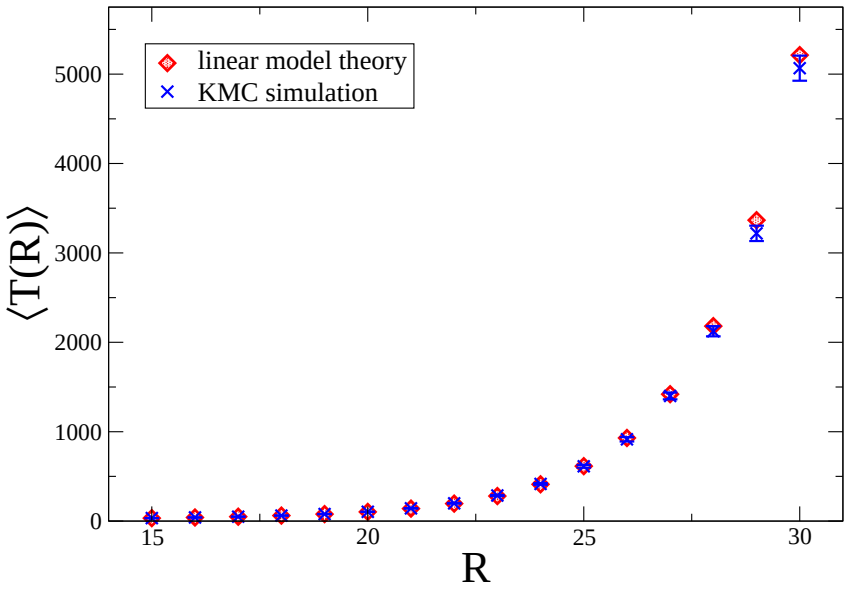

Figure 5.1: Graph showing the mean FPT as a function of R for the linear model with a source (red diamonds) and the KMC simulation of the full model with competition (blue marks) for the first parameter set. The error bars represent a 95% confidence level for the simulation mean FPTs.

value for g and the analytic expression for $f_N(R,t)$

$$f_N(R,t) = gR \int_0^t dt' \, \frac{e^{-(w+z)t'} I_R(wt')}{t'} \exp\left[-gR \int_0^t dt' \, \frac{(t-t')e^{-(w+z)t'} I_R(wt')}{t'} \right] \tag{5.5}$$

allows for a numerical calculation of $f_N(R,t)$ and its moments. The moments of the measured FPT PDF for R are of course simply calculated from the results of the N_{sims} runs via

$$\langle T^j(R) \rangle_{\text{sim}} = \frac{1}{N_{\text{sims}}} \sum_{k=1}^{N_{\text{sims}}} t_k(R)^j, \tag{5.6}$$

where $t_k(R)$ is the value of the FPT to the point R in the k-th simulation.

Figure 5.1 shows a comparison between simulation (of the nonlinear model) and theory (of the linear model with a source) for the mean FPT (the first moment of $f_N(R,t)$) for R between 15 and 30. The agreement between the two is excellent, with the theoretical value of the MFPT from the linear model with a source within a few percent of the measured value of the MFPT from the model with competition for all lattice points. This result bodes well for the effectiveness of the linear model with a source, but it is necessary to examine the higher moments as well as the full form of $f_N(R,t)$.

Table 5.2 shows the second and fifth moments of $f_N(R,t)$ for various values of R. The agreement here is very good, though it appears that, as with the mean FPT from Figure 5.1, the higher moments in the simulation are lower

Table 5.2: Comparison of predictions from the linear model with a source for the second and fifth moments of $f_N(R,t)$ with Monte Carlo data from the model with interactions. The quoted errors represent a 95% confidence interval.

R	$\langle T^2\rangle_{\rm th}$	$\langle T^2\rangle_{\rm sim}$	$\langle T^5\rangle_{\rm th}$	$\langle T^5\rangle_{\rm sim}$
10	173.739	164.97 ± 2.38404	5.78947E5	$(5.38868 \pm .208015)$E5
15	1203.87	1223.91 ± 21.8565	9.67825E7	$(9.95067 \pm .713879)$E7
20	14509.5	14691.1 ± 572.021	2.06877E11	$(1.79262 \pm .320831)$E11
25	6.91791E5	$(7.00186 \pm .424694)$E5	7.29976E15	(8.42756 ± 3.50113)E15
30	5.36637E7	$(5.13892 \pm .321111)$E7	4.39059E20	(4.00704 ± 1.21406)E20

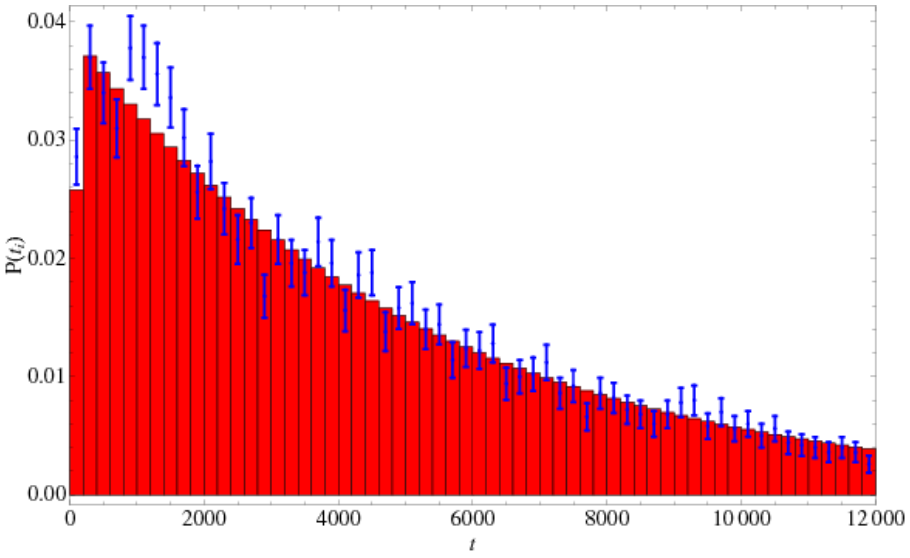

Figure 5.2: Histogram of 5000 FPTs for $R = 30$. The i-th solid bar represents the probability from the linear theory that the site at $R = 30$ is hit in the i-th time bin, and each small mark with error bars represents the simulation value of this probability. Each time bin has a width of $\Delta t = 200/w$.

than the theoretical value for $R = 30$.

Comparing moments from the simulation of the full model with the predicted values from the linear model with a source is certainly useful, but it is even more illuminating to look at the form of $f_N(R,t)$ suggested by the simulation results and compare this with the analytical prediction from the linear model with a source. I will do this in two ways: by binning first passage times and constructing a histogram, and by using kernel density estimation techniques.

The first of these methods is easy to explain: for a given set of first passage times to a point R, a bin width time Δt is chosen, and all runs that hit between $(k-1)\Delta t$ and $k\Delta t$ are placed in the k-th bin, where $k = 1, 2, \ldots$. The number of runs in each bin is then divided by the total number of runs $N_{\rm sims}$, and the result is a histogram of FPT probabilities which can be compared with theory. The linear theory with a source predicts that the probability P_k

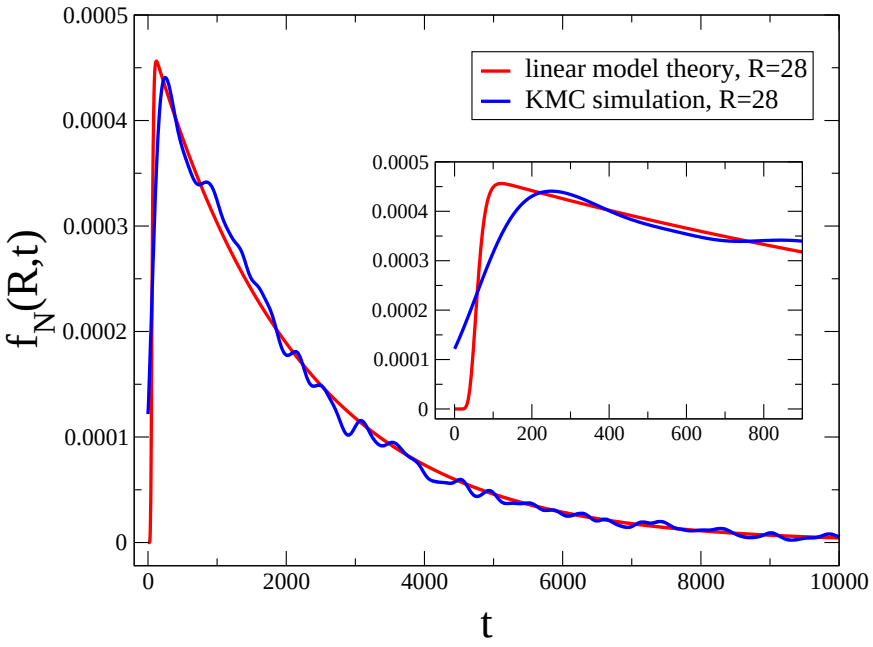

Figure 5.3: Main window: plot showing $f_N(R,t)$ for $R = 28$ for the linear model with a source (red line) and the estimate for $f_N(R,t)$ for $R = 28$ from the simulation results using kernel density estimation (blue line). Inset: a blowup of the graph for small times.

of a run hitting in the k-th bin is:

$$P_k = \int_{(k-1)\Delta t}^{k\Delta t} dt\, f_N(R,t) = P_{\text{none}}(R,(k-1)\Delta t) - P_{\text{none}}(R,k\Delta t). \qquad (5.7)$$

Figure 5.2 shows a comparison of the histogram obtained from the simulations with the predictions from the linear model with a source for $R = 30$. The agreement is good, and it appears that the linear model with a source correctly predicts the form of $f_N(R,t)$.

The second method used to compare the FPT PDF suggested by the simulation results with theory is kernel density estimation. This method uses the simulation results—which are samples from some underlying FPT PDF—to construct a smooth estimate for the underlying FPT PDF. This is done as follows: the FPT PDF $f_N(R,t)$ at time t is estimated to be given by a weighted sum of N_{sims} terms, with each term corresponding to a sample (simulation result). The effect of the i-th sample on the estimate for the PDF at time t depends on the difference between the sample's value t_i and t: samples closer to t will have more weight. In this way, regions of t which are close to many samples (and thus probably correspond to greater values of the PDF) will have a higher estimated value of $f_N(R,t)$. The general formula for

constructing an estimate $\hat{f}_N(R,t)$ of the PDF is [77]

$$\hat{f}_N(R,t) = \frac{1}{N_{\text{sims}}\, h} \sum_{i=1}^{N_{\text{sims}}} K\left(\frac{t-t_i}{h}\right), \tag{5.8}$$

where h is a bandwidth and $K(\cdot)$ is a function known as the kernel. The kernel is often taken to be a Gaussian of unit variance, although other choices are common; as far as the bandwidth is concerned, there is a sizable literature devoted to different methods for determining an optimal bandwidth. I used the Sheather-Jones method [77] for choosing a bandwidth and a Gaussian kernel, resulting in the estimate for $f_N(R,t)$ shown in Figure 5.3 alongside the FPT PDF from the linear theory with a source. The agreement is quite good, although the early time behavior seems to be a bit off. This is really not a concern, however, as the mean FPT (and higher moments) is dominated largely by the long-time behavior of the FPT PDF, which the linear theory with a source appears to capture well.

Table 5.3: Parameters used in the second of three sets of simulations of a two oasis system in $d = 1$.

Parameter	**Description**	**Value**
a	oasis radius	2
$R_<$	min. dist. measured	5
$R_>$	max. dist. measured	24
w	hopping rate	1.0
y	birth rate	2.5
z	death rate	0.2
b	compet. rate	.02
$c_0(0)$	starting pop.	62
N_{sims}	number of runs	1300

The second set of parameters for which runs were made is listed in Table 5.3. The total hopping rate w was again set to 1.0, and so time can again be thought of as being measured in units of $1/w$. Note that the competition rate is much larger in this parameter set than it was in the other set.

Figure 5.4 shows a comparison between the mean FPT from the linear theory with a source and the simulations. The agreement is again very good, though there is again the suggestion of a slight deviation at the larger values of R.

Figures 5.5 and 5.6 show the kernel density estimates for the FPT PDF for the second parameter set and the exact FPT PDF from the linear theory with a source at $R = 24$ and $R = 8$, respectively. The linear theory with a source again does a nice job of predicting the long-time behavior of the FPT PDF for large R, but, as expected, it completely fails for small R, as can be seen in Figure 5.6.

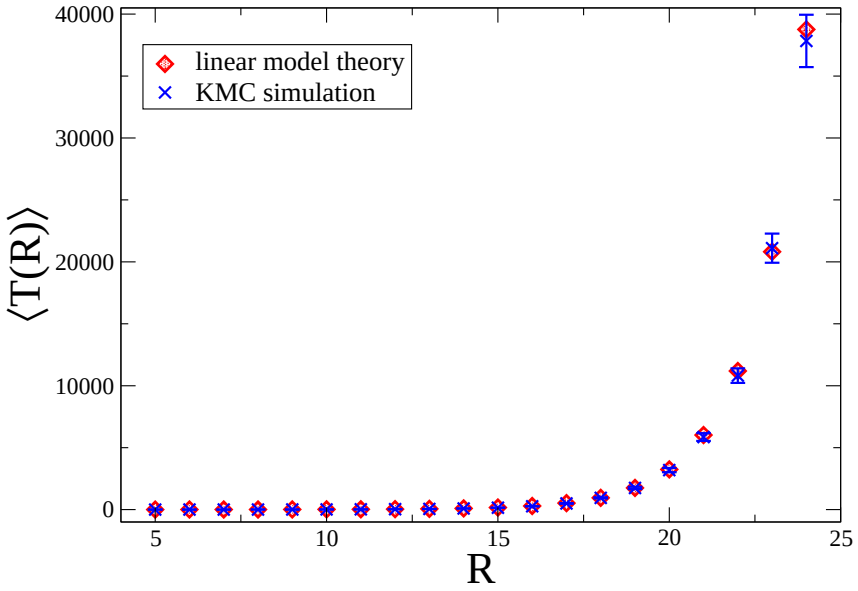

Figure 5.4: Graph showing the mean FPT as a function of R for the linear model with a source (red diamonds) and the KMC simulation of the full model with competition (blue marks) for the second parameter set. The error bars represent a 95% confidence level for the simulation mean FPTs.

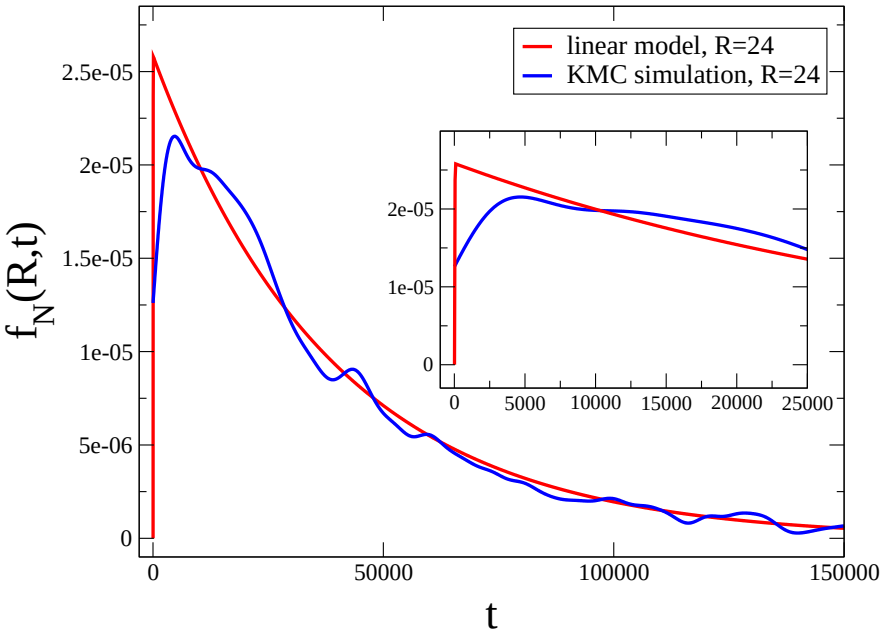

Figure 5.5: Main window: plot showing $f_N(R,t)$ for $R = 24$ for the linear model with a source (red line) and the estimate for $f_N(R,t)$ for $R = 24$ from the simulation results using kernel density estimation (blue line). Inset: a blowup of the graph for small times.

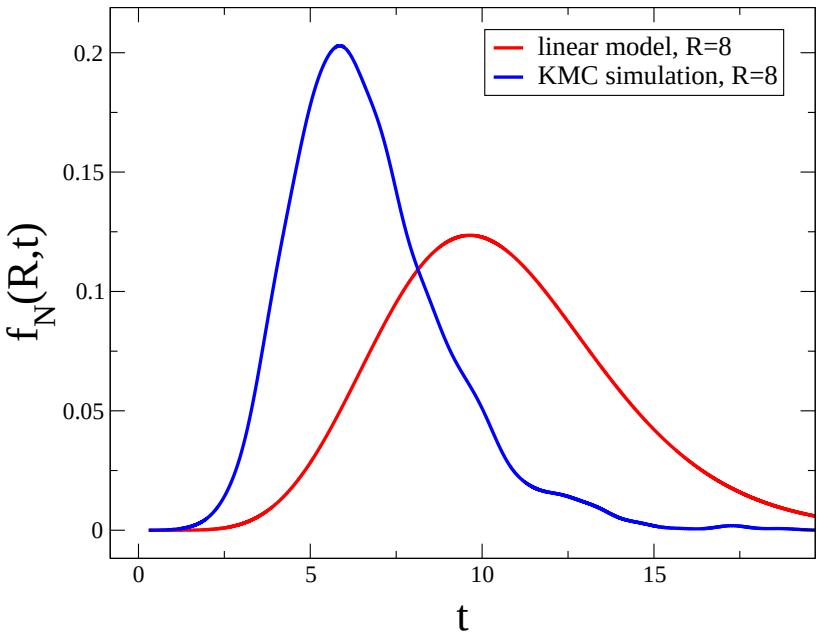

Figure 5.6: Plot showing $f_N(R,t)$ for $R = 8$ for the linear model with a source (red line) and the estimate for $f_N(R,t)$ for $R = 8$ from the simulation results using kernel density estimation (blue line).

Table 5.4: Parameters used in the third of three sets of simulations of a two oasis system in $d = 1$.

Parameter	**Description**	**Value**
a	oasis radius	2
$R_<$	min. dist. measured	15
$R_>$	max. dist. measured	45
w	hopping rate	1.0
y	birth rate	7.5
z	death rate	0.025
b	compet. rate	.1
$c_0(0)$	starting pop.	37
N_{sims}	number of runs	1533

Table 5.4 lists the parameters for the third set of runs. For this set of simulations, the competition rate was turned up yet again so that it exceeded the death rate; competition is a more significant source of particle destruction than death for a lattice site with more than one particle for this set of parameters.

Figure 5.7 shows the mean FPT as a function of R for both the KMC simulations and the linear theory with a source. The agreement is clearly quite poor; the simulation mean FPT is smaller than the theoretical value for all distances. What is the source of the disparity between the linear theory with a source and the model with competition?

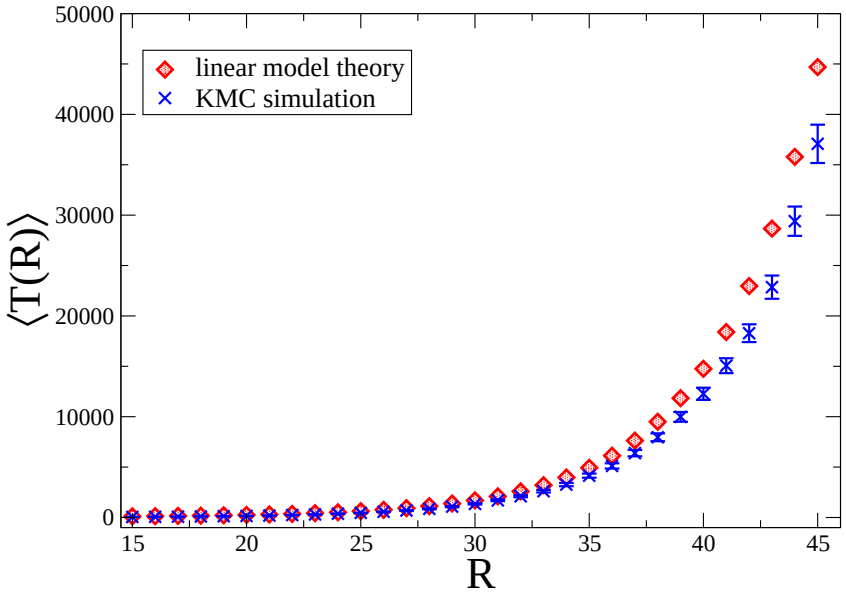

Figure 5.7: Graph showing the mean FPT as a function of R for the linear model with a source (red diamonds) and the KMC simulation of the full model with competition (blue marks) for the third parameter set. The error bars represent a 95% confidence level for the simulation mean FPTs.

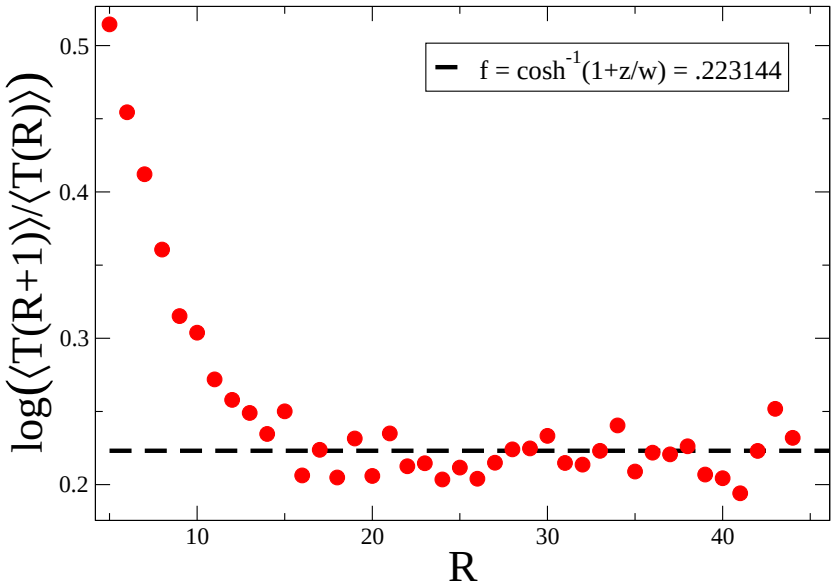

Figure 5.8: Graph showing that the mean FPT grows exponentially with the value of f given by the linear theory with a source.

Figure 5.8 is a plot of $\log[\langle T(R+1)\rangle/\langle T(R)\rangle]$; this quantity should, according to the linear theory, approach $f = \cosh^{-1}(1 + z/w)$ as R gets large, and the simulation results certainly do this. This suggests that the mean FPT rises exponentially with R for large R as $\sim e^{fR}$, as predicted by the linear theory. Figure 5.9 shows the kernel density estimate for $f_N(R,t)$ for the third parameter set at $R = 45$ along with the prediction for $f_N(R,t)$ from the linear theory with a source. Although the two do not match up nearly as well as they did for the first two parameter sets, it should be clear that the $f_N(R,t)$ suggested by the simulations looks like an exponential distribution for large times, as predicted by the linear theory with a source. Together with the results for the first two parameter sets, all of this suggests the following:

- The value of g obtained by matching the tails of the mean-field theory solutions for the two models (the solutions to (4.4) and (4.12)) works well to predict the moments of $f_N(R,t)$ only when the competition rate b is relatively small; when it is large, the value of g obtained in this manner is too small, and the linear theory with a source overestimates the mean FPT (and higher moments). A little thought shows why this is the case: since the mean-field theory approximates $\langle c_\nu(c_\nu - 1)\rangle$ by $\langle c_\nu\rangle^2$, it overestimates the importance of the competition term at small particle concentrations. The tail of the steady-state mean-field solution is thus "too small," and matching it with the mean-field solution of the linear model with a source leads to an underestimate of g and an overestimate of the mean FPT.

- Even for larger values of b, however, the linear theory with a source correctly predicts the shape of $f_N(R,t)$ for large values of R. This function looks like an exponential distribution save for its small time behavior, which does little to affect the value of the moments.

It is possible to "fit" the linear theory with a source to the simulation data by varying g. Figure 5.10 shows the best fit result for the mean FPT for the third parameter set. It should be clear that the linear theory matches the simulation data very well for this value of g.

What can one conclude about the linear theory with a source? For small values of the competition rate, it performs admirably, and even for larger values of b it correctly predicts the form of $f_N(R,t)$. This is ultimately what is important; it is the exponential growth of $\langle T(R)\rangle$ with R that allows for the use of ideas from percolation theory to predict the infection time, and it is the fact that $f_N(R,t)$ looks like an exponential distribution that allows the analogy with the Eden model and first passage percolation to work, paving the way to a prediction for the large-scale front roughness. The linear theory with a source gets both of these features correct. That it fails to accurately predict what is essentially a prefactor in front of the mean FPT for large values of the competition rate does not substantially alter its effectiveness.

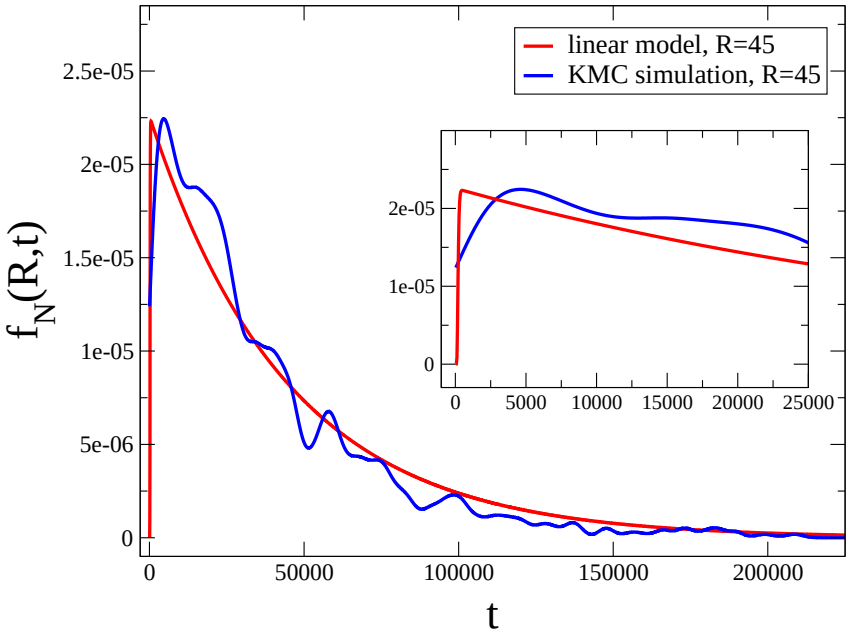

Figure 5.9: Main window: plot showing $f_N(R,t)$ for $R = 45$ for the linear model with a source (red line) and the estimate for $f_N(R,t)$ for $R = 45$ from the simulation results using kernel density estimation (blue line). Inset: a blowup of the graph for small times.

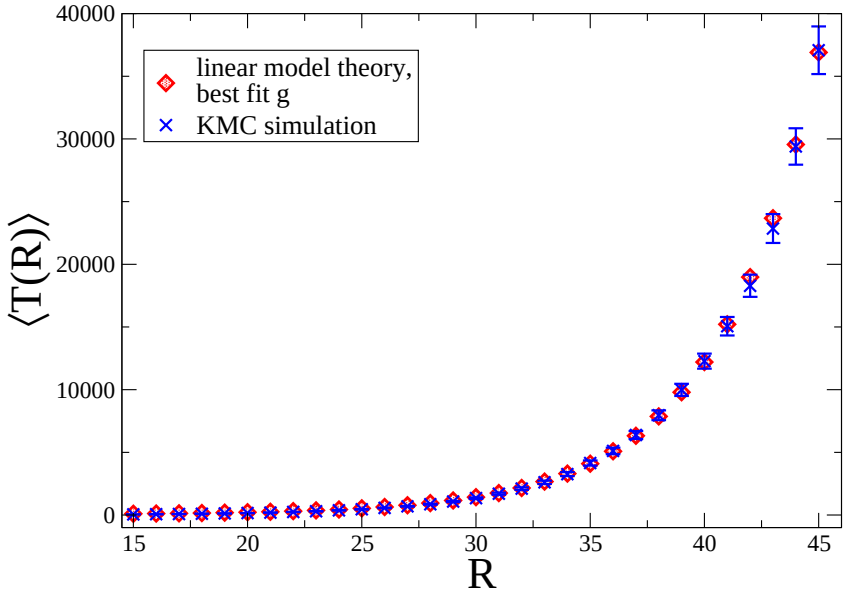

Figure 5.10: Graph showing the mean FPT as a function of R for the linear model with a source (red diamonds) and the KMC simulation of the full model with competition (blue marks) for the third parameter set with g chosen to provide the best fit between the data sets.

5.3 Simulations of a Large System in $d = 2$

5.3.1 Simulating at the Proper Level of Detail

It should now be clear that the linear model with a source adequately captures the first passage properties of a two oasis system for the case of large oasis separation. The two main conclusions that can be drawn from this are as follows: first, the mean FPT grows exponentially with oasis separation for large oasis separation; second, the distribution of first passage times is nearly exponential for large oasis separation.

The next challenge, then, is to simulate a large system comprised of many oases at low density in $d = 2$ or $d = 3$. Given the fact that the KMC algorithm simulates every event, it might seem foolish to try such a method on a large system comprising many oases; indeed, this is the case. Though there are certainly many methods which can be used to speed up KMC simulations—the τ-leaping method, for instance, zooms past unimportant events [78, 79]—none will be able to sufficiently speed up a simulation of the magnitude needed to test the predictions of Chapter 4. To see why this is the case, recall that that the predictions made for $T_{\text{infection}}$ and for the roughness of a front were for the case of a system much larger than L_0, the correlation length of the particle current-carrying network. A block of size L_0 in $d = 2$ contains, according to (4.59), on the order of $(\kappa R_{\max})^{8/3}$ oases; since $\kappa R_{\max} > 1$ for the low oasis density regime, the number of oases per block can be quite large even for modest values of $\kappa R_{\max}$. For instance, for $\kappa R_{\max} = 5$, there are $\simeq 73$ oases per block; a large system consisting of, say, 100 blocks per edge (10000 blocks total) would contain $\simeq 73000$ oases. Simulating such a system would simply take too long.

The solution to this problem lies in using the known properties of the FPT PDF to formulate a simulation of the system at a lower level of detail. For the case of low oasis density—the case I am interested in—it is the large oasis separations that must be crossed which largely determine the transit time. For these large separations, the FPT PDF $f_N(R, t)$ is close to an exponential distribution with a mean that rises exponentially with R. Given these facts, it seems that simply *assigning* first passage times between randomly placed oases rather than simulating individual particle events should be sufficiently accurate for the purpose of determining the infection time and front properties. This should work for the case of low oasis density, where the transit time between oases is much larger than the growth time on an oasis.

For the simulations I performed in $d = 2$, then, I used the approximate FPT PDF between oases separated by a distance R:

$$f_N(R, a, t) = \frac{gK_0(\kappa R)}{K_0(\kappa a)} \exp\left[-g\left(K_0(\kappa R)/K_0(\kappa a)\right) t\right]. \tag{5.9}$$

Although this FPT PDF is not accurate for small values of R, the contributions to the transit time from such separations are negligible. For the important oasis separations, (5.9) is quite accurate. Note that, because the distribution in (5.9) is an exponential distribution, this new coarse-grained model can be simulated unambiguously; it is itself governed by a master equation and represents a type of off-lattice Eden model.

There are four further simplifications and adjustments which I incorporated into the simulation in the interest of computational efficiency. First, time in the simulations is measured in units of $\tau = gtK_0(\kappa R_{\max})/K_0(\kappa a)$; that is, time is measured in units of the time needed to cross a link of size $R_{\max}$. In these units, the FPT PDF becomes

$$f_N(R,\tau) = \frac{K_0(\kappa R)}{K_0(\kappa R_{\max})}\, \exp\left[-\frac{K_0(\kappa R)}{K_0(\kappa R_{\max})}\,\tau\right]. \tag{5.10}$$

The advantage of this scaling should be obvious: the dependence of the transit time on g and a is removed, thus eliminating the need to input dummy values for these variables into the simulation.

The second simplification is to replace $K_0(\kappa R)$ and $K_0(\kappa R_{\max})$ by their large argument asymptotic forms. This approximation is poor for small oasis separations, but the contribution of the time to cross such separations to the infection time is negligible, anyway; for large oasis separations R, the asymptotic form for $K_0(\kappa R)$ is quite close to the actual value. This approximation makes the FPT PDF

$$f_N(R,\tau) = \sqrt{\frac{R_{\max}}{R}}\, e^{-\kappa(R-R_{\max})}\, \exp\left[-\sqrt{\frac{R_{\max}}{R}}\, e^{-\kappa(R-R_{\max})}\,\tau\right]. \tag{5.11}$$

The third simplification is the neglect of the finite size of the oases—they are treated as points in the simulation. This will, of course, produce some errors: for instance, oases whose centers are separated by less than $2a$ are obviously overlapping, and the transit time between them should be 0. The transit time assigned between such oases in the simulation will still be very small, however—$\sim e^{-\kappa(R_{\max}-a)}$—and so the errors should have a negligible effect upon the infection time. An additional error introduced by the neglect of the finite size of the oases is illustrated in Figure 5.11. When an oasis of *finite* size (labeled 3 in panel b of the figure) is placed in a space previously consisting of only two oases (labeled 1 and 2 in panels a and b), there are two effects on the first passage properties between the original two oases: the first stems from the fact that a particle from oasis 1 can hit oasis 3 and ignite it, and that a particle from that oasis can then hit oasis 2; the second stems from the fact that oasis 3 changes the death rate in a finite region, and by doing so alters the first passage properties for a particle going directly from $1 \to 2$. The first of these effects is taken into account in the simulations: once oasis 3 is

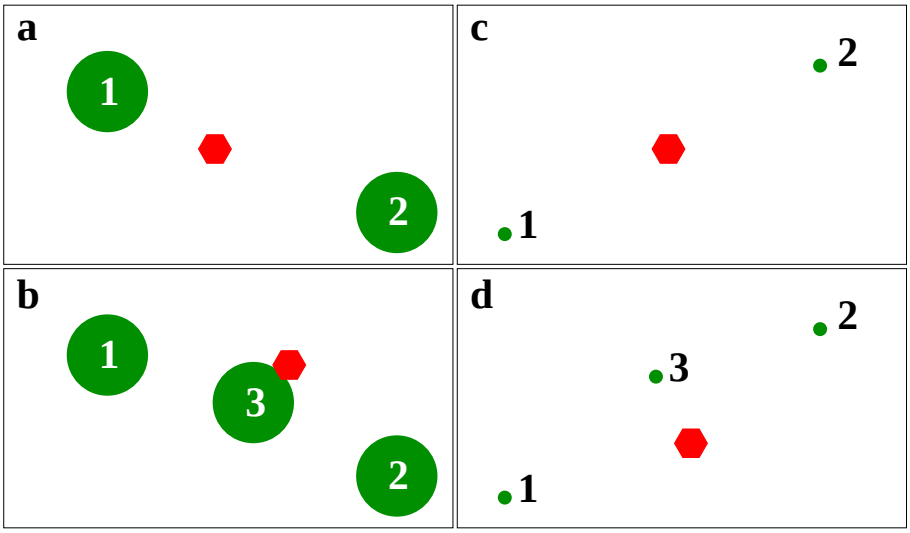

Figure 5.11: Diagram to aid in the visualization of the effects of additional oases on two oasis first passage properties. The green circles are oases and the red hexagon is a particle.

hit, passage times between it and oasis 2 are generated, and the total time for transit from $1 \to 3 \to 2$ may be less than the time from $1 \to 2$. The second of these effects, however, depends strongly on the size of the oases. For the point oases depicted in panels c and d, this effect is nonexistent, and so treating the oases as points in the simulations neglects this effect. The errors stemming from this should be very minor for pairs of oases with no oases directly between them, and the largest oasis separations—the rate-limiting links—fit this description. Thus, treating the oases as points should not significantly alter the infection time.

The final—and most significant—approximation is the imposition of a cutoff distance R_{cut} beyond which oases are disconnected. For oases separated by more than this distance, the possibility of direct infection is neglected. I will show in the next section that this modification allows for a much faster simulation, but for now, I will simply offer a derivation of the value of R_{cut} based on the model parameters.

The basic idea behind the selection of an appropriate value for R_{cut} is to ensure that the probability P_{miss} of missing an event—that is, the probability that an oasis infection event across a distance greater than R_{cut} would occur during the simulation if there were no cutoff—is below some small threshold value Π. To estimate this probability, it is necessary to know the system size L (for a system area of L^2), the oasis density n, κ, and the simulation time T. This last quantity must be estimated: since time is scaled so that it takes one unit of time to cross a separation of size R_{max}, and since this time should determine the time needed to cross a block of size L_0, the time to cross a system of size L—and thus the simulation time—should be of order L/L_0.

An upper limit on $P_{\rm miss}$ can be obtained by taking all oases in the system to be initially infected and calculating the probability (averaged over oasis configurations) that a jump larger than $R_{\rm cut}$ occurs before time $T = L/L_0$ (even a jump to an oasis outside the system). Each oasis (labeled by j) has a total rate $r_>$ to infect far away oases given by

$$r_> = \sum_{k|R_{jk}>R_{\rm cut}} \sqrt{\frac{R_{\rm max}}{R_{jk}}}\, e^{-\kappa(R_{jk}-R_{\rm max})}, \tag{5.12}$$

where R_{jk} is the distance between oases j and k. This total rate to infect a far away oasis is, of course, dependent on the oasis configuration. Averaging over configurations gives an approximation for $r_>$:

$$\begin{aligned} r_> &\simeq 2\pi n \int_{R_{\rm cut}}^{\infty} dR\, R \sqrt{\frac{R_{\rm max}}{R}}\, e^{-\kappa(R-R_{\rm max})} \\ &\simeq \frac{\pi n e^{-\kappa(R_{\rm cut}-R_{\rm max})}}{\kappa^2} \sqrt{\frac{R_{\rm max}}{R_{\rm cut}}}\, \left[1+\kappa R_{\rm cut}\right]. \end{aligned} \tag{5.13}$$

The probability $1 - P_{\rm miss}$ that none of the $N_{\rm oas}$ oases in the system have infected a far away neighbor after time T is simply given by a product of one-oasis probabilities—$1 - P_{\rm miss} = (e^{-r_> T})^{N_{\rm oas}}$—and replacing $N_{\rm oas}$ by its average value nL^2 leads to:

$$1 - P_{\rm miss} \simeq e^{-r_> n L^3/L_0}. \tag{5.14}$$

Setting $P_{\rm miss} < \Pi$, assuming Π is very small, and expressing the result in terms of $R_{\rm max}$ and κ leads to a transcendental equation for the minimum value of $R_{\rm cut}$ necessary to fulfill the "no miss" condition with probability $1 - \Pi$:

$$\frac{e^{-\kappa R_{\rm cut}}}{\sqrt{\kappa R_{\rm cut}}}\left(1+2\kappa R_{\rm cut}\right) = \Pi \sqrt{\frac{\pi}{B_c(2)^5}} \left(\frac{R_{\rm max}}{L}\right)^3 \left[\kappa R_{\rm max}\right]^{17/6}\, e^{-\kappa R_{\rm max}}. \tag{5.15}$$

Remember that this is really an upper limit on $R_{\rm cut}$ for a given value of Π; I have assumed an initial condition which allows all oases in the system the duration of the simulation to try to infect a distant neighbor, whereas in actuality the oases only have the portion of the simulation after they are hit.

To summarize: the model which will be simulated consists of point oases between which first passage times are picked from the distribution given in (5.11). Because this distribution is an exponential distribution, the entire process is memoryless, and can be described by a master equation. This model can be thought of as an off-lattice version of the Eden model with long-range interactions: just as the lattice Eden model and lattice FPP with times taken from an exponential distribution are really the same thing—one is couched in the language of dynamics and the other in the language of optimization, but they describe the same system—so too is this model, with first passage times

assigned between randomly placed points, just a different description of a dynamic process. In Chapter 6, I will explore this further.

5.3.2 Details of the Large System Simulation

Now that the relevant simplifications to the model have been described, I can detail the method used to simulate a large system in $d = 2$. The basic idea is to proceed one oasis infection event at a time, but the manner in which events are chosen is different than in the two oasis simulation. The reason for the change is that, in this simulation, because each oasis infection event occurs with a different rate (since the rate depends on the separation between oases), there is no easy way to group events with the same rate into classes. This grouping is what allowed for efficient random selection of events in the simulation of two oases: the total rate for each event type was kept, and then the n-fold way algorithm was used to select first an event type and then an event of that type. For the large system simulation, events are instead placed in a priority queue and then executed. As mentioned in Section 5.3.1, because the events are taken to be Poisson processes—the FPT PDF between each pair of oases is an exponential distribution—assigning times to events when they first become possible and then simply executing them in order is completely equivalent to a kinetic Monte Carlo simulation, just as lattice FPP with an exponential FPT PDF is completely equivalent to the Eden model. Priority queues are useful for simulating systems with disordered reaction rates, and have been used recently in a simulation of the contact process with disorder [80]. The queue, of course, must be updated as the simulation proceeds. The use of a cutoff distance R_{cut} allows for the system to be broken into blocks of edge length $2R_{\text{cut}}$; when an oasis' neighbors need to be determined, only the oasis' block and three neighboring blocks need to be searched. This greatly speeds up the simulation.

The basic algorithms used for studying the nature of the coarse-grained front and for studying the infection time are the same. All that differs between the two cases are the initial conditions and the types of data gathered. The steps which must be completed to set up each simulation run are:

1. Read in the appropriate parameters, including κ, n, and R_{cut}. For the front simulation, read in the approximate system lengths $L_\perp$ in the direction perpendicular to the direction of travel of the front and $L_\parallel$ in the direction of travel of the front as well as a set of coarse-graining length scales and cutoffs (ξ and λ from Section 4.5.2) and the frequency at which coarse-grained front data output is desired. For the infection time simulation, read in a set of distances L_i to which infection data is to be gathered and a tolerance δ specifying how far an oasis may be from one of the rings with radii $L_1, L_2, \ldots$ to be considered to be located at that distance. The reason for doing the simulation this way should be

clear: in one simulation run, infection time data for a given L_i can be gathered from $\simeq 4\pi L_i n\delta$ oases rather than one oasis. In practice, $\delta \ll R_{\max}$, so that all oases in a given ring can be considered to be located at the distance L_i from the starting oasis.

2. Calculate $R_{\max}$ and L_0 from n and κ using (4.52) and (4.59). For the front simulation, determine the actual system width $L_\perp$ and "height" $L_\parallel$ by finding the smallest numbers larger than the approximate values read in which are common multiples of $2R_{\text{cut}}$ and all of the values of the coarse-graining scale ξ read in. This ensures that the system can be broken into blocks of size $2R_{\text{cut}}$ *and* that the system can be coarse-grained at each value of ξ without any space left over. For the infection time simulation, set the system size in each dimension to be the closest number to $8L_{\max}$ that is also an exact multiple of $2R_{\text{cut}}$, where $L_{\max}$ is the largest distance to which FPT statistics are to be gathered.

3. Set up an array of blocks, each of edge length $2R_{\text{cut}}$. For the front simulation, initialize the entire bottom row of $L_\perp/2R_{\text{cut}}$ blocks. For the infection time simulation, initialize one block in the middle of the system. The initialization is done as follows:

   (a) For each block, pick a random number from a Poisson distribution with mean $4n{R_{\text{cut}}}^2$, the average number of oases per block. Record this number—the number of oases in the block—and initialize an array of this number of oasis objects.

   (b) For each oasis object in each block, pick a random x coordinate and a random y coordinate that lie within the block being set up. Set the infection time for each oasis to 0 since it is initially infected. In the infection time simulation, check to see whether the oasis is within a distance δ of one of the L_i; if it is, tag it so that its infection time can be recorded once it is hit.

4. Now set up the event queue. The queue will be kept in a binary tree structure, sorted by infection time. It is important to note that each oasis need only appear in the tree *once*; it is wasteful to keep infection events in the tree which correspond to second (or third, etc.) oasis hits. Due to this fact, the oasis objects themselves form the leaves of the tree: each contains its impending infection time and pointers to left and right children. In the front simulation, the event queue is set up as follows:

   (a) Determine the uninfected neighbors—that is, oases within a distance R_{cut}—of the first oasis which lies in the upper half of the first block in the bottom row. Since all of the oases in blocks in the bottom row are initially infected, these neighbors will be found in the second row of blocks. These blocks—and indeed all blocks in

the system besides the bottom row—are initialized *as needed*; that is, each block is initialized when an oasis within R_{cut} of it becomes infected. In the present case, two blocks will need to be initialized: the block directly above the first block in the first row, and either the second block in the second row or the last block in the second row (periodic boundary conditions are used in the direction perpendicular to the front propagation), depending on the position of the oasis.

(b) Once the uninfected neighbors are determined, generate the first passage times to these neighbors using (5.11) and place the oases into the tree structure sorted by infection time.

(c) For each remaining oasis in the bottom row of blocks, find the uninfected neighbors (generating the necessary blocks "on-the-fly") and then, for each neighbor, do the following: if the neighbor does not have an impending infection time, generate one and add the neighbor to the tree. If it already has an impending infection time, generate a new first passage time from (5.11) and compare the two; if the new time is less than the old one, remove the oasis from the tree, change its impending infection time, and add it back to the tree. At the end of this step, there exists a tree—sorted by infection time—consisting of all those oases within R_{cut} of at least one initially infected oasis.

For the infection time simulation, the queue is set up in a similar fashion, with the change that only the neighbors of the one initially infected oasis need to be found. Thus, at the end of this step, the event tree consists of all oases within R_{cut} of the initially infected oasis.

5. For the front simulation, initialize a set of population arrays to hold the number of infected oases in each coarse-graining block. Each array corresponds to a different coarse-graining length scale ξ and contains $L_\perp L_\parallel/\xi^2$ entries, one for each coarse-graining block in the system. These arrays must be kept in order to output the state of the coarse-grained front efficiently.

Once these steps are complete, the actual simulation can begin. Oases are infected one at a time; the set of steps for each infection event are as follows (see also Figure 5.12):

1. Remove the oasis with the smallest infection time from the event tree. Set the oasis to infected, and update the current time T to the infection time of the oasis. For the front simulation, update each coarse-grained block population array based on the location of the newly infected oasis. For the infection time simulation, check to see if the newly infected oasis

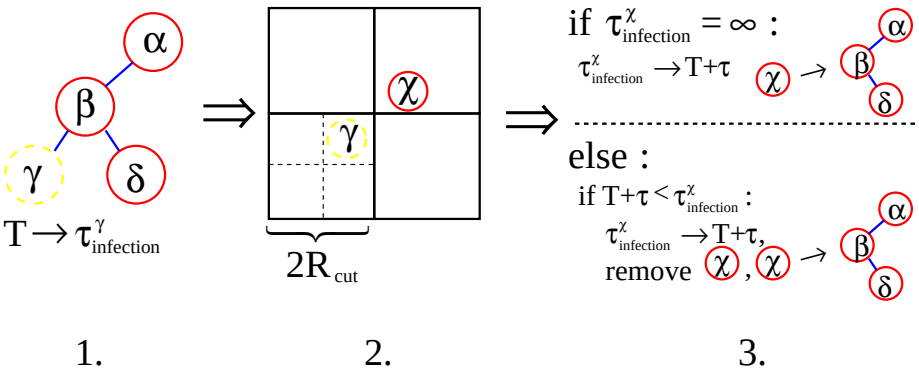

Figure 5.12: Schematic of the set of steps involved in each oasis infection event in the simulation of a large system in $d = 2$. The numbers correspond to the steps described on this page and the previous one; steps 4 and 5 are not depicted. The oases in the figure are labeled by Greek letters: oasis γ is the oasis being infected, and oasis χ is an uninfected neighbor of γ. Note that the blocks shown in 2. are the only blocks which must be searched for neighbors of γ, which is in the upper right hand quadrant of its block. The notation $\tau^{\chi}_{\text{infection}} = \infty$ is meant to indicate that χ does not yet have an impending infection time.

has been tagged as being close to one of the distances L_i from the start oasis. If it has, record the infection time.

2. Find the uninfected neighbors of the newly infected oasis, setting up blocks as needed. Only four blocks need be searched through: the block in which the newly infected oasis is located and the nearest three neighboring blocks to the newly infected oasis. These can be determined based on what quadrant of the current block the newly infected oasis is located in.

3. For each neighbor without an impending infection time, generate a first passage time τ from (5.11) with R given by the distance between the oases, and place the neighbor in the event tree with impending infection time $T + \tau$. For each neighbor *with* an impending infection time, generate a first passage time τ and compare $T + \tau$ with the existing impending infection time. If the new time is less than the old time, remove the oasis from the tree, change its impending infection time to $T + \tau$, and add it back to the tree. At the end of this step, the tree is correctly sorted.

4. Free the memory taken up by the newly infected oasis—it is not needed anymore.

5. For the front simulation, check to see whether the current time T is a multiple of the output period. If it is, compute the front roughness from (4.67) for each combination of ξ and λ and output the result.

This process repeats until an end condition is met. For the front simulation, the end condition is simple: once the first oasis in any of the blocks

in the top row is infected, the simulation ends. The end condition is different for the infection time simulation: all oases in all rings must be infected before the simulation can end. This condition presents some practical problems which serve to illuminate a few subtleties about the infection time not touched on in Section 4.4.2; in the next section, I will discuss some of these subtleties.

I have already remarked upon one obvious advantage of using a cutoff distance R_{cut}—namely, that the search for neighbors need only extend over a small subset of the oases in the system. There is one further advantage: because the oases can be created "on-the-fly" as the simulation proceeds and can be thrown away after they are hit, the amount of memory required by the simulation at any one time is less than the memory needed to store all oases. It is thus possible to go to very large system sizes without running out of memory.

A brief comment on the computational complexity of this algorithm: since each oasis must be addressed during the course of the simulation, there are $\mathcal{O}(L^2)$ steps required for a system of size L. Each step requires that the newly infected oasis' neighbors be found, a process which, while potentially very time-consuming, does not depend on L. However, each change to the event tree takes $\mathcal{O}(\log_2(N_{\text{tree}}))$ time, where N_{tree} is the number of events (uninfected oases with infected neighbors) in the event tree. This quantity obviously grows as the simulation proceeds (at least for the infection time simulation), but an upper limit can be obtained by taking it to be of $\mathcal{O}(L^2)$; thus, the simulation time scales with $L^2 \log_2(L)$.

5.3.3 Effects of Oasis Configuration on the Infection Time

In Section 4.4.2, I made predictions for the mean infection time—the time for a population to go from one oasis to an oasis located a distance L away—and for the fluctuations of the infection time. The mean infection time predictions can be found in (4.62), (4.63), and (4.64), while the prediction for the fluctuations in $T_{\text{infection}}$ is given in (4.65). In these expressions, the angle brackets denote averaging over *internal* noise—that is, averaging over different realizations of the infection process for the same oasis configuration. But what are the effects of different oasis configurations on the infection time distribution? How can these effects be taken into account? By considering the simplified model used in the simulations described in the previous section, it is easy to determine the nature and significance of these effects.

Consider the following situation: a system of oases is set up, a starting and target oasis are selected (separated by a distance L), and the system is allowed to evolve. According to (4.62), the time taken for the target oasis to be hit should be of the order L/L_0 if time is being measured in units of $\langle T(R_{\max})\rangle$, as it is in the simulations. Because the infection time is the minimum time

needed to get from the starting to the target oasis, it should be relatively insensitive to changes in the oasis configuration from realization to realization; a "bad link" will simply be shunted by neighbors, and will have little effect on the infection time. But what if the target oasis is isolated from the rest of the cluster—what if it is a "bad oasis?" The link to the target oasis cannot be overcome by neighboring links, and for this reason it should provide the dominant effect of disorder on the infection time distribution.

For the case of a bad target oasis, the mean infection time should be something like $(L/L_0) + \langle T(R_{\text{near}})\rangle$, where R_{near} is the distance from the target oasis to the nearest oasis on the current-carrying cluster which also contains the starting oasis. This "extra" time $\langle T(R_{\text{near}})\rangle$ can be considerable since the mean FPT between oases rises exponentially with distance. Still, as $L \to \infty$, this extra contribution to the time will become smaller and smaller compared to L/L_0; for this reason, the predictions made in Section 4.4.2 for the mean infection time—which are supposed to be valid for $L \gg L_0$—can be considered to be independent of oasis configuration. This is strictly true only in the limit $L \to \infty$, of course.

To see exactly how this might affect the results of the simulation, consider the following heuristic argument: assume that a given oasis chosen at random has a probability p_b to be a "bad" oasis isolated from the rest of the cluster. For a ring of radius L, there are $\simeq 4\pi nL\delta$ oases located within a distance δ of the ring, and a fraction p_b of them should be bad. The measured mean infection time—the average of the infection times to the oases in the ring—will really be an average over oasis configurations (or disorder) as well as over internal noise. I will denote this quantity by $\overline{\langle T(L)\rangle}$. Its value should be approximately

$$\overline{\langle T(L)\rangle} \simeq \langle T(L)\rangle + p_b\langle T(R_{\text{near}})\rangle, \tag{5.16}$$

where $\langle T(L)\rangle$ is the "true" configuration-independent value of the mean infection time (technically, the $L \to \infty$ limit of $\overline{\langle T(L)\rangle}/L$ times L). The fractional deviation of the measured mean infection time from the $L \to \infty$ configuration-independent value is thus:

$$\frac{\overline{\langle T(L)\rangle} - \langle T(L)\rangle}{\langle T(L)\rangle} \simeq \frac{\langle T(R_{\text{near}})\rangle}{\langle T(L)\rangle} \propto \frac{1}{L}. \tag{5.17}$$

As claimed, then, the contributions to the mean infection time stemming from a "bad" oasis become fractionally less important as L grows larger, justifying the neglect of oasis configuration effects in making the predictions of Section 4.4.2. To determine $\langle T(L)\rangle$ in the simulations, I simply averaged together the infection times from all oases in a ring, ignoring the effects of any possible "bad" oases.

What about the fluctuations of $T_{\text{infection}}$? The heuristic argument from above can be repeated, resulting in the following expression for the standard

deviation of $T_{\text{infection}}(L)$, which I will denote by σ_T:

$$\sqrt{\frac{\overline{{\sigma_T}^2} - {\sigma_T}^2}{{\sigma_T}^2}} \simeq \sqrt{p_b}\, \frac{\sigma_{T(R_{\text{near}})}}{\sigma_T} \propto \frac{1}{L^{1/3}}, \tag{5.18}$$

where $\sigma_{T(R_{\text{near}})}$ is the standard deviation of the FPT distribution for the last link. There are two important points to note here: first, as before, the $L \to \infty$ behavior is oasis configuration-independent, as expected. Second, the decay of oasis configuration effects on the quantity σ_T is very slow. This suggests that these effects might need to be taken into account in the simulations when measuring the fluctuations in $T_{\text{infection}}$; in the next section, I will discuss this further.

Everything that has been said about a bad target oasis also applies to a bad starting oasis. Thankfully, it is easy to rectify this problem in the infection time simulation: after the event tree has been set up and the simulation has begun, each new oasis is checked to see how far from the starting oasis it is located. Once an oasis beyond some distance of the order of R_{max} is hit, the simulation is restarted with that oasis as the new starting oasis. In this way, any potential large first steps are avoided. For the simulations I performed, I used $2R_{\text{max}}$ as my restart distance.

Besides possibly skewing the simulation results of the fluctuations in $T_{\text{infection}}$, the presence of "bad" target oases has one further effect on the infection time simulation: because events are executed in order, a bad oasis forces the simulation to run for a very long time in order for the end condition—all oases in all rings infected—to be met. This is problematic; to deal with this issue, uninfected oases in rings are periodically checked to see if they have any uninfected neighbors. If a particular oasis doesn't—which is often the case if it is isolated from the rest of the cluster—then clearly the impending infection time for that oasis will be the actual infection time, and the event can be executed "ahead of schedule."

5.3.4 Results of the Large System Simulations in $d = 2$

I will now present the results of the simulations described in the previous section, beginning with the front simulation. Recall from Section 4.5.2 that the RMS coarse-grained front roughness $\sqrt{\langle w^2(\Lambda,\tau)\rangle}$ is expected to follow the scaling form

$$\sqrt{\langle w^2(\Lambda,\tau)\rangle} = \Lambda^{\zeta} f\left(\frac{\tau}{\Lambda^z}\right), \tag{5.19}$$

where $\Lambda = L_\perp/\xi$ is the system width in units of the coarse-graining length scale ξ and $f(x)$ is some scaling function which goes as $x^{\zeta/z}$ for small arguments. The exponents ζ and z are expected to be $1/2$ and $3/2$, respectively, as in the Eden model.

The front simulation was run for various values of $L_\perp$ with $\kappa = 1.0$ and

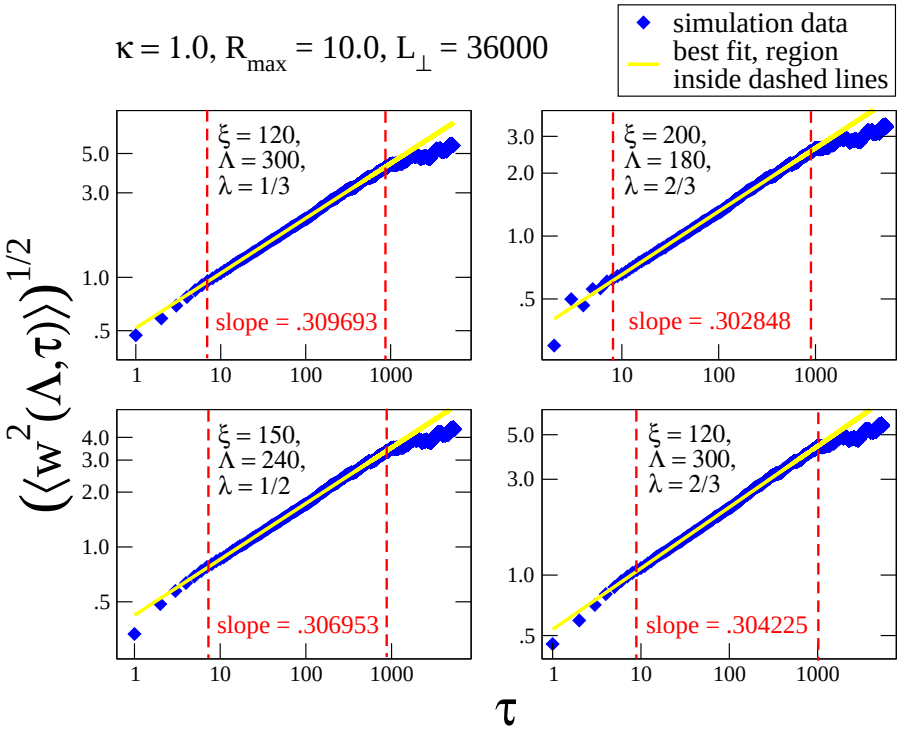

Figure 5.13: Graphs of the coarse-grained front roughness as a function of time (blue diamonds) for different values of the coarse-graining block size ξ and cutoff λ. The results are the average of 87 runs performed with $\kappa = 1.0$, $R_{\max} = 10.0$, and $L_\perp = 36000$. Best-fit lines for the regions between the dashed red lines are also shown, along with their slopes.

$R_{\max} = 10.0$, which is well within the hopping/low oasis density regime. For each value of $L_\perp$, a number of trials were performed in order to obtain a good value for $\langle w^2(\Lambda,\tau)\rangle$; for larger values of $L_\perp$, fewer trials were performed due to the longer time needed for each trial. Various coarse-graining scales ξ and cutoffs λ were used to measure $\sqrt{\langle w^2(\Lambda,\tau)\rangle}$. Unfortunately, it was impossible to run enough trials for long enough for enough values of $L_\perp$ to obtain decent steady state statistics (that is, to allow $f(x)$ to reach its $x \to \infty$ value), which would allow for a data collapse; thus, the exponents ζ and z could not be measured independently. However, by looking at the short-time behavior of $\sqrt{\langle w^2(\Lambda,\tau)\rangle}$, it was possible to determine the exponent $\beta = \zeta/z$, which is 1/3 for KPZ fronts in $d = 2$.

Figure 5.13 shows the front roughness averaged over 87 runs with $L_\perp = 36000$ on a log-log plot. It should be clear that the early-time behavior is indeed power-law, although, as in the Eden model, the *very* early time behavior is not as neat. By the end of the simulations, the roughness was clearly beginning to saturate, as can be seen by the flattening of the average roughness near the right edge of the graphs. To determine the exponent β, then, requires fitting the curves only at those times large enough for the very

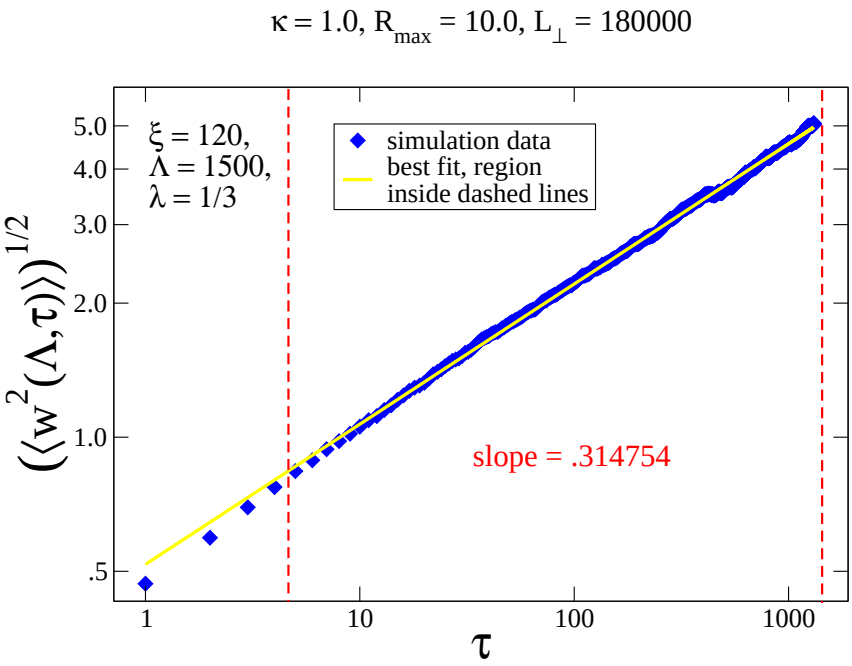

Figure 5.14: Graph of the coarse-grained front roughness as a function of time (blue diamonds) for $\xi = 120$ and $\lambda = 1/3$. The results are the average of 15 runs performed with $\kappa = 1.0$, $R_{\max} = 10.0$, and $L_\perp = 180000$. The best-fit line for the region between the dashed red lines is also shown, along with its slope.

early time effects to wear off but small enough for the finite-size effects to be negligible. I determined this region by inspection; the edges of the fitted regions are indicated by dashed red lines in the figure.

The best-fit values of β are reassuringly close to 1/3, and are, as expected, slightly lower than 1/3 due to the effects of the intrinsic width discussed in Chapter 3. Moreover, the specific choice of cutoff and coarse-graining block size seems to be unimportant, though of course a value of $\xi \gg L_0$ *would* change the nature of the coarse-grained front, as would a value of λ near 1. But for $\xi = \mathcal{O}(L_0)$, it appears that the arguments presented in Section 4.5.2 are correct: the coarse-grained front is in the KPZ universality class. To confirm this, however, it would be useful to look at a larger system.

Figure 5.14 shows the results of 16 runs conducted at a much larger system size, $L_\perp = 180000$, with $\xi = 120$ and $\lambda = 1/3$. At this system size, the front does not "see" the finite-size effects at any point during the course of the simulation; for this reason, only the very early time data points were excluded from the fit. The fitted value of $\beta = .314754$ is even closer to the expected value of 1/3 than the fits for the smaller system size, which is not surprising given the decreasing importance of the intrinsic width as system size increases.

The infection time simulation was significantly easier to perform than the front simulation, since only one run was needed for each parameter set to obtain good results. Recall from Section 4.4.2 that the first passage time to an

oasis a distance L away is expected to be of the order

$$\langle T_{\text{infection}}(L)\rangle \simeq \frac{L}{L_0}\langle T(R_{\max}, a)\rangle; \tag{5.20}$$

in the simulation units, this translates to

$$\langle \tau_{\text{infection}}(L)\rangle \simeq \frac{L}{L_0}. \tag{5.21}$$

Recall that $\tau = t/\langle T(R_{\max}, a)\rangle$; that is, time is measured in units of the time to cross a link of size $R_{\max}$.

According to (5.21), a plot of $\langle \tau_{\text{infection}}(L)\rangle$ vs. L/L_0 should have slope of $\mathcal{O}(1)$. Furthermore, the slope should only depend on κ and $R_{\max}$ through the combination $\kappa R_{\max}$. The reason for this is as follows: imagine stretching out the space inhabited by a set of oases by some scaling factor ℓ while at the same time reducing κ by a factor $1/\ell$. Under this scaling, the product $\kappa R_{\max}$ remains constant, and the FPT PDF between oases—given by (5.11)—remains unchanged. (This is assuming that $n \ll 1/a^2$; that is, the oases are much further apart, on average, than their radii. For the point oases of the simulations, this is always the case.) The average time to cross a correlation length-sized block does not change at all, but the size of the block does get scaled by a factor ℓ. This means that two systems with the same $\kappa R_{\max}$ will have the same infection time properties so long as space is measured in units of L_0 in each system. Thus one can write:

$$\langle \tau_{\text{infection}}(L)\rangle = \frac{L}{L_0} F(\kappa R_{\max}), \tag{5.22}$$

where $F(\cdot)$ is some function of order unity.

Figure 5.15 shows the results of the infection time simulation for various values of κ and $R_{\max}$. The infection time is indeed of order L/L_0, which suggests that the picture of transport put forth in Chapter 4 is correct: links of size $\simeq R_{\max}$ serve to limit the propagation of the population through space, and these links are separated by a typical distance of order L_0. There are a few additional things to note about the data in Figure 5.15. First, the two data sets with $\kappa R_{\max} = 12.0$ are indeed on top of one another, as expected. Second, the data sets for the largest values of $\kappa R_{\max}$ are incomplete. This is due to the fact that it was not possible to allow some oases from the rings at those values of L to be infected before the simulation was forced to end for practical reasons; rather than report average values of $\tau_{\text{infection}}$ without all infection times from all oases in the rings, I simply omitted those data points from the graph. It is not surprising that this effect should be more pronounced at larger values of $\kappa R_{\max}$: as $\kappa R_{\max}$ increases, off-cluster target oases take exponentially longer to be infected. Again, in the limit of $L \to \infty$, the effects of these bad oases should be negligible.

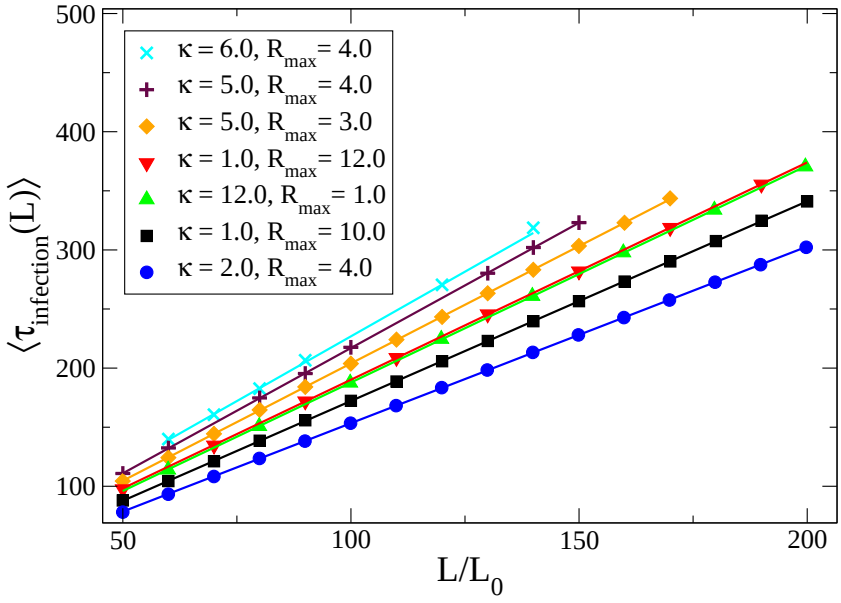

Figure 5.15: Plot of the mean infection times to various distances for different values of κ and $R_{\max}$. Every other data point marker has been removed from each of the two $\kappa R_{\max} = 12.0$ sets for visibility.

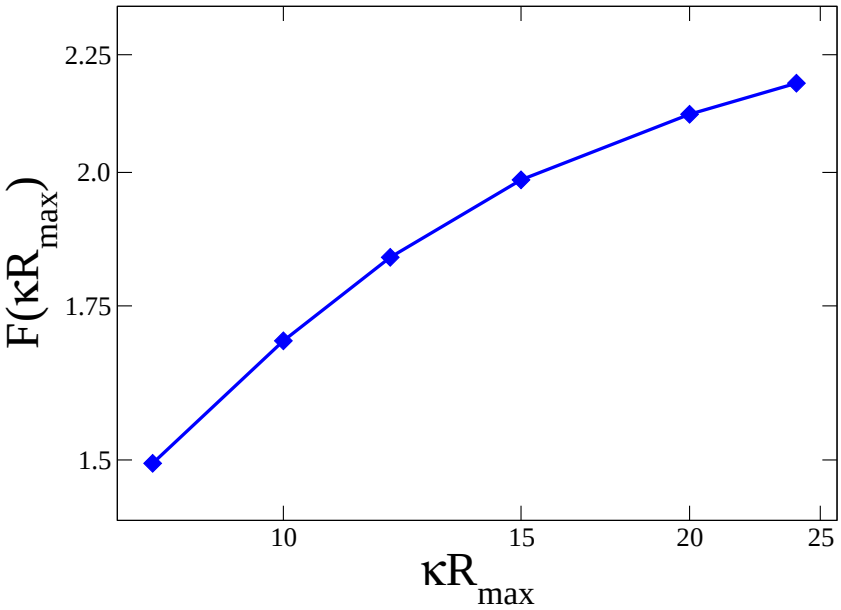

Figure 5.16: Plot of the function $F(\kappa R_{\max})$ as determined by the best-fit lines to the data in Figure 5.15.

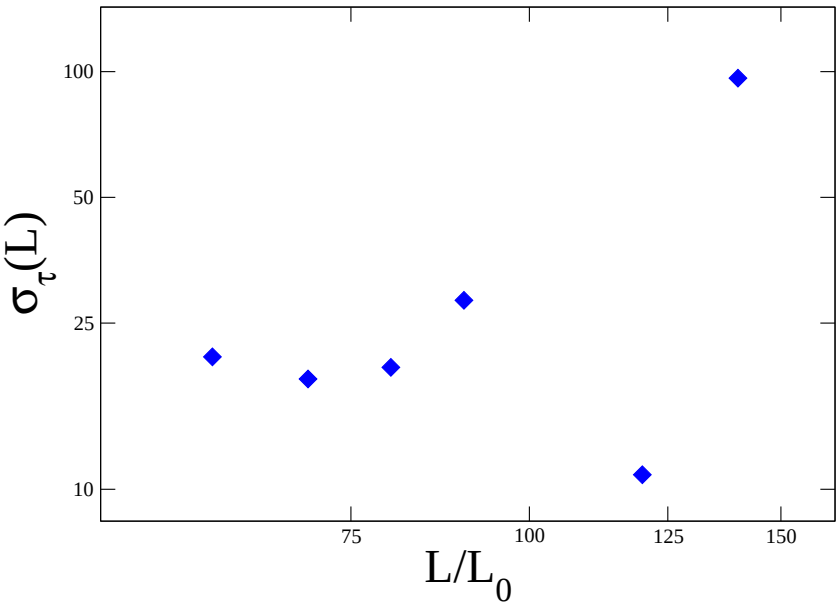

Figure 5.17: Plot of the fluctuations about the mean infection time versus L/L_0 for $\kappa = 6.0$, $R_{\max} = 4.0$.

The function $F(\kappa R_{\max})$ is simply equal to the slope of the $\langle \tau_{\text{infection}}(L) \rangle$ versus L/L_0 curve. Figure 5.16 shows the measured values of $F(\kappa R_{\max})$ from Figure 5.15 plotted versus $\kappa R_{\max}$. Note that $F(\kappa R_{\max})$ grows with increasing $\kappa R_{\max}$. This can be explained by noting that, as $\kappa R_{\max}$ rises, the correlation length L_0 also rises; thus, there are more smaller links in a correlation-length sized box for larger values of $\kappa R_{\max}$. However, what is significant is that $F(\kappa R_{\max})$ is of order 1.

It should be clear that the mean infection time behaves as expected; what about the fluctuations? As mentioned in Section 5.3.3, any "bad" oases should affect the quantity $\sigma_T(L)$ (and thus $\sigma_\tau(L)$, the fluctuations measured in the simulation units of time) more than they affect $\langle T_{\text{infection}} \rangle$ at a given value of L, and the simulation data bears this out. Figure 5.17 shows a plot of the measured values of $\sigma_\tau(L)$ versus L for $\kappa = 6.0$, $R_{\max} = 4.0$. The pattern in the data is difficult to discern, and it seems impossible to test the $\sigma_\tau(L) \sim L^{1/3}$ prediction of Section 4.4.2 with such noisy data.

The source of the noise is indeed the presence of "bad" oases, as can be seen in Figure 5.18, which shows a normalized histogram of the infection times to the furthest distance ($L/L_0 = 140$) shown in Figure 5.17. Note the two red circles around the spikes at large τ: these two spikes correspond to "bad" oases whose infection times greatly skew the measured value of $\sigma_\tau(L)$. Ideally, one would simulate a very large system so that these effects could be minimized; however, in the present case I will simply remove the data points corresponding to the "bad" oases. To reiterate: the effects of these oases are legitimate, but I am interested in the asymptotic scaling of $\sigma_\tau(L)$ as $L \to \infty$,

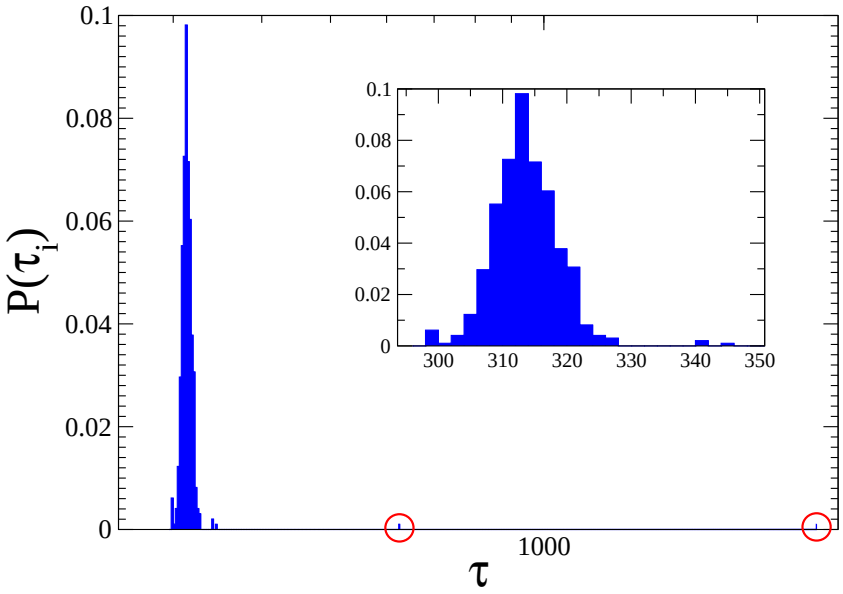

Figure 5.18: Histogram of infection times to the distance $L/L_0 = 140$, taken from the same simulation data that produced Figure 5.17 Note the two spikes at large times which drive up $\sigma_\tau(L)$.

which is not affected by oasis configuration effects.

How to determine which data points to remove? This is, of course, a highly contentious subject, but in the present case the outliers seem so obvious that any reasonable criterion should work. Perhaps the easiest criterion to implement is Chauvenet's criterion, which is usually used to decide whether or not to reject a single spurious measurement [81]. It is not totally appropriate for cases in which there are multiple measurements which may be omitted, but I have used it regardless; again, the "bad" data points are, for the most part, obvious enough that any reasonable criterion should prune them out. (Peirce's criterion [82] is more appropriate for the case of pruning multiple data points, but it is significantly harder to implement.) Chauvenet's criterion can be stated as follows: for a given set of data of size N (N runs) taken from a normal distribution with mean μ and standard deviation σ, a data point with value x can be discarded if the probability of attaining that value or higher times N is below $1/2$. In other words, if the data point is extreme enough that one would expect to see a value that high less than one half of one time on average for a set of N runs, the data point is discarded.

To eliminate unwanted points from the simulation data, I began by applying Chauvenet's criterion to the largest infection time in each set of infection times; if it was sufficiently extreme, the point was eliminated and the mean and standard deviation of the set were recalculated. This was repeated until no more points fit the criterion.[3] Figure 5.19 shows the simulation values

[3]It should be stressed that this is *not* usually the proper way to apply Chauvenet's criterion, as it can remove data which is evidence of a real effect. In the present case, however, that is

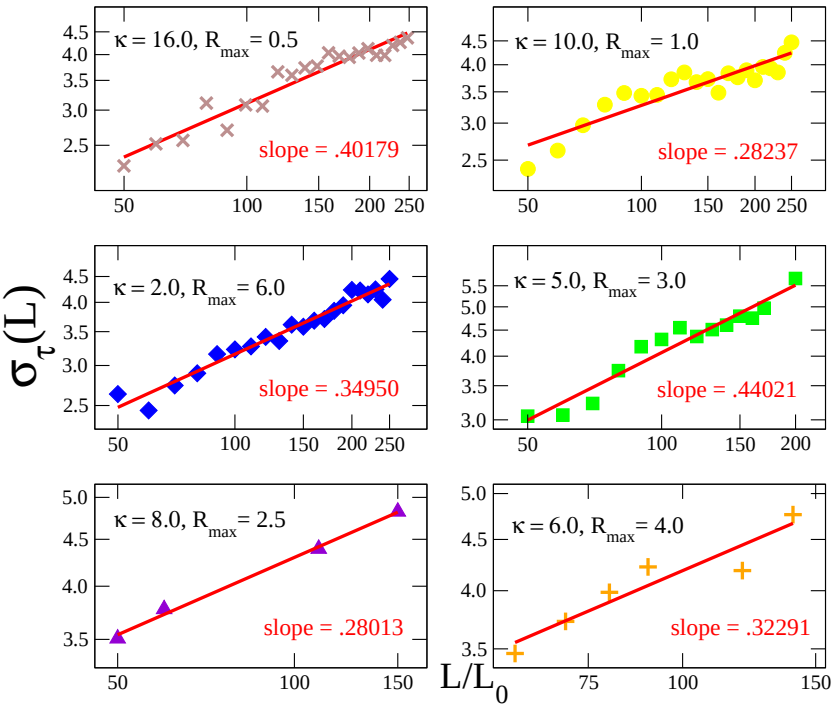

Figure 5.19: Plots of $\sigma_\tau(L)$ vs. L/L_0 for different values of κ and $R_{\max}$. The graph in the lower right hand corner is the "fixed" version of Figure 5.17.

of $\sigma_\tau(L)$ versus L—with large values of the infection time taken out in the manner described above—for various values of κ and $R_{\max}$. As before, the missing data points are due to rings which contained oases which could not be hit by the end of the simulation. Although these values would almost certainly be taken out by the application of Chauvenet's criterion, the times for these rings were not output at all by the simulation; hence, these points are simply missing.

The conclusions that can be drawn from Figure 5.19 are murky: it seems plausible that $\sigma_\tau(L)$ could grow as $L^{1/3}$ for large L, but it is not totally clear from the data. The data is certainly not *inconsistent* with that prediction, but it does not confirm it, either. To resolve this ambiguity through simulation would require simulating infection times to much larger distances L. However, as the simulation time grows roughly as $L^2 \log_2(L)$, this is not feasible.

5.4 Summary

In this chapter, I have presented the details of and results from three simulations designed to test the predictions made in Chapter 4. The first simulation is built around a simple kinetic Monte Carlo algorithm, and seeks

precisely what I am trying to do: I know that there are "bad" oases driving up the fluctuations in the infection time, and I *want* to remove their effects from the data. Hence, a liberal application of Chauvenet's criterion, which would usually be improper, is wholly warranted.

to determine whether the linear model with a source introduced in Section 4.3.2 accurately captures the first passage properties of the full model with competition. In Section 5.2.3, I showed that the linear model does accurately predict these first passage properties—namely, the exponential rise of the mean FPT with oasis separation and the asymptotic nature of the FPT PDF. However, the parameter g which appears in the linear model cannot be determined by matching mean-field solutions when the competition rate b is high.

In Section 5.3, I described two simulations designed to test the predictions made in Sections 4.4 and 4.5 for a system in two dimensions comprised of many oases. The two simulations share the same basic algorithm, described in detail in Section 5.3.2. The first simulation involves a front moving through a large system in $d = 2$. In Section 4.5.2, I claimed that a coarse-grained version of this front should be governed by the KPZ equation, and should thus have a roughness exponent $\beta = 1/3$ in $d = 2$. In Section 5.3.4, I presented the results of the front simulation, which confirm this prediction.

The second simulation described in Section 5.3.2 is designed the test the predictions for the mean infection time $\langle T_{\text{infection}}(L)\rangle$ and the fluctuations about this mean. In Section 5.3.4, I presented compelling evidence from this simulation that the mean infection time is indeed dominated by the time needed to cross links of size $R_{\max}$, but the results for the fluctuations of $T_{\text{infection}}$ are more ambiguous.

6 First Passage Percolation and the Contact Process

In the previous two chapters, I explored a particular reaction-diffusion model with disorder in the reaction rates using a variety of analytical and numerical tools. In order to simulate this model, it was necessary to make certain simplifications, as detailed in Section 5.3.1. The simplified model, which consists of points between which first passage times are picked from an exponential distribution whose mean depends on oasis separation, should capture the properties of the full model in the regime I have been studying—namely, the regime of low oasis density.

However, the simplified model is more than just an approximation that makes simulation easier; it is itself a new stochastic model somewhat related to—though in some ways quite distinct from—the Euclidean FPP discussed in Chapter 3. Additionally, just as the lattice Eden model can be made into the contact process through the introduction of a death process, so too can this new model be turned into an off-lattice version of the contact process by allowing the points to become unoccupied after being infected. In this chapter, I will discuss the simplified model as both a new kind of off-lattice FPP and as an off-lattice version of the contact process. In each case, I will present both analytic predictions and simulation results.

6.1 Off-Lattice First Passage Percolation

6.1.1 Introduction to the Model

The simplified model used in the simulations discussed in Chapter 5 is itself an interesting subject for study. The model consists of sites[1] randomly placed in $d = 2$ between which first passage times are assigned. For a pair of sites separated by a distance R, the first passage time is chosen from the distribution given by

$$f_N(R,\tau) = \sqrt{\frac{R_{\max}}{R}}\, e^{-\kappa(R-R_{\max})}\, \exp\left[-\sqrt{\frac{R_{\max}}{R}}\, e^{-\kappa(R-R_{\max})}\, \tau\right]. \qquad (6.1)$$

[1] For this chapter, I will cease discussing "oases," instead referring to the points which can be occupied as "sites." This change in nomenclature is meant to reinforce the notion that the model being studied in this chapter, though inspired by the model of Chapters 4 and 5, is its own entity.

As discussed in the last chapter, this model works as an approximation for the oasis problem for the case of low oasis density ($\kappa R_{\max} \gg 1$).

In this section, I will explore the behavior of this model for all values of $\kappa R_{\max}$, as well as for different powers of the prefactor. That is, I will consider rate functions of the form

$$r(R) = \left(\frac{R_{\max}}{R}\right)^{\alpha} e^{-\kappa(R-R_{\max})}, \tag{6.2}$$

where α is allowed to take any nonnegative value. Passage times between sites are then chosen from $f_N(R,\tau) = r(R)e^{-r(R)\tau}$. I will show that there are two distinct kinds of transport that take place depending on the values of $\kappa R_{\max}$ and α: for large $\kappa R_{\max}$ or large α (or large values of both parameters), the rate of transport is limited by the links of size $R_{\max}$ which must be crossed, and so large leaps are not common. In this regime, the underlying structure of sites is very important in determining the infection time. This is the kind of hopping behavior studied in the last two chapters. When both parameters are small, however, the transport is mediated by large leaps of size $> R_{\max}$, and the underlying structure of the cluster is relatively unimportant—that is, the length scales $R_{\max}$ and L_0 cease to have much importance.

6.1.2 Analytical Predictions

I will first examine the system in the hopping regime—large $\kappa R_{\max}$ or large α or both. Site separations of $\simeq R_{\max}$ should dominate the infection time in the hopping regime, and so the only quantity that needs to be determined in order to make a prediction for the infection time is the correlation length L_0, which serves as an order of magnitude estimate of the separation of the rate-limiting links. In order to determine L_0, it is necessary to use the Shklovskii argument presented in Section 4.4.1: links with first passage times larger than $\simeq e\langle T(R_{\max})\rangle$ will in all likelihood be shunted by smaller links, and so the correlation length should be roughly equal to that of the spanning cluster which includes such links as its largest members. The size R_{large} of such links can be determined by solving the transcendental equation

$$\alpha \log\left(\frac{R_{\text{large}}}{R_{\max}}\right) + \kappa\left(R_{\text{large}} - R_{\max}\right) = 1. \tag{6.3}$$

Using $R_{\text{large}} = R_{\max}(1+\delta)$, this can be rewritten as

$$\alpha \log(1+\delta) + \kappa R_{\max}\delta = 1. \tag{6.4}$$

Since δ should be small, this can be solved, leading to the approximation

$$R_{\text{large}} \simeq R_{\max}\left(1 + \frac{1}{\alpha + \kappa R_{\max}}\right), \tag{6.5}$$

which, when used together with (4.55) gives:

$$L_0 \sim (\alpha + \kappa R_{\max})^{\nu} . \tag{6.6}$$

Various numerical prefactors have been removed from this expression, and it of course is unitless. To get a numerical estimate for L_0, it is necessary to multiply by a length scale—namely, $n^{-1/2}$:

$$L_0 \simeq \frac{(\alpha + \kappa R_{\max})^{\nu}}{n^{1/2}}. \tag{6.7}$$

Note that this expression agrees with (4.59) for the limit $\kappa R_{\max} \gg \alpha$, as was the case in the last two chapters, when $\alpha = 1/2$ and $\kappa R_{\max} \gtrsim 10$.

With this expression in hand, it is possible to make an order of magnitude prediction for the infection time as a function of site separation L in the limit of large L:

$$\langle \tau_{\text{infection}}(L) \rangle \simeq \frac{L}{L_0}, \tag{6.8}$$

or, with all factors written out,

$$\langle \tau_{\text{infection}}(L) \rangle \simeq \frac{L\, n^{1/2}}{(\alpha + \kappa R_{\max})^{\nu}}. \tag{6.9}$$

Recall that time is being measured in units of the time needed to cross a link of size $R_{\max}$.

What about the small α and small $\kappa R_{\max}$ behavior? The key feature of the transport in this regime is the fact that the largest leaps of size $R_{\max}$ are no longer rate-limiting; the minimizing path will in general include many large leaps of size $> R_{\max}$. It is actually quite difficult to attain a good estimate—or even scaling argument—for the leap size, and thus the velocity, in this regime. This difficulty can be understood best by thinking of the wave-like nature of the advancing front of occupied sites: contrary to the case of large α or large $\kappa R_{\max}$, the front advances not when the rate-limiting site separations of size $R_{\max}$—which are necessarily at the edge of the front—are finally crossed, but instead when leaps which may originate in the *interior* of the infected region are made. A somewhat useful analogy may be to the case of pushed fronts in RD models [39]. In pushed fronts, the growth behind the front causes the motion of the front ("pushes" the front forward) rather than the growth at the edge (as in pulled fronts). As a result, the front speed may be much higher than the spreading speed of small perturbations to the unstable state, and is quite hard to predict analytically.

Nonetheless, it is possible to obtain an estimate of the infection time using a somewhat heuristic method. Consider the rough picture of transport in the small α and small $\kappa R_{\max}$ regime depicted in Figure 6.1: the population spreads out from the starting site in a front moving with velocity v_s. After

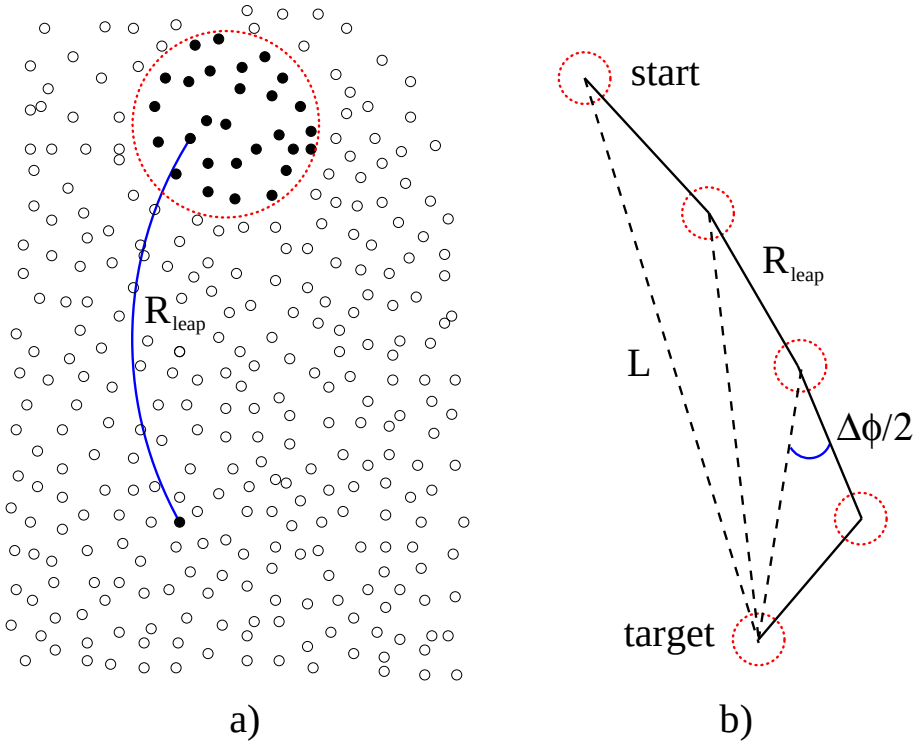

Figure 6.1: a) Rough picture of transport in the small $\alpha + \kappa R_{\max}$ regime: the population spreads out with some velocity v_s, and after some time a large leap is made to a faraway site. The dark circles denote infected sites, the open circles uninfected sites, and the large red circle is the border between the two kinds of sites. b) Picture of transport on a larger scale. The minimizing path includes leaps which deviate from a straight-line path to the target by no more than some angle $\Delta\phi/2$.

some characteristic time, a large leap of size R_{leap} is made from somewhere in the ball of occupied sites to a distant site, and a new ball starts growing. This process repeats, and space is eventually filled by these growing balls of infected sites. Now consider two sites separated by a large distance L: the transport between these two sites can be thought of as being mediated by a series of large leaps, with each leap being in the general direction of the target site. This is depicted in Figure 6.1b. If the typical leap deviates from the straight line to the target by an angle $\Delta\phi/2$, then the infection time is given approximately by

$$\langle \tau_{\text{infection}}(L) \rangle \simeq \frac{\tau_{\text{leap}} L}{R_{\text{leap}} \cos(\Delta\phi/2)}. \tag{6.10}$$

The time τ_{leap} in this equation is the typical time one would have to wait for a leap of size $\geq R_{\text{leap}}$ that deviates from a straight line path to the target site by no more than $\Delta\phi/2$. In order to obtain a value for $\langle \tau_{\text{infection}}(L) \rangle$, it is necessary to estimate v_s, determine τ_{leap} as a function of R_{leap} and $\Delta\phi$, and then minimize (6.10) with respect to $\Delta\phi$ and R_{leap}. This procedure is explained in detail in Appendix C, and the results of this method are compared with simulation results in the next section.

Thus far I have been presenting analytical predictions for the infection time, but it would be good to restate these predictions in terms of the time constant from the theory of first passage percolation. Recall from Chapter 3 that the time contant μ for off-lattice FPP is defined as

$$\mu = \lim_{L \to \infty} \frac{T_{\text{infection}}}{L}. \tag{6.11}$$

The results of this section can be expressed in terms of the time constant as follows: for $\kappa R_{\max} + \alpha \gg 1$, $\mu \simeq n^{1/2}/(\kappa R_{\max} + \alpha)^{4/3}$, where n is the number density of sites and time is measured in units of time needed to cross a link of size $R_{\max}$. For the case where $\kappa = 0$ and $\alpha \gg 1$, this result should actually apply to the Euclidean FPP studied by Newman *et. al* [60, 61]. In their model, the density n is fixed at 1 and time is not scaled; thus, $\mu \simeq [(B_c/\pi)^{\alpha/2}]/\alpha^{\nu}$. For small $\kappa R_{\max} + \alpha$, there is not such a nice closed-form expression, but it is possible to arrive at a numerical estimate by making some basic assumptions about the nature of transport.

There is one further statement that can be made: for any $\kappa > 0$, $\mu > 0$; but for $\kappa = 0$, $\mu = 0$ for $\alpha \leq 2$. This is due to the fact that, for $\alpha \leq 2$ and $\kappa = 0$, the total rate for an infected site to infect *any* other site diverges:

$$r_{tot} = \sum_i \left(\frac{R_{\max}}{R_i} \right)^{\alpha} \simeq 2\pi n {R_{\max}}^{\alpha} e^{\kappa R_{\max}} \int_0^{\infty} dR\, R^{1-\alpha}. \tag{6.12}$$

(Of course, this integral diverges at 0 for $\alpha \geq 2$, but this is just an artifact of the approximation of the sum in (6.12) by this integral.) Thus, the starting site infects some other site in some arbitrarily small amount of time, that site

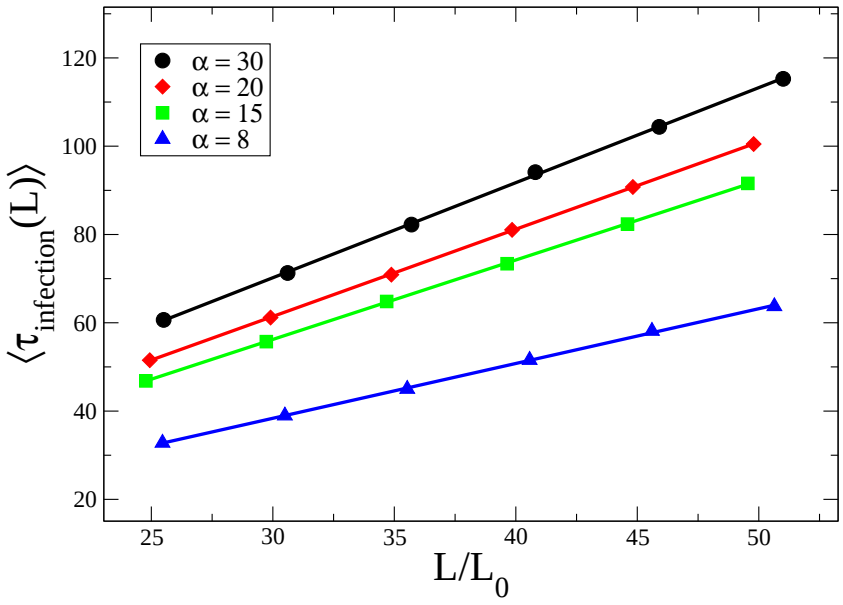

Figure 6.2: Plot of the mean infection times to various distances for different values of α with $\kappa = .4$, $R_{\max} = 1.0$.

infects some other site in an arbitrarily small amount of time, and so on.

6.1.3 Simulation Results

There are two predictions that need to be tested: first, the large α, small $\kappa R_{\max}$ hopping behavior needs to be confirmed. Second, the numerical estimates for the infection time in the small $\kappa R_{\max} + \alpha$ regime obtained from the method described in the last section and in Appendix C need to be checked. The simulation used to test these predictions is the same one described in detail in Section 5.3.2.[2]

The first set of results, which is for the case of large α, is shown in Figure 6.2. Because of the site configuration effects discussed in Section 5.3.3, it was necessary to "treat" some of this data by removing anomalously large infection times in the manner described in Section 5.3.4. As stressed in that section, these effects are "real" in the sense that they are due to a real phenomenon—sites that are isolated from the rest of the cluster—but they should diminish in significance as $L \to \infty$. As it is the $L \to \infty$ behavior of the infection time that I am interested in, I have removed these data points. The resulting data clearly confirms the "hopping" picture of transport and the expression for L_0 given in (6.7): the slopes of the best-fit lines through the data are all of order 1, as expected.

[2] Actually, there is one small difference: the blocks used to shorten the search for neighbors are of size R_{cut} in the present case, and all nine blocks near an site are searched for neighbors. This is in contrast to the simulations presented in Chapter 4, which used a block size of $2R_{\text{cut}}$ but only searched over four neighboring blocks. The "new" method, all other things being equal, should speed up the neighbor search by a factor of 16/9.

Table 6.1: Table comparing simulation results for the time constant μ to the predictions from the heuristic leaping model introduced in the last section.

$\kappa, R_{\max}, \alpha$	μ_{sim}	μ_{theor}	R_{leap}	τ_{leap}	v_s
$0.25, 1.0, 0.5$	.0014083	.0048490	13.8716	.057824	57.0068
$0.5, 1.0, 0.5$	.0066808	.0334923	7.17501	.206502	12.9397
$1.0, 1.0, 0.5$	.026591	.176645	3.94241	.60454	3.77136
$0.3, 1.0, 2.5$	.023188	.244048	6.89319	1.45952	2.46042

The second set of results, which is for the small $\kappa R_{\max} + \alpha$ regime, is shown in Table 6.1. For each $\kappa R_{\max}, \alpha$ pair, the table lists the value of μ obtained from fitting the $\langle \tau_{\text{infection}}(L) \rangle$ versus L simulation data to a straight line (the slope of this line is μ) and the value of μ obtained from the method described in the previous section and in Appendix C. Also listed are the leap size R_{leap}, leap time τ_{leap}, and front velocity v_s obtained from this method (see Appendix C for details).

The performance of the "leaping" method is clearly somewhat lacking, though not terrible: for each parameter set, the method manages to provide an estimate for μ within about an order of magnitude of the simulated value. The fact that the estimate is consistently too high suggests that the errors associated with taking each leap to be of size R_{leap} and taking each leap to be off-target by an angle $\Delta\phi/2$—errors that tend to lead to an overestimate of the infection time—are more significant than the error associated with using a value of v_s that is almost assuredly too high (see Appendix C).

The somewhat poor performance of the leaping method speaks to the difficulty of estimating the front velocity of pushed fronts. Still, the method at least offers a means of obtaining a ballpark figure of the infection time (or time constant), and also provides an intuitive picture of the nature of transport for the case of small $\kappa R_{\max} + \alpha$.

6.2 The Off-Lattice Contact Process

6.2.1 Introduction to the Model

If the lattice sites in the Eden model are allowed to "die"—that is, to become unoccupied after being occupied—the resulting stochastic process is simply the contact process (CP). It is possible to include a death event in the off-lattice FPP model discussed in the last chapter and the first part of this chapter: upon becoming infected, a lattice point can die with rate γ (the process is taken, as always, to be a Poisson process).

It should be clear that, as γ is raised, the system will eventually be unable to support a stable population, and will undergo a transition to the absorbing state. Given the disorder in the system (the random placement of sites), it

seems natural that this transition should be in the same universality class as the active to absorbing state transition in the disordered lattice CP models discussed in Section 2.2.2. This conjecture can be supported by appealing to a recent classification of phase transitions in the presence of quenched disorder proposed by Vojta [83, 84]. This classification suggests that if the effective dimension d_{eff} of the rare disordered regions is equal to the lower critical dimension of the model without disorder, then the transition in the presence of disorder should be controlled by the strong disorder fixed point mentioned in Chapter 2. The off-lattice CP model can be thought of as a lattice CP model (with exponentially decaying interactions with all other lattice sites) with sites randomly pushed out of place. The rare disordered regions have $d_{\text{eff}} = 0$, which is the same as the lower critical dimension of the contact process; thus, the model's critical behavior should be the same as that of the disordered lattice CP. In this section, I will explore the ramifications of this conjecture for the critical properties of the model and present some simulation results which support this conjecture.

Before doing so, however, it is necessary to introduce one small modification to the model: rather than using the rate function (6.2) to pick transit times between sites, I will use

$$r(R) = \min\left\{\left(\frac{R_{\max}}{R}\right)^{\alpha} e^{-\kappa(R-R_{\max})}, \left(\frac{R_{\max}}{2a}\right)^{\alpha} e^{-\kappa(2a-R_{\max})}\right\}, \qquad (6.13)$$

where a is some small length. This is effectively the same as giving the sites a finite radius a and setting the hopping rate between all pairs of overlapping sites to the same value $r_{\max} = r(2a)$. The reason for this modification mostly has to do with speeding up simulations, and so I will discuss it in Section 6.2.3.

6.2.2 Analytical Predictions

Recall from Section 2.2.2 the details of the diluted contact process on a lattice: each infected site can infect a neighboring uninfected site with a rate $\lambda/2d$, and can die out at some rate μ; disorder is introduced by the removal of a fraction p of sites. The model is thus characterized by two quantities: the ratio λ/μ and the fraction of sites removed p. The transition of interest occurs as λ is lowered (or, equivalently, as μ is raised) for $p < p_c$, where p_c is the percolation threshold. This transition is characterized by logarithmically slow critical dynamics and a large Griffiths phase below the critical point in which the dynamics are governed by nonuniversal (parameter-dependent) power laws—that is, the relaxation to the absorbing state is algebraic. For smaller values of λ, the relaxation to the absorbing state is exponential.

For the off-lattice contact process, the relevant quantities that characterize the system are:

1. The dimensionless product $\kappa R_{\max}$.

2. The prefactor power α.

3. The modified death rate γ', defined as the death rate γ divided by the rate to cross a link of size $R_{\max}$; that is,

$$\gamma' = \gamma {R_{\max}}^{\alpha} e^{\kappa R_{\max}}. \tag{6.14}$$

   This is really nothing more than the death rate measured in the units of time that I have been using throughout this chapter.

4. The length a.

There is one more quantity of interest: the average total infection rate $r_{\rm tot}$ for a site; that is

$$\begin{aligned} r_{\rm tot} &= 2\pi n \int_0^\infty dR\, R\, r(R) \qquad (6.15) \\ &= B_c\, e^{\kappa R_{\max}} \left[\left(\frac{R_{\max}}{2a} \right)^{\alpha-2} e^{-2\kappa a} + 2(\kappa R_{\max})^{\alpha-2} \Gamma(2-\alpha, 2\kappa a) \right], \end{aligned}$$

where $\Gamma(\cdot,\cdot)$ is the incomplete gamma function. This total rate is analogous to the rate λ in the lattice CP, and thus it should be expected that the critical death rate γ_c' should be of order $r_{\rm tot}$. The ratio $r_{\rm tot}/\gamma'$ in the off-lattice CP model plays the role of λ/μ in the lattice CP model. For the remainder of this section, I will assume that the critical point is reached by tuning γ' while keeping all other quantities the same.

At this point it is necessary to define some of the quantities whose critical and sub-critical behavior is of interest and to give their known behavior in the disordered contact process. There are typically two initial conditions used when studying the disordered CP: a fully occupied lattice and a single infected site. Since I will be performing simulations starting from a small set of occupied sites (similar to the second scenario), I will define the quantities associated with spreading. First, there is the mean number of particles $N(\tau) \equiv \langle n(\tau) \rangle$, where $n(\tau)$ is the total number of occupied sites at time τ in a given trial and the averaging is over trials. In the active phase, $N(\tau) \to \infty$ as $\tau \to \infty$, while in the absorbing phase $N(\tau) \to 0$ at large τ. In the Griffiths regime of the absorbing phase, $N(\tau) \sim \tau^{-\zeta}$ for large τ, where ζ depends on the parameters of the model [28]. At the critical point, $N(\tau) \sim \log[\tau/\tau_0]^{\bar\theta}$, where τ_0 is some nonuniversal time scale [30].

The other important measure is the survival probability $S(\tau)$, which is simply the probability that the system is still active after a time τ; clearly, $S(\tau) \to 0$ as $\tau \to \infty$ in the absorbing phase, while $S(\tau) > 0$ as $\tau \to \infty$ in the active phase. In the Griffiths portion of the absorbing phase, $S(\tau) \sim \tau^{-\phi}$ for large τ, where ϕ is a parameter-dependent power law.[3] At criticality, $S(\tau) \sim \log[\tau/\tau_0]^{-\bar\delta}$ [30].

[3] I have slightly oversimplified things here: the decay of $S(\tau)$ in the Griffiths phase is power

I expect that this same behavior should be found in the off-lattice contact process with the same critical exponents, provided that $\kappa > 0$ or $\alpha > 2$. If both of these conditions are violated, then the system should only exhibit an active phase since $r_{\text{tot}} = \infty$.

6.2.3 Simulating the Off-Lattice Contact Process

The simulation of the off-lattice contact process proceeds in the same basic way as the infection time simulation of Chapter 5 and the off-lattice FPP simulation of earlier in this chapter save for a few modifications:

1. When a site is infected, a death time τ_{death} is picked from the distribution $\gamma' e^{-\gamma'\tau}$. The site is then kept in the queue (search tree) along with the uninfected sites with impending infection times. When generating transit times to uninfected sites, the proposed times are checked against τ_{death}; if they are greater than τ_{death}, they are rejected.

2. When a site dies, its infected neighbors generate infection times to that site, and the lowest one is picked (unless each proposed infection time is greater than its source's death time, in which case the just-deceased site has no impending infection time and is removed from the tree).

3. It is not possible to "throw away" information about infected sites since they can die out and become reinfected. Thus, it is necessary to hold in memory at all times *all* sites that have been set up.

These modifications serve to slow down the simulation of the off-lattice CP. Given that the dynamics being investigated are very slow to begin with, and that many runs are needed to obtain good statistics, it is quite time-consuming to investigate this model. It is for this reason that I have changed the rate function from (6.2) to (6.13); without this modification, the simulation would run even slower. To see why, consider the case in which the starting site has a very close neighbor. If the rate function (6.2) were to be used, it might be possible for γ' to be much less than the transit rate between these two sites, thus allowing the system to persist for a long enough time to prevent other runs from being performed. Of course, this localized cluster of sites that reinfects itself is precisely what leads to the logarithmic critical scaling and the Griffiths phase, but when allowed to "run rampant," as it were, it also leads to unacceptably long simulation times. By introducing a cutoff and "capping" the rate at some maximum value, as I have done in (6.13), it is possible to ensure that no one simulation run takes too long.

Even with this change, it has not yet been possible to investigate the critical dynamics to confirm the conjecture that they are the same as the critical dynamics of the diluted CP on a lattice; nevertheless, there are

law, but the decay at the transition from the Griffiths phase to the conventional absorbing phase has a stretched exponential character [30], as mentioned in Chapter 2.

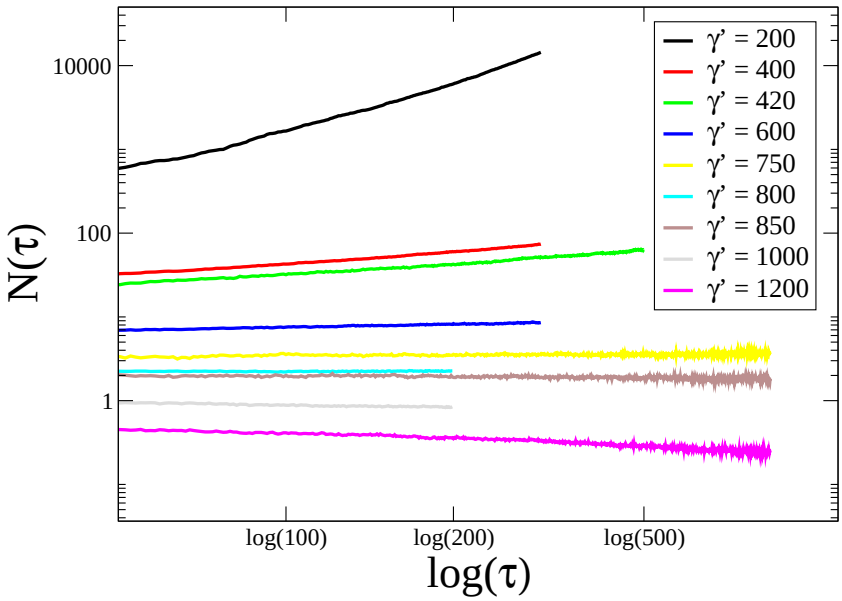

Figure 6.3: Plot of $N(\tau)$ versus $\log(\tau)$ for various values of γ'. Each line represents an average over many runs, with the number of runs varying from line to line. Since the smaller values of γ' are in the active phase, each run at these values took fairly long; as a result, fewer runs were performed for these values of γ'. Each run began with 5 sites infected near the center of the system, and proceeded until all sites were empty or the edge of the system was reached. Note that the key is in the same order, top to bottom, as the lines.

promising preliminary results. Figure 6.3 shows a plot of $N(\tau)$ versus $\log(\tau)$ on a log-log plot for various values of γ'. Such a plot is useful for picking out the critical behavior as only those values of γ' near γ'_c will produce straight lines for large τ; supercritical and subcritical values of γ' should curve away. Figure 6.3 suggests that $750 \lesssim \gamma'_c \lesssim 850$ for the parameters in the simulation ($\kappa = 1.0$, $R_{\max} = 10.0$, $\alpha = 1.0$, $a = 0.5$); since $r_{\text{tot}} \simeq 11000$ for these parameters, the prediction that γ'_c should be of order r_{tot} is not too terribly far off, though it is somewhat surprising that the critical death rate is so low.[4] However, in order to test the conjecture that the active to absorbing phase transition in this off-lattice CP model belongs to the same universality class as the disordered lattice CP transition, it will be necessary to perform much longer simulation runs.

6.3 Summary and Future Work

In this chapter, I have taken the simplified model used in Chapter 5 for simulating a multi-oasis system and, by making a few generalizations, turned

[4]Perhaps not that surprising; the rate r_{tot} is, after all, an average, and much of the contribution to this average comes from sites with many close neighbors. There is thus much site-to-site variability in the total rate, and sites without many close neighbors will be affected much more greatly by the death rate.

it into two new models: a new kind of off-lattice first passage percolation model, and a new off-lattice version of the contact process. In Section 6.1, I explored the behavior of the FPP model both in the hopping regime and the "leaping" regime. For the former case, I obtained an estimate of the infection time that agrees well with simulation results; for the latter case, I developed a heuristic model which allows for a rough approximation of the infection time that agrees marginally well with simulation results.

In Section 6.2, I introduced a new model: the off-lattice contact process. I conjectured that this model should have the same critical properties as the much-studied lattice contact process with quenched disorder, and detailed the relevant time scales in this model. I then explained how to modify the algorithm used in Chapter 5 to simulate a many-oasis system and in this chapter to study off-lattice FPP to simulate this new model. Finally, I presented preliminary simulation results for this model.

There is much work yet to be done on the models studied in this chapter. The most obvious future avenue of research is the continuation of the off-lattice CP simulations; specifically, it is necessary to simulate the system at the critical point and measure the exponents $\bar{\delta}$ and $\bar{\theta}$. Because the off-lattice CP model of this chapter should capture the behavior of the full multi-particle oasis model of Chapters 4 and 5, finding its critical behavior would shed light on the critical behavior of that model, which is significantly more difficult to simulate.

This brings me to the second avenue of research: simulating the multi-particle system of Chapters 4 and 5 in $d \geq 2$ on a large scale. Efforts are already underway to apply the τ-leaping method [78, 79], heretofore employed mostly to study non-spatial models of chemical reactions, to disordered reaction-diffusion models of the type studied herein. It remains to be seen whether it will be feasible to study large systems using such an approach.

A Mean-Field Solutions

A.1 Solution of the Steady-State Mean-Field Equation in $d = 1$

The equation that needs to be solved is

$$0 = D\bar{c}_{ss}''(x) + U(x)\bar{c}_{ss}(x) - b\bar{c}_{ss}(x)^2, \tag{A.1}$$

where $U(x) = (y + z)\Theta(a - |x|) - z$ and the primes denote differentiation with respect to x. To solve this, one can find solutions in the oasis ($|x| < a$) and desert ($|x| > a$) and then match at the boundaries. In the desert, the relevant equation is $0 = D\bar{c}_{ss}''(x) - z\bar{c}_{ss}(x) - b\bar{c}_{ss}(x)^2$. Defining $u(c) \equiv u(\bar{c}_{ss}(x)) \equiv \bar{c}_{ss}'(x)$ leads to the first order equation

$$0 = u\frac{du}{dc} - \frac{z}{D}c - \frac{b}{D}c^2, \tag{A.2}$$

where I have written $\bar{c}_{ss}(x)$ as c for simplicity. This equation can be integrated to give

$$u(c) = \frac{dc(x)}{dx} = -\sqrt{\frac{z}{D}}\, c(x)\sqrt{1 + \frac{2bc(x)}{3z}}, \tag{A.3}$$

which can in turn be integrated to obtain the function $\bar{c}_{ss}(x)$ quoted on the second line of (4.5). A very similar procedure can be done for the area inside the oasis, leading to

$$u(c) = -\sqrt{\frac{2b}{3D}}\sqrt{c(x)^3 - c(0)^3 - \frac{3y}{2b}\left(c(x)^2 - c(0)^2\right)}, \tag{A.4}$$

which can also be integrated, leading to the function quoted on the first line of (4.5). Since the derivatives must match at the boundary, (A.3) and (A.4) can be set equal at $|x| = a$ to obtain the following relation:

$$\bar{c}_{ss}(a) = \bar{c}_{ss}(0)\sqrt{\frac{3y - 2b\bar{c}_{ss}(0)}{3(y + z)}}. \tag{A.5}$$

A.2 Derivation of the Formula for y_c

The cutoff value of the growth rate y below which a population placed on an oasis will die out as $t \to \infty$ can be estimated using the mean-field equation

(4.1) with $b = 0$. For values of y greater than the cutoff, the population will continue to increase without limit as $t \to \infty$; for $y < y_c$, the population will eventually die out. At y_c, there will be a steady-state solution. Hence, one way of finding the cutoff is to try to match solutions to the steady-state equation for $|\boldsymbol{x}| < a$ and $|\boldsymbol{x}| > a$ at $|\boldsymbol{x}| = a$. Only along a certain line in parameter space will this be possible.

In one dimension, the steady-state mean-field equation with $b = 0$ is solved by $c(0)\cos(\sqrt{y/D}\,x)$ for $|x| < a$ and $c(a)e^{-\kappa(|x|-a)}$ for $|x| > a$. Matching the functions and derivatives at $|x| = a$ leads to:

$$y_c = z\cot^2\left(\sqrt{\frac{y_c}{D}}\,a\right), \qquad \text{(1D)} \tag{A.6}$$

which is precisely (4.7). In two dimensions, a similar calculation leads to

$$y_c = z\left[\frac{J_0\left(\sqrt{\frac{y_c}{D}}\,a\right)K_1\left(\kappa a\right)}{J_1\left(\sqrt{\frac{y_c}{D}}\,a\right)K_0\left(\kappa a\right)}\right]^2, \qquad \text{(2D)} \tag{A.7}$$

while in three dimensions I have obtained

$$y_c = z\tan^2\left(\pi - \sqrt{\frac{y_c}{D}}\,a\right). \qquad \text{(3D)} \tag{A.8}$$

These equations can be solved numerically to determine y_c. A plot of y_c as a function of z in one, two, and three dimensions, with all other parameters fixed, is shown in Figure A.1.

Note that y_c only has meaning in the mean-field limit; taking fluctuations into account leads to the conclusion that single isolated oasis will die out with probability 1 as $t \to \infty$.

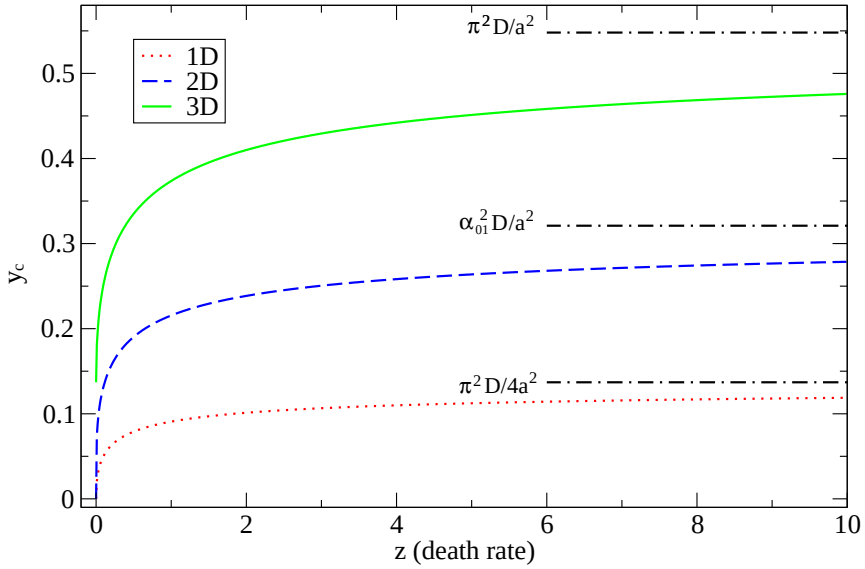

Figure A.1: Cutoff growth rate y_c as a function of death rate z with $a = 3.0$, $D = 0.5$. Here α_{01} is the first zero of J_0. Note that in one and two dimensions, an arbitrarily small growth rate with $z = 0$ will allow a stable population to take hold; in three dimensions, $y_c(z = 0) = \pi^2 D/4a^2$.

B Asymptotic Analysis of the Moments of $f_N(\boldsymbol{x}, t)$

In this appendix, I derive the results for the asymptotic moments of $f_N(\boldsymbol{x}, t)$ for the continuum in $d = 1, 2, 3$ quoted in (4.31), (4.36), and (4.37). In any dimension, $P_{\text{none}}(R, a, t) \simeq \exp[-gY(R, a, t)]$, where $Y(R, a, t)$ is given by

$$Y(R,a,t) = \frac{(a/R)^{d/2-1}}{2\pi\imath} \int_{\mathcal{L}} ds\, \frac{e^{st}}{s^2}\, \frac{K_{d/2-1}\left(\sqrt{\frac{s+z}{D}}\, R\right)}{K_{d/2-1}\left(\sqrt{\frac{s+z}{D}}\, a\right)}. \tag{B.1}$$

Although in $d = 1$ and $d = 3$ this Laplace transform machinery is unnecessary—one can simply perform the integral over time appearing in (4.23)—it is easier to determine the asymptotic behavior of the moments of $f_N(R, a, t)$ in all dimensions by using these tools. Changing variables to $p = s + z$ leads to $Y(R, a, t) = [(a/R)^{d/2-1} e^{-zt}/(2\pi\imath)] Q_1(R, a, t)$, where

$$Q_1(R,a,t) = \int_{\mathcal{L}} dp\, \frac{e^{pt}}{(p-z)^2}\, \frac{K_{d/2-1}\left(\sqrt{\frac{p}{D}}\, R\right)}{K_{d/2-1}\left(\sqrt{\frac{p}{D}}\, a\right)}. \tag{B.2}$$

This integral can be evaluated using contour integral techniques. There is one second-order pole at $p = z$ and a branch cut which I will take to lie on the real p axis from $p = 0$ to $p = -\infty$. The countour will be taken to enclose the pole at $p = z$, and consists of three parts: Q_1, the value of which I wish to find; and Q_2 and Q_3, whose values must add with that of Q_1 to equal $2\pi\imath\Xi$, where Ξ is the residue at $p = z$. The space is shown schematically in Figure B.1. Using the residue theorem and changing integration variables to $u = -p$ gives:

$$\begin{aligned} Q_1(R,a,t) &= 2\pi\imath\, t e^{zt}\, \frac{K_\mu(\kappa R)}{K_\mu(\kappa a)} \\ &- 2\pi\imath \frac{e^{zt} R K_{\mu+1}(\kappa R)\, K_\mu(\kappa a)}{\sqrt{4Dz}\, [K_\mu(\kappa a)]^2} \\ &+ 2\pi\imath \frac{e^{zt} a K_\mu(\kappa R)\, K_{\mu+1}(\kappa a)}{\sqrt{4Dz}\, [K_\mu(\kappa a)]^2} \\ &- \int_0^\infty du\, \frac{e^{-tu}}{(u+z)^2}\, \frac{M_\mu(R,a,u)}{K_\mu\left(\imath\sqrt{\frac{u}{D}}\, a\right) K_\mu\left(-\imath\sqrt{\frac{u}{D}}\, a\right)}, \end{aligned} \tag{B.3}$$

where I have used $\mu = d/2 - 1$ and $M_\mu(R, a, u) = 2\imath \text{Im}\left[K_\mu\left(\imath\sqrt{\frac{u}{D}}\, R\right) K_\mu\left(-\imath\sqrt{\frac{u}{D}}\, a\right)\right]$. One can see that $Y(R, a, t)$ thus has the form $C_1 t - C_2 + C_3 h(t)$, where the C_n are constants in time and $h(t)$ is given by some complicated integral. Since $Y(R, a, 0) = 0$, one can let $C_3 = C_2$ and

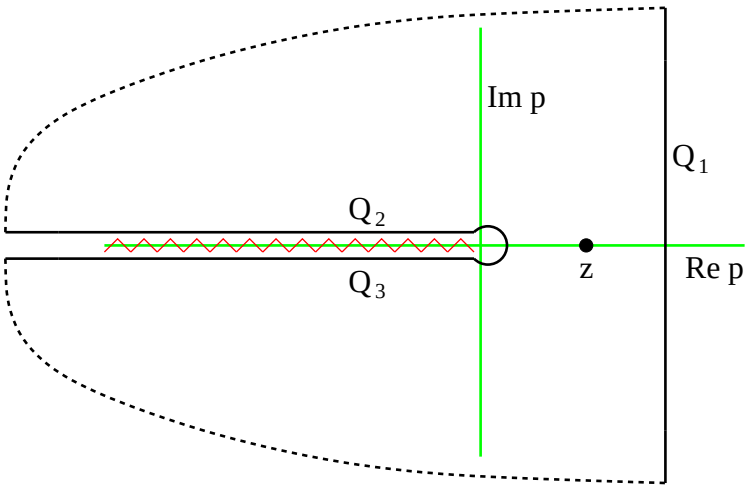

Figure B.1: Schematic of the contour integral which must be done to find $Y(R,a,t)$. The dashed lines represent contributions to the integral that vanish as they are moved further from the origin.

$h(0)=1$. It should be clear that $h(\infty)=0$, and that $h(t)\leq 1$ for all t. This is enough to prove the asymptotic results for the moments of $f_N(R,a,t)$ quoted in Section 4.3.3. These moments are given by $\langle T^j(R,a)\rangle = j\int_0^\infty dt\, P_{\rm none}(R,a,t)t^{j-1}$; plugging in the form for $Y(R,a,t)$ gives:

$$\langle T^j(R,a)\rangle = j\int_0^\infty dt\, e^{-g[C_1 t - C_2(1-h(t))]}\, t^{j-1} \tag{B.4}$$

The constant C_2 goes to 0 as $R\to\infty$, so one can Taylor expand $\exp[gC_2(1-h(t))]$ and arrive at

$$\langle T^j(R,a)\rangle = j\int_0^\infty dt\, e^{-gC_1 t}\, t^{j-1}\,[1+gC_2(1-h(t))+\ldots] \tag{B.5}$$

Keeping only the lowest order term, one gets $\langle T^j(R,a)\rangle = j!(gC_1)^{-j}$ as $R\to\infty$. Looking at (B.3), one sees that $C_1 = (a/R)^{d/2-1}K_{d/2-1}(\kappa R)/K_{d/2-1}(\kappa a)$. I am now ready to plug in the functional forms for $K_{d/2-1}$ and arrive at the final asymptotic expressions for $\langle T^j(R,a)\rangle$:

$$\begin{aligned}
\langle T^j(x)\rangle &= j!\,\frac{e^{\kappa|x|j}}{g^j} \qquad \text{1D} \\
\langle T^j(R,a)\rangle &= j!\left[\frac{K_0(\kappa a)}{g\,K_0(\kappa R)}\right]^j \qquad \text{2D} \\
\langle T^j(R,a)\rangle &= j!\left(\frac{R}{a}\right)^j \frac{e^{\kappa(R-a)j}}{g^j} \qquad \text{3D,}
\end{aligned} \tag{B.6}$$

where $|x| = R-a$ (the distance from the origin to the edge of the oasis nearest the origin).

C Estimating the Infection Time for Off-Lattice FPP with Large Leaps

In this appendix, I will provide details of a method for estimating the infection time in the off-lattice first passage percolation model studied in Chapter 6 for the case of small α and small $\kappa R_{\max}$. In Section 6.1.2, I proposed that transport in this regime is mediated by large leaps of size R_{leap} which originate from growing balls of infected sites (see Figure 6.1). There is some typical time τ_{leap} after a ball first starts growing that a large leap of size $\geq R_{\text{leap}}$ is made from somewhere in this ball towards the target site. An estimate for the infection time is then given by optimizing the expression $L\tau_{\text{leap}}/[R_{\text{leap}}\cos(\Delta\phi/2)]$ with respect to R_{leap} and $\Delta\phi$, the allowed angular deviation of the leaps from the straight line path to the target. In order to do this optimization, however, it is necessary to know two things: the dependence of τ_{leap} on R_{leap} and $\Delta\phi$; and the front velocity v_s of the growing balls.

I will first derive an approximate expression for τ_{leap} as a function of R_{leap} and $\Delta\phi$. Consider a growing ball of sites which is centered at the origin. At time τ', a new ring of sites located a distance $v_s\tau'$ from the origin is infected for the first time. For each of these sites, one can define a local coordinate system in which the "allowed leaping region"—the slice of a circle centered on the origin of the ball of angular width $\Delta\phi$ extending from $R_{\text{leap}} \to \infty$—is described by some complicated boundary function. However, this local coordinate system has a region that largely overlaps with the allowed leaping region that is simple to describe. The two regions are shown in Figure C.1.

It is not too terrible of an approximation to simply replace the allowed leaping region by this other region, thus making calculations considerably easier. The distance R which defines the beginning of the approximate allowed leaping region is given by $R^2 = (v_s\tau')^2 + R_{\text{leap}}^2 - 2v_s\tau' R_{\text{leap}}\cos(\theta)$, where θ is the angle to the site from the line down the middle of the actual allowed leaping region. The total rate r_{leap} for a site to infect any site in the (approximate) allowed leaping region is then given by

$$\begin{aligned} r_{\text{leap}}(R) &\simeq n\Delta\phi \int_R^\infty d\rho\, \rho \left(\frac{R_{\max}}{\rho}\right)^\alpha e^{-\kappa(\rho - R_{\max})} \\ &= \frac{B_c \Delta\phi (\kappa R_{\max})^{\alpha-2} e^{\kappa R_{\max}}}{\pi} \Gamma(2-\alpha, \kappa R), \end{aligned} \tag{C.1}$$

where I have used $n = B_c/\pi R_{\max}^2$ with $B_c = 4.5$ and $\Gamma(\cdot,\cdot)$ is the incomplete gamma function.

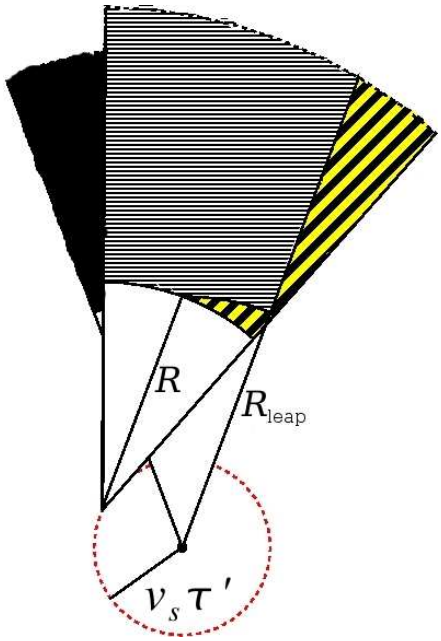

Figure C.1: Figure showing the relationship between the actual allowed leaping region and the approximate region used to make calculations tractable. The section with thin horizontal lines corresponds to the overlap of the two regions; the section with thick vertical lines corresponds to the portion of the approximate leaping region not actually in the allowed leaping region; and the dark section corresponds to the portion of the allowed leaping region not in the approximate region.

The calculation now proceeds largely in the same manner as the first passage time calculation of Section 4.3.3; that is, I will find the probability that *no* large leaps have occurred by a time τ, given that the site at the origin (the center of the ball) was first infected at $\tau = 0$. I will denote this probability by $P_{\text{nl}}(\tau)$; it is given roughly by

$$P_{\text{nl}}(\tau) = \prod_{v_s\tau'=0, v_s\Delta\tau', \ldots}^{v_s\tau} \prod_{\theta=0,\Delta\theta,\ldots}^{2\pi} \left[e^{-r_{\text{leap}}(R)(\tau-\tau')} \right]^{n v_s^2 \tau' \Delta\tau' \Delta\theta}. \tag{C.2}$$

Taking the logarithm of each side and allowing $\Delta\tau'$ and $\Delta\theta$ to go to 0 gives:

$$\log P_{\text{nl}}(\tau) = -\frac{{B_c}^2 \Delta\phi (\kappa R_{\max})^{\alpha-2} e^{\kappa R_{\max}}}{(\pi R_{\max})^2} \int_0^{v_s\tau} ds\, s \int_0^{2\pi} d\theta\, \Gamma(2-\alpha, \kappa R) \left[\tau - \frac{s}{v_s} \right], \tag{C.3}$$

where $R^2 = s^2 + R_{\text{leap}}^2 - 2sR_{\text{leap}}\cos(\theta)$. To determine τ_{leap}, one needs to set this expression equal to -1; that is, τ_{leap} is defined by $P_{\text{nl}}(\tau_{\text{leap}}) = 1/e$.

What about v_s? This is a more troubling matter than finding τ_{leap}, it turns out. Indeed, there is no reason to suppose *a priori* that the motion on scales $< R_{\text{leap}}$ can even be defined by a front, but I will nonetheless attempt to estimate the speed of such a front. To do so, I will assume that transport is

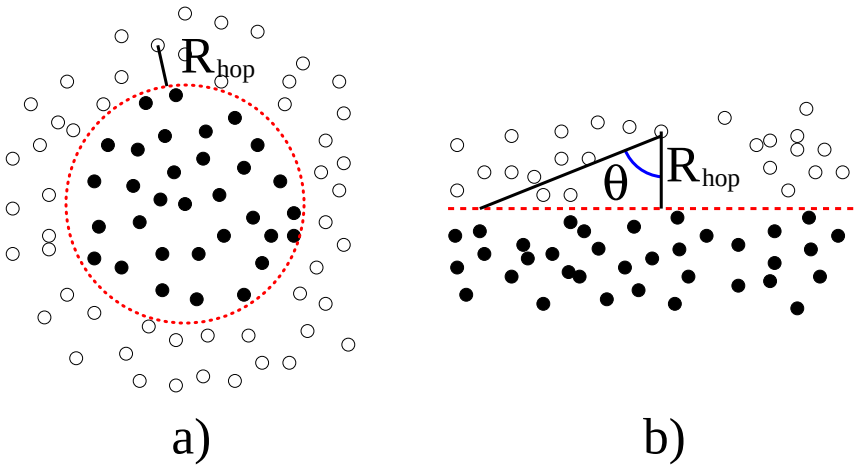

Figure C.2: a) Rough picture of front motion: sites a distance R_{hop} away from the front are infected, moving the front forward. b) Picture of an infinite front. In this case, the integration over the ball can be taken to be over an infinite rectangular region, simplifying the calculation.

mediated by small hops of size R_{hop} so that the speed of the front is given approximately by $R_{\text{hop}} r_{\text{hop}}$, where r_{hop} is the rate for all of the occupied sites inside the ball to infect an unoccupied site a distance R_{hop} from the front. The situation is depicted in Figure C.2a. It should be clear that the front speed in this approximation will depend on the radius of the ball—indeed, this makes intuitive sense given that the front will clearly gain speed rapidly at first as more sites are infected—but that there is an asymptotic front speed. It is this speed that I will try to solve for and then maximize with respect to R_{hop}. This asymptotic front speed is given by (see Figure C.2b)

$$v_s = \frac{B_c}{\pi R_{\max}^2} \int_{-\frac{\pi}{2}}^{\frac{\pi}{2}} d\theta \int_{\frac{R_{\text{hop}}}{\cos(\theta)}}^{\infty} d\rho\, \rho \left(\frac{R_{\max}}{\rho}\right)^{\alpha} e^{-\kappa(\rho - R_{\max})}. \tag{C.4}$$

After maximizing this equation and using the result to estimate the infection time, it is important to make sure that $L/\langle \tau_{\text{infection}}(L) \rangle > v_s$; that is, the leaps are allowing for transit faster than the front velocity.

To summarize: in order to estimate the infection time for the case of small $\kappa R_{\max} + \alpha$, it is necessary to first estimate the front speed v_s of the growing balls by maxizing (C.4), then use this result to minimize $\tau_{\text{leap}}/R_{\text{leap}}$ with respect to $\Delta\phi$ and R_{leap}. The leap time τ_{leap} is given in (C.3). Note that some of the errors in the various approximations should negate each other to some extent: R_{leap} is really the *minimum* leap distance, and $\Delta\phi$ is the *maximum* angular deviation from the target site, so these approximations tend to lead to an overestimate of the infection time; on the other hand, the speed v_s is undoubtedly an overestimate of the true front speed, and this will tend to lead to an underestimate of the infection time.

References

[1] R. Kroon, H. Fleurent, and R. Sprik, Phys. Rev. E **47**, 2462 (1993).

[2] J. D. Murray, *Mathematical Biology* (Springer-Verlag, New York, 1993).

[3] D. R. Nelson and N. M. Shnerb, Phys. Rev. E **58**, 1383 (1998).

[4] K. A. Dahmen, D. R. Nelson, and N. M. Shnerb, arXiv:cond-mat/9903276v1.

[5] K. A. Dahmen, D. R. Nelson, and N. M. Shnerb, J. Math. Bio. **41**, 1 (2000).

[6] M. Mimura, H. Sakaguchi, and M. Matsushita, Physica A **282**, 283 (2000).

[7] K. Page, N. Monk, and P. Maini, Phys. Rev. E **76**, 11902 (2007).

[8] J. von Hardenberg, E. Meron, M. Shachak, and Y. Zarmi, Phys. Rev. Lett. **87**, 198101 (2001).

[9] D. Birch, Y. Tsang, and W. Young, Phys. Rev. E **75**, 66304 (2007).

[10] N. G. van Kampen, *Stochastic Processes in Physics and Chemistry* (Elsevier Science Publishers B.V., Amsterdam, The Netherlands, 2007).

[11] D. Johnson, *Kinetic Monte Carlo: Bare Bones and a Little Flesh*, from the UIUC Materials Computation Center Computational Materials Science Summer School 2001.

[12] G. Ódor, Rev. Mod. Phys. **76**, 663 (2004).

[13] P. Grassberger and A. de la Torre, Annals of Physics **122**, 373 (1979).

[14] H. Janssen, Zeit. Phys. B **42**, 151 (1981).

[15] H. Hinrichsen, Adv. Phys. **49**, 815 (2000).

[16] H. Janssen and U. Täuber, Annals of Physics **315**, 147 (2005).

[17] U. Täuber, M. Howard, and B. P. Vollmayr-Lee, J. Phys. A: Math. Gen. **38**, R79 (2005).

[18] P. Grassberger, Zeit. Phys. B **47**, 365 (1982).

[19] J. Marro and R. Dickman, *Nonequilibrium Phase Transitions in Lattice Models* (Cambridge University Press, Cambridge, UK, 1999).

[20] A. Harris, J. Phys. C **7**, 1671 (1974).

[21] J. Cardy, *Scaling and Renormalization in Statistical Physics* (Cambridge University Press, Cambridge, UK, 1996).

[22] W. Kinzel, Zeit. Phys. B **58**, 229 (1985).

[23] A. Noest, Phys. Rev. Lett. **57**, 90 (1986).

[24] H. Janssen, Phys. Rev. E **55**, 6253 (1997).

[25] J. Hooyberghs, F. Iglói, and C. Vanderzande, Phys. Rev. Lett. **90**, 100601 (2003).

[26] J. Hooyberghs, F. Iglói, and C. Vanderzande, Phys. Rev. E **69**, 66140 (2004).

[27] T. Vojta and M. Dickison, Phys. Rev. E **72**, 036126 (2005).

[28] A. G. Moreira and R. Dickman, Phys. Rev. E **54**, R3090 (1996).

[29] T. Vojta and M. Y. Lee, Phys. Rev. Lett. **96**, 035701 (2006).

[30] T. Vojta, A. Farquhar, and J. Mast, arxiv:0810.1569v1.

[31] R. Griffiths, Phys. Rev. Lett. **23**, 17 (1969).

[32] I. Webman, Phil. Mag. B **77**, 1401 (1998).

[33] G. Szabó, H. Gergely, and B. Oborny, Phys. Rev. E **65**, 066111 (2002).

[34] F. Sagués, J. Sancho, and J. García-Ojalvo, Rev. Mod. Phys. **79**, 829 (2007).

[35] M. Freidlin, *Markov Processes and Differential Equations: Asymptotic Problems* (Birkhäuser Verlag, Basel, 1996).

[36] T. Lee and F. Torcaso, Ann. Prob. **26**, 1179 (1998).

[37] J. Carpenter, Ph.D. thesis, University of Illinois at Urbana-Champaign (2004).

[38] R. A. Fisher, Ann. Eugenics **7**, 353 (1937).

[39] D. Panja, Phys. Rep. **393**, 87 (2004).

[40] E. Brunet and B. Derrida, Phys. Rev. E **56**, 2597 (1997).

[41] J. Krug and H. Spohn, in *Solids Far From Equilibrium*, edited by C. Godrèche (Cambridge University Press, Cambridge, UK, 1992).

[42] F. Family, J. Phys. A: Math. Gen. **18**, L75 (1985).

[43] E. Moro, Phys. Rev. Lett. **87**, 238303 (2001).

[44] M. Kardar, G. Parisi, and Y. Zhang, Phys. Rev. Lett. **56**, 889 (1986).

[45] J. Riordan, C. R. Doering, and D. ben Avraham, Phys. Rev. Lett. **75**, 565 (1995).

[46] G. Tripathy and W. van Saarloos, Phys. Rev. Lett. **85**, 3556 (2000).

[47] G. Tripathy, A. Rocco, J. Casademunt, and W. van Saarloos, Phys. Rev. Lett. **86**, 5215 (2001).

[48] R. A. Blythe and M. R. Evans, Phys. Rev. E **64**, 051101 (2001).

[49] J. Hammersley and D. Welsh, in *Bernoulli, Bayes, Laplace Anniversary Volume*, edited by J. Neyman and L. M. Le Cam (Springer-Verlag, Berlin, 1965).

[50] H. Kesten, Lecture Notes in Math **1180**, 125 (1986).

[51] C. Howard, in *Probability on Discrete Structures*, edited by H. Kesten (Springer-Verlag, Berlin, 2004).

[52] S. Alm and R. Parviainen, Combinatorics, Probability and Computing **11**, 433 (2002).

[53] K. Alexander, Ann. Appl. Prob. **3**, 81 (1993).

[54] H. Kesten, Ann. App. Prob. **3**, 296 (1993).

[55] M. Eden, in *Symposium on Information Theory in Biology, Gatlinburg, Tennessee, October 29-31, 1956* (Pergamon Press, Symposium Publications Division, 1958), p. 359.

[56] J. Zabolitzky and D. Stauffer, Phys. Rev. A **34**, 1523 (1986).

[57] M. T. Batchelor, B. I. Henry, and S. D. Watt, Phys. Rev. E **58**, 4023 (1998).

[58] J. Kertesz and D. Wolf, J. Phys. A: Math. Gen. **21**, 747 (1988).

[59] D. Wolf and J. Kertesz, J. Phys. A: Math. Gen. **20**, L257 (1987).

[60] C. Howard and C. Newman, Probability Theory and Related Fields **108**, 153 (1997).

[61] C. Howard and C. Newman, Ann. Prob. **29**, 577 (2001).

[62] C. Wang, P. Liu, and J. Bassingthwaighte, J. Phys. A: Math. Gen. **28**, 2141 (1995).

[63] E. Kuennen and C. Wang, J. Stat. Mech.: Theory and Exp. **2008**, P05014 (2008).

[64] V. Ambegaokar, B. I. Halperin, and J. S. Langer, Phys. Rev. B **4**, 2612 (1971).

[65] J. Kurkijärvi, Phys. Rev. B **9**, 770 (1974).

[66] J. Joo and J. Lebowitz, Phys. Rev. E **72**, 36112 (2005).

[67] A. L. Lin, B. A. Mann, G. Torres-Oviedo, B. Lincoln, J. Kas, and H. L. Swinney, Biophys. J. **87**, 75 (2004).

[68] M. Assaf and B. Meerson, Phys. Rev. E **75**, 031122 (2007).

[69] S. Redner, *A Guide to First-Passage Processes* (Cambridge University Press, Cambridge, UK, 2001).

[70] M. Abramowitz and I. A. Stegun, *Handbook of Mathematical Functions with Formulas, Graphs, and Mathematical Tables* (Dover, New York, 1964).

[71] B. I. Shklovskii and A. L. Efros, *Electronic Properties of Doped Semiconductors* (Springer-Verlag, Berlin, 1984).

[72] A. Hunt, *Percolation Theory for Flow in Porous Media* (Springer-Verlag, Berlin, 2005).

[73] D. Stauffer and A. Aharony, *Introduction to Percolation Theory* (Routledge, London, 1994).

[74] V. Ambegaokar, S. Cochran, and J. Kurkijärvi, Phys. Rev. B **8**, 3682 (1973).

[75] D. Gillespie, J. Comp. Phys. **22**, 403 (1976).

[76] A. Bortz, M. Kalos, and J. Lebowitz, J. Comp. Phys. **17**, 10 (1975).

[77] S. Sheather and M. Jones, J. Royal Stat. Soc. Series B: Meth. **53**, 683 (1991).

[78] M. Rathinam, L. Petzold, Y. Cao, and D. Gillespie, J. Chem. Phys. **119**, 12784 (2003).

[79] D. Gillespie, J. Chem. Phys. **115**, 1716 (2001).

[80] S. Fallert, J. Ludlam, and S. Taraskin, Phys. Rev. E **77**, 51125 (2008).

[81] J. Taylor, *An Introduction to Error Analysis* (University Science Books, Mill Valley, CA, 1997).

[82] B. Peirce, Astron. J. **2** (1852).

[83] T. Vojta and J. Schmalian, Phys. Rev. B **72**, 045438 (2005).

[84] T. Vojta, J. Phys. A: Math. Gen. **39**, R143 (2006).

Author's Biography

Andrew Royce Missel was born to Gary and Elizabeth Missel in Redwood City, California, on January 6th, 1981. He headed to the East Coast to attend Cornell University in Ithaca, New York in 1999, then headed to the Midwest for graduate school in physics at the University of Illinois, Urbana-Champaign in 2003. At UIUC, he studied population dynamics in disordered systems with Karin Dahmen. He is now planning on heading back to the West Coast for a postdoc with Alex Levine at UCLA, thus completing his round-trip journey.